Université de Montréal

Calculs ab initio de structures électroniques pour un meilleur design de polymères photovoltaïques

par
Nicolas Bérubé

Département de physique
Faculté des arts et des sciences

Thèse présentée à la Faculté des études supérieures
en vue de l'obtention du grade de Philosophiæ Doctor (Ph.D.)
en physique

Avril, 2014

Université de Montréal
Faculté des études supérieures

Cette thèse intitulée:

Calculs ab initio de structures électroniques pour un meilleur design de polymères photovoltaïques

présentée par:

Nicolas Bérubé

a été évaluée par un jury composé des personnes suivantes:

Carlos Silva,	président-rapporteur
Michel Côté,	directeur de recherche
William Skene,	membre du jury
Johannes Hachmann,	examinateur externe
Christian Pellerin,	représentant du doyen de la FES

Thèse acceptée le: 11 avril 2014

RÉSUMÉ

La présente thèse porte sur l'utilité de la théorie de la fonctionnelle de la densité dans le design de polymères pour applications photovoltaïques.

L'étude porte d'abord sur le rôle des calculs théoriques pour la caractérisation des polymères dans le cadre de collaborations entre la théorie et l'expérience. La stabilité et les niveaux énergétiques de certaines molécules organiques sont étudiés avant et après la sulfuration de leurs groupements carbonyles, un procédé destiné à diminuer le band gap. Les propriétés de dynamique électronique, de séparation des porteurs de charges et de spectres de vibrations Raman sont également explorées dans un polymère à base de polycarbazole.

Par la suite, l'utilité des calculs théoriques dans le design de polymères avant leurs synthèses est considérée. La théorie de la fonctionnelle de la densité est étudiée dans le cadre du modèle de Scharber afin de prédire l'efficacité des cellules solaires organiques. Une nouvelle méthode de design de polymères à faible band gaps, basée sur la forme structurale aromatique ou quinoide est également présentée, dont l'efficacité surpasse l'approche actuelle de donneur-accepteur. Ces études sont mises à profit dans l'exploration de l'espace moléculaire et plusieurs candidats de polymères aux propriétés électroniques intéressantes sont présentés.

Mots clés:Photovoltaïque, polymères, matériaux organiques, structure électronique, calculs ab initio, théorie de la fonctionnelle de la densité.

ABSTRACT

This thesis focuses on the role of density functional theory in the design of polymers for photovoltaic applications.

Theoretical calculations are first studied in the characterization of polymers in the context of collaborations between theory and experiment. The stability and the energy levels of some organic molecules are studied before and after a sulfurization of their carbonyl groups, a process destined to lower the band gaps. The dynamics of the electronic processes and the Raman vibration spectra are also explored in a polycarbazole-based polymer.

From then, the usefulness of theoretical calculations in the design of polymers before their syntheses is explored. Density functional theory calculations are studied under the Scharber model in order to predict the efficiency of organic solar cells. Then, a new approach for the design of low band gap polymer based on the aromatic or quinoid structures is established, whose efficiency surpasses the actual donor-acceptor approach. These studies are used in the exploration of the chemical space and several candidate for polymers with interesting electronic properties are presented.

Keywords: Photovoltaics, polymers, organic materials, electronic structure, ab initio calculations, density functional theory.

TABLE DES MATIÈRES

LISTE DES TABLEAUX

LISTE DES FIGURES

REMERCIEMENTS

J'aimerais tout d'abord remercier tous mes collègues au sein de mon groupe de recherche de m'avoir guidé, inspiré, accompagné et supporté (dans tous les sens du terme) au sein de ces 5 années de travail et d'avoir été des amis très chers: Merlin Delaval-Lebel, Jonathan Laflamme-Janssen, Simon Blackburn, Gabriel Antonius, Vincent Gosselin, Bruno Rousseau, Bénédict Plante, Jason Beaudin, Jean-Frédéric Laprade, Paul Boulanger, Simon Pesant, Josiane Gaudreau et Simon Lévesque.

Un énorme merci à Françoise Provencher d'être une collègue de travail exemplaire, un modèle à suivre et une source contagieuse de passion. Je suis ravi d'avoir pu faire mon doctorat à tes côtés.

Merci au groupe de Mario Leclerc pour les collaborations, spécialement à Pierre-Olivier Morin de m'avoir guidé dans le monde pluridisciplinaire de la chimie de synthèse.

Merci également aux employés de notre département d'apporter leur aide, leurs conseils, leur support inconditionnel et leur joie méthodique au cours de nos études, spécialement à Anne Gosselin, Lynda Syvrais, Élise Saint-Jacques et à notre cher Louis Lemay.

Merci à la PHYSUM et à mes collègues d'avoir construit ma vie sociale, mon implication et d'avoir partagé mes passions. Merci à Guillaume Lavoie, Étienne Raymond, Jessica Nasica, et Laura-Isabelle Dion-Bertand d'avoir partagé mes projets extrascolaires. Merci également aux membres de la troupe de chant a cappella de physique.

Merci aux organismes subventionnaires et aux bourses reçues de m'avoir donné la chance de compléter mes études.

Merci à ma mère pour tout son support moral et financier, et de s'être soucié de ma santé en me préparant un nombre incalculable de repas excellents.

Il va sans dire que les plus chers remerciements vont à mon directeur de recherche, Michel Côté, sans qui cette thèse n'aurait jamais vu le jour. Merci de m'avoir guidé au cours de mes études, ainsi qu'au travers de la bureaucratie académique. Merci pour ton attention, tes soucis à mon égard et pour ton support dans les durs moments. Merci pour

tous les conseils, les réflexions, et les discussions quant à la recherche, à nos passe-temps ou au sens général de la vie.

CHAPITRE 1

INTRODUCTION

Le monde a des besoins énergétiques de plus en plus grands. En 2012, la consommation énergétique mondiale dépassait les douze milliards de tonnes d'équivalents pétrole. Le pétrole, le charbon et le gaz naturel composent 87% de cette consommation.[32] Un des grands défis de notre génération est de diminuer notre dépendance envers les sources d'énergie non renouvelables pour pouvoir combler nos besoins futurs.

L'énergie solaire est un candidat de plus en plus populaire pour résoudre cette crise énergétique. En effet, cette technologie occupe une place de plus en plus grande dans notre culture et dans notre économie. Nous pouvons soutirer de l'énergie du Soleil de nombreuses façons, avec des processus tels l'énergie thermique ou la photosynthèse. La technologie actuelle la moins coûteuse pour la production d'électricité à partir du Soleil est l'utilisation de l'effet photoélectrique,[1] par lequel un photon excite directement un électron dans un semi-conducteur, qui peut ensuite être utilisé pour construire une différence de potentiel et donc, un courant électrique. Ce processus de transformation énergétique est appelé énergie photovoltaïque.

L'énergie solaire est actuellement limitée par ses coûts d'exploitation qui peinent à concurrencer les sources d'énergie actuelles. Par exemple, au Québec, l'hydroélectricité est fournie à un tarif de 5,4 sous par kilowattheure en avril 2013.[178] En comparaison, les coûts moyens de l'énergie photovoltaïque sont situés à 14,4 sous par kilowattheure.[1] Cependant, les coûts des énergies renouvelables ont tendance à diminuer alors que ceux des énergies non renouvelables augmentent. Le principe de parité réseau[1] a lieu lorsque les coûts d'une énergie alternative sont égaux au prix de vente actuel d'un réseau électrique, et la parité a été récemment atteinte en Espagne.[70] Lorsque la parité réseau est atteinte, le développement de l'énergie solaire à grande échelle devient alors économiquement viable. Il est donc crucial pour le développement de l'énergie solaire d'améliorer la technologie actuelle et de diminuer ses coûts.

[1] en anglais: *grid parity*

La diminution des coûts d'un panneau solaire passe par la compréhension de son fonctionnement. Dans un semi-conducteur, les électrons occupent tous les niveaux d'énergie disponibles jusqu'au niveau de Fermi, et il existe ensuite une plage d'énergie inaccessible appelée *band gap*[2], au-dessus de laquelle d'autres états inoccupés se situent. Les derniers états occupés constituent la *bande de valence*, et les premiers états inoccupés au-dessus du band gap constituent la *bande de conduction*. Via l'effet photoélectrique, un photon peut exciter un électron de la bande de valence à la bande de conduction, laissant ainsi une absence d'électron, un *trou*, dans le niveau précédemment occupé. L'électron et le trou sont encore couplés par la force de Coulomb et forment un *exciton*. Pour pouvoir retirer de l'énergie de ce phénomène, il faut un processus pour éviter que cet électron ne se recombine avec le trou en revenant dans son état original. Les panneaux solaires dits inorganiques utilisent le principe d'une jonction p-n pour créer un champ électrique qui sépare physiquement l'électron du trou, empêche la recombinaison de l'exciton et transporte ces porteurs de charges aux interfaces du dispositif. Les porteurs ainsi séparés peuvent être utilisés pour fournir un courant électrique.[203] Le fonctionnement est illustré à la Figure 1.1.

Les panneaux solaires à base de silicium sont actuellement les plus populaires, puisque le silicium est présent en très grande proportion dans la croûte terrestre et que les technologies de traitement et de dopage du silicium forment des dispositifs pouvant très facilement retirer l'énergie d'un électron excité. Cependant, cette technologie est limitée par son fort coût autant financier qu'énergétique. En effet, pour produire l'énergie nécessaire pour fabriquer un panneau solaire à base de silicium, il faudrait utiliser un panneau solaire pendant 6 à 16 ans.[228] Cela limite l'énergie solaire à des usagers pouvant se permettre un fort investissement de départ.

Plusieurs autres technologies inorganiques existent, par exemple les cellules solaires à plusieurs jonctions où l'énergie de plusieurs photons se combine pour augmenter l'efficacité, mais ces cellules particulièrement coûteuses sont réservées à des usages sous des concentrateurs de lumière ou dans des milieux distants où l'énergie est peu accessible.

[2] Bien que le terme français soit *largeur de bande interdite*, l'appellation *band gap*, couramment utilisée dans la communauté, sera favorisé pour alléger le texte.

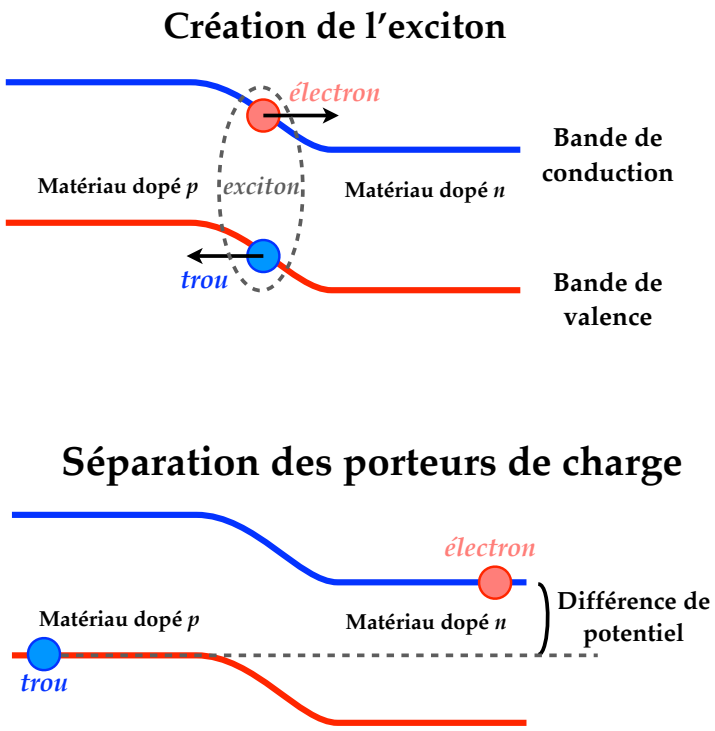

Figure 1.1 – Fonctionnement d'une cellule solaire inorganique.

Les cellules à couche minces à base de Cadmium-Tellurium ou Cuivre-Indium-Gallium-Sélénium utilisent moins de matériau que les cellules à base de silicium et procurent une alternative intéressante, mais ne pourront pas combler les besoins énergétiques de la planète puisque ces matériaux sont rares et souvent toxiques.[62]

Chacune de ces technologies peut trouver une utilisation spécifique, mais plusieurs usages demeurent inaccessibles. Une technologie émergente pouvant pallier les lacunes actuelles du domaine est la photovoltaïque organique dans laquelle les semi-conducteurs sont à base de carbone. Ces composés sont beaucoup moins coûteux à fabriquer et nécessitent aussi un investissement initial plus faible.[10, 63, 115] Ils présentent aussi la possibilité d'être dissouts et incorporés à des encres. Celles-ci peuvent bénéficier de l'énorme expertise en technique d'impression, d'un faible coût et d'une très grande rapidité de production. De plus, les dispositifs organiques peuvent être fabriqués sur des substrats flexibles ou semi-transparents, et peuvent ainsi profiter de nou-

velles applications, par exemple des textiles solaires qui s'enroulent pour un transport facile, des vitres teintées photovoltaïques ou une inclusion facile à l'architecture des édifices.[40, 50, 136, 153, 201]

Les cellules solaires organiques fonctionnent de manière similaire à leurs équivalents inorganiques, mais leurs composants ne peuvent être dopés de manière aussi efficace pour créer une jonction p-n. Ainsi, la jonction p-n est remplacée par une hétérojonction entre deux matériaux distincts appelés *donneur* et *accepteur* d'électrons, comme illustré dans la Figure 1.2. Les niveaux énergétiques de ces deux matériaux sont placés de sorte que le champ à leur interface sépare les porteurs de charge. Pour minimiser la distance que l'exciton doit parcourir et pour ainsi éviter sa recombinaison, il est donc important de maximiser l'interface entre le matériau donneur et le matériau accepteur à l'aide d'une hétérojonction volumique illustrée à la Figure 1.3, de sorte qu'une interface soit toujours à proximité de l'exciton pour le dissocier.[53]

La limitation principale de la photovoltaïque organique reste sa faible efficacité par rapport à ses homologues inorganiques. Pour pouvoir être économiquement viable et compétitif, il est crucial d'augmenter cette efficacité. Pour ce faire, il faut pouvoir trouver les composés organiques qui possèdent les propriétés électroniques les plus utiles, entre autres un band gap optimal et des niveaux énergétiques permettant une hétérojonction efficace. Cependant, l'espace moléculaire des différents composés organiques possibles est énorme. La synthèse de tous les composés est complètement impossible, et il est crucial de pouvoir sonder les propriétés de façon théorique pour une meilleure efficacité. Le Harvard Clean Energy Project utilise la puissance combinée d'un gigantesque réseau d'ordinateurs résidentiels pour calculer les propriétés de millions de molécules organiques et explorer ainsi cet espace moléculaire.[86] Néanmoins, ce projet s'attaque seulement aux composés moléculaires, et se n'intéresse pas encore aux systèmes périodiques comme les chaines de polymères ou aux cristaux moléculaires.

Scharber et al. a proposé un modèle semi-empirique en 2006 pour expliquer le fonctionnement des dispositifs organiques et prévoir une efficacité maximale de 11% basée sur ce modèle.[189] Il existe une grande disparité entre cette limite de Scharber la limite de Shockley-Queisser de 33,7%[197] sur les jonctions p-n utilisée dans les dispositifs

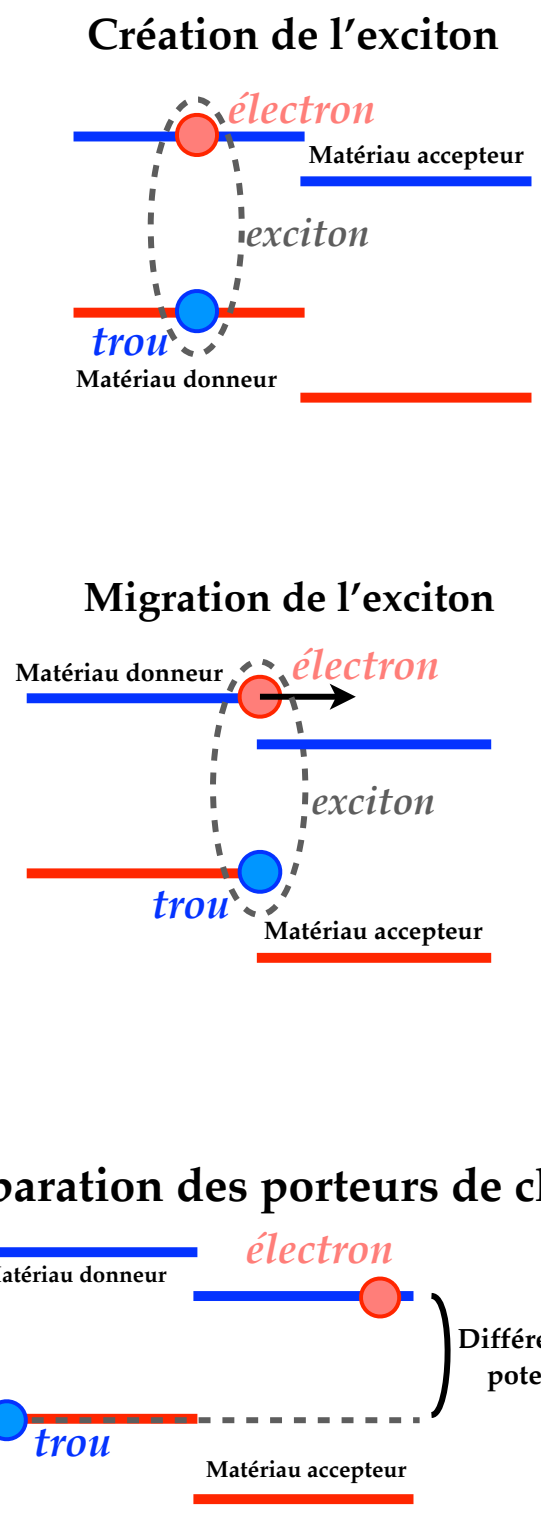

Figure 1.2 – Fonctionnement d'une cellule solaire organique à hétérojonction.

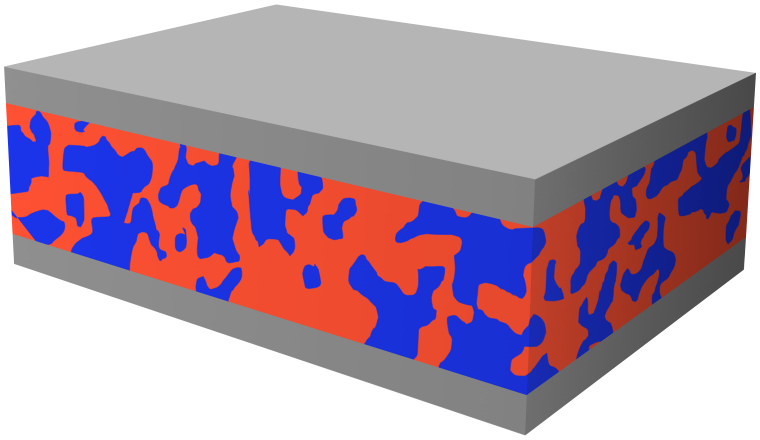

Figure 1.3 – Représentation d'une cellule solaire organique à hétérojonction volumique.

inorganiques. Le facteur limitant du modèle de Scharber est la présence de pertes empiriques totalisant 0,6 eV lors de la séparation des porteurs de charge. Cette perte empirique est mesurée dans beaucoup de dispositifs, mais est encore particulièrement mal comprise dans la communauté scientifique.

Les calculs théoriques peuvent apporter des précisions aux résultats expérimentaux pour sonder des propriétés difficiles à mesurer et procurer de nouveaux liens nécessaires à la compréhension des dispositifs organiques. La compréhension de la perte énergétique de 0,6 eV des dispositifs organiques pourrait mener à son élimination, et ainsi doubler leur efficacité. Plusieurs outils de calculs théoriques permettent de sonder les propriétés de matériaux. Pour avoir une bonne compréhension des propriétés électroniques, il est utile de partir de principes premiers et de résoudre l'équation de Schrödinger. Ces méthodes de calculs qui ne sont pas basées sur des données expérimentales sont appelées *ab initio*.

Une technique intéressante pour résoudre l'équation de Schrödinger est la théorie de la fonctionnelle de la densité (DFT).[41, 148] Cette dernière est basée sur le théorème de Hohenberg-Kohn, qui stipule que n'importe quel observable du système, y compris l'énergie totale, peut être exprimé en tant que fonctionnelle de la densité de l'état fondamental grâce à un principe de minimisation de l'énergie.[96] La difficulté à la base de la DFT consiste à trouver cette fonctionnelle. L'utilisation de cette fonctionnelle pour

obtenir les propriétés de notre système a été développée par Kohn et Sham.

La stratégie de Kohn-Sham consiste à supposer l'existence d'un système d'électrons non interagissant qui possède la même densité d'état fondamental que notre système réel. Puisque nos deux systèmes ont la même densité d'état fondamental, ils ont donc la même énergie totale, puisque cette dernière est une fonctionnelle de la densité. En supposant que ce système d'électrons non interagissant existe et possède des fonctions électroniques ψ^i_{KS}, nous pouvons dériver l'énergie totale de notre système par ψ^i_{KS} et obtenir une équation très semblable à l'équation de Schrödinger à un corps. Nous pouvons facilement résoudre cette équation pour obtenir de nouveaux ψ^i_{KS}, et ainsi une nouvelle densité d'état fondamental. À partir de cette densité, nous obtenons une nouvelle énergie totale, et le processus recommence jusqu'à obtenir une convergence de notre énergie. Le processus est illustré à la Figure 1.4.

La DFT se limite aux propriétés de l'état fondamental, et bien que les valeurs propres des états de Kohn-Sham peuvent être interprétées comme une approximation d'ordre zéro des énergies des états excités, il n'y a pas de justification rigoureuse derrière cette pratique. Une variante de la DFT, la DFT dépendante du temps (TDDFT), permet de sonder les propriétés des états excités en analysant les résonances de la réponse temporelle du système.[146] Bien que la TDDFT soit efficace pour les molécules, elle ne fonctionne pas très bien pour les systèmes étendus comme les polymères. D'autres méthodes plus poussées et plus exigeantes existent, comme la GW et les équations de Bethe-Saltpeter et sont réputées pour leur exactitude. Cependant, l'avantage de la DFT est sa rapidité. Il s'agit de l'outil de compromis idéal pour de multiples collaborations nécessitant l'analyse de multiples polymères.

La fonctionnelle utilisée dans la majorité de cette thèse est la B3LYP,[20] une fonctionnelle semi-empirique dont les paramètres sont tirés d'une fonctionnelle semblable, la B3PW91[81]. Ces paramètres ont été fixés sur les propriétés d'un ensemble de diverses molécules. Il est important de noter que malgré sa popularité actuelle dans le domaine, la B3LYP est désuette. Cependant, aucune fonctionnelle plus récente a remplacé objectivement la B3LYP dans la communauté. Puisque cette thèse porte sur les collaborations entre les théoriciens et les expérimentateurs et non sur le peaufinement des outils théo-

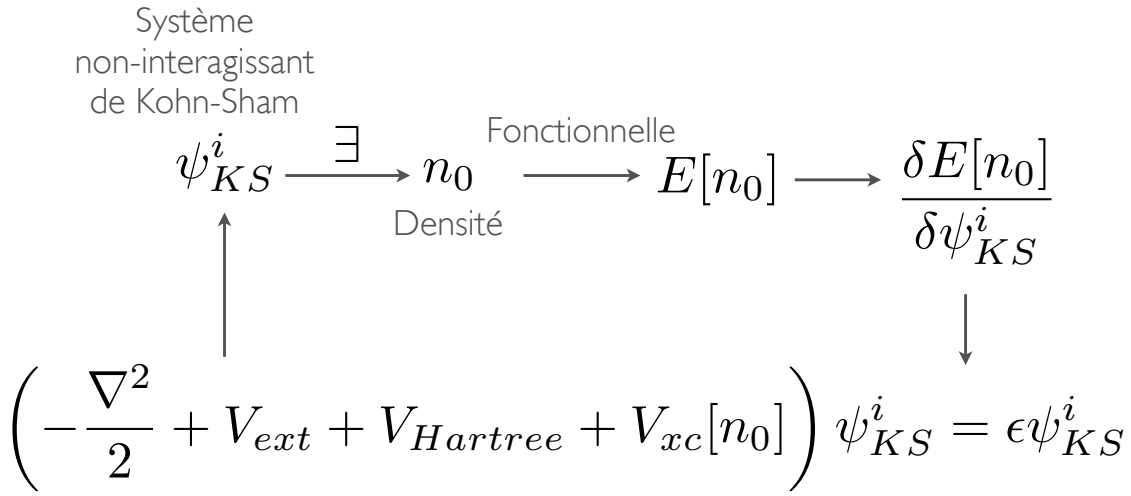

Figure 1.4 – Schéma résumant la de la théorie de la fonctionnelle de la densité:
1) On construit une fonctionnelle exprimant l'énergie totale en fonction de la densité.
2) On suppose l'existence d'un système de Kohn-Sham possédant des fonctions d'onde ψ^i_{KS}.
3) À partir d'une densité obtenue ou supposée, on obtient l'énergie totale à partir de notre fonctionnelle.
4) On dérive l'énergie totale par ψ^i_{KS} pour obtenir une équation de type Schrödinger.
5) On résout cette équation pour obtenir de nouveaux ψ^i_{KS}.
6) Ces ψ^i_{KS} nous donnent une nouvelle densité.
7) On répète les étapes 3 à 6 jusqu'à obtenir une convergence de nos quantités.

riques, il a été jugé préférable d'utiliser le standard de la communauté des chimistes organiques. Comme il est discuté au cours de cette thèse, la B3LYP détient un bon pouvoir prédictif lorsqu'elle analyse les orbitales frontières des molécules et des polymères. Ces orbitales frontières sont majoritairement situées sur la chaîne principale qui définissent les propriétés électroniques, à l'inverse des chaînes secondaires qui dictent les propriétés morphologiques.

Cette thèse s'attarde autour de quatre articles qui étudieront différentes contributions théoriques au champ de recherche de la photovoltaïque organique. Le premier article discute de la caractérisation de nouveaux composés du diketopyrrolopyrrole (DPP) et du thienopyrroledione (TPD). Un procédé de sulfuration appliqué sur ces composés permet de réduire leur band gap et ainsi augmenter l'absorption solaire pour permettre d'aug-

menter l'efficacité des dispositifs photovoltaïques. Puisque ces composés sont nouveaux, il est important d'avoir des résultats théoriques pour confirmer les résultats expérimentaux. Les calculs théoriques permettent également de sonder l'origine de la diminution du band gap et ainsi ouvrir la porte à un processus pour diminuer les band gaps de façon méthodique sur d'autres polymères. De plus, la technique de sulfuration affecte la stabilité des molécules, et la DFT peut étudier la structure moléculaire du polymère et l'effet de la répartition de la charge sur ce dernier.

Le second article parle d'une nouvelle technique expérimentale permettant de sonder la dynamique électronique à des échelles de temps de l'ordre de la femtoseconde. La dynamique électronique des cellules solaires organiques à hétérojonction volumique est particulièrement complexe et mal comprise. Le fait de pouvoir sonder ce processus permet de comprendre l'origine des pertes empiriques de 0,6 eV des dispositifs, la différence principale avec les dispositifs inorganiques. En plus de donner de la crédibilité au nouveau spectre expérimental parfois controversé et d'expliquer partiellement la disparition de certains pics due à la réorganisation de la charge, les calculs théoriques aident à la caractérisation particulièrement complexe des vibrations des polymères. Ces vibrations sont centrales à l'identification des états excités. En effet, en étudiant la progression du spectre de vibrations au fil du temps, on étudie ainsi la progression des états excités.

Le troisième article aborde le modèle de Scharber. Ce modèle semi-empirique a été développé en 2006 pour pouvoir prédire le potentiel de polymères nouvellement synthétisé à partir de leurs propriétés électroniques. L'avantage de ce modèle, en plus de fournir une limite réaliste d'efficacité qui n'était pas atteinte à l'époque, est d'éviter d'entreprendre la fabrication d'un dispositif photovoltaïque pour les polymères incompatibles. Cependant, la DFT permet de prédire les propriétés électroniques des polymères avant leurs synthèses, qui sont parfois des processus longs et complexes. L'article s'intéresse à l'efficacité de la DFT sur la prédiction des propriétés des polymères lorsqu'utilisés dans un dispositif, dans le cadre du modèle de Scharber, et proposera un certain nombre de candidats non synthétisés à l'époque pouvant potentiellement atteindre une haute efficacité.

Le dernier article de cette thèse montre le potentiel des calculs théoriques dans la

quête pour trouver des polymères avec des band gaps de plus en plus petits. L'étude utilise la DFT pour établir une relation entre les structures atomiques et le band gap des polymères pour une banque de plus de 200 polymères provenant de différentes familles. Un tel lien permet de développer une nouvelle technique pour synthétiser des copolymères à faible band gaps à partir de leurs structures atomiques qui s'avère plus efficace que la technique précédente utilisant les niveaux énergétiques.

CHAPITRE 2

SULFURATION DU DIKETOPYRROLOPYRROLE

2.1 Mise en contexte

Un des grands défis de l'électronique organique est de trouver des polymères aux band gaps de plus en plus petits. Par exemple, selon une étude récente, le band gap optimal pour les panneaux solaires organiques est situé entre 1,1 et 1,4 eV.[189] En effet, la majorité des polymères ont un band gap trop élevé pour des applications électroniques efficaces, et diminuer ce band gap favoriserait l'absorption de la lumière visible. La création de nouveaux polymères aux propriétés intéressantes demande du temps, entre autres pour établir des méthodes efficaces de synthèse et de traitement. Il est donc utile de trouver des techniques pouvant modifier le band gap de polymères de façon méthodique pour pouvoir bénéficier de l'expertise les entourant. Le diketopyrrolopyrrole (DPP) et le thienopyrroledione (TPD) sont deux molécules utilisées en chimie organique pour leurs faibles band gaps et leur grande planarité.[60, 114, 198] Il est vu dans ce chapitre que cette planarité est assurée partiellement par les groupements carbonyles qui les composent.

Le DPP est couramment synthétisé à partir de molécules de thiophène pour des applications photovoltaïques,[60, 114] et à partir de benzène pour des utilisations en tant que pigment.[91, 133] Cependant, plusieurs calculs théoriques utilisant la théorie de la fonctionnelle de la densité (DFT), accomplis par Simon Lévesque et moi-même, ont démontré que la substitution de la molécule de thiophène ou de benzène par d'autres molécules affecte grandement le band gap de la molécule de DPP.

Malheureusement, ces molécules interfèrent avec les groupes carbonyles du DPP, et les modifications de ces derniers ont alors été explorées. L'oxygène et le soufre étant dans la même colonne du tableau périodique et possédant ainsi le même nombre d'électrons de valence, il est possible de remplacer les groupes carbonyles par des groupes thiocarbonyles par un processus appelé sulfuration à l'aide du réactif de Lawesson. Il

faut cependant étudier les effets de cette substitution sur les propriétés photoélectriques ainsi que sur la stabilité de notre composant.

C'est ici que l'importance du théoricien surgit. La synthèse et la caractérisation de nouveaux composants pour de nouvelles applications sont des projets pluridisciplinaires qui nécessitent la collaboration entre chimistes et physiciens. Par exemple, puisque les effets de la sulfuration sur ces molécules organiques sont peu documentés, les calculs théoriques servent à rajouter de la crédibilité aux mesures expérimentales sur ces nouveaux composants. De plus, les calculs théoriques permettent de caractériser la molécule d'une manière complètement différente et guider ainsi les développements de la synthèse. Dans le cadre de cette étude, plusieurs calculs de DFT ont pu identifier que la sulfuration des composés contribuait à diminuer leurs band gaps.

Malheureusement, les composants recherchés souffraient d'une grande instabilité en laboratoire. Une analyse de charge électronique a été accomplie dans le but de trouver la source de cette instabilité. Des calculs subséquents sur la substitution du thiophène par du furane créaient une attraction électronique plus grande avec la molécule du DPP, contribuant ainsi à une plus grande stabilité dans le noir tout en conservant de faibles band gaps. Les composants contenant les groupes thiocarbonyles sont malheureusement tous instables à la lumière pour des raisons encore inconnues. Il est donc crucial de continuer cette étude si on souhaite obtenir des résultats utiles pour la photovoltaïque.

Les calculs DFT ont été principalement accomplis par Simon Lévesque, entre autres les calculs de stabilité de la Table 2.III et des Figures 2.4 et 2.5, ainsi que les calculs de charges des Figures 2.6 et 2.7. Suite à un empêchement de la part de Simon, j'ai dû prendre le relais du projet et procéder à l'analyse des résultats et la collaboration avec les chimistes du groupe de Mario Leclerc. Les parties théoriques et la structure générale de l'article ont été rédigées par moi-même, plus spécifiquement les parties théoriques des Sections 2.2.2, 2.2.3.1 et 2.2.3.2.

2.2 Thiocarbonyl Substitution in 1,4-Dithioketopyrrolopyrrole and Thienopyrroledithione Derivatives: An Experimental and Theoretical Study

Simon Lévesque,[1] David Gendron,[2] Nicolas Bérubé,[1] François Grenier,[2] Mario Leclerc[2] and Michel Côté[1]

[1] *Département de Physique, Université de Montréal, Montréal, Québec H3C 3J7, Canada* [2] *Département de Chimie, Université Laval, Québec City, Québec G1V 0A6, Canada*

A series of new 1,4-dithioketopyrrolopyrrole and thienopyrrolodithione derivatives have been synthesized and characterized by spectroscopy and electrochemistry measurements. The replacement of carbonyl by thiocarbonyl has a direct effect on the optical gap and on the ionization potential and electron affinity energies. For example, the optical gaps have been lowered by 0.5 eV, a fact that has been correctly predicted by density functional theory and time-dependent density functional theory calculations. A theoretical analysis on the stability of the new molecules is also presented.

2.2.1 Introduction

Since the first publication by Farnum in 1974,[69] the 1,4-diketopyrrolopyrrole (DPP) unit has been intensely studied and used as a pigment or dye in a variety of applications.[91, 133] Indeed, many articles[107, 224] report the use of different substituents on the aromatic cycles flanking the DPP core (Ar, see Figure 2.1), such as nitro, *tert*-butyl, or nitrile group, and on different positions, such as *meta* or *para* of a benzene ring or the 4- or 5-positions of a thiophene. This strategy is efficient to modulate the optical properties and the structural organization in the solid state. Nowadays, DPP materials are mostly used in organic field-effect transistors and organic solar cells because of their exceptional ambipolar mobilities (> 1 cm^2/Vs) and their high power conversion efficiencies (up to 6.05 % in single-layer cells, 8.62 % in tandem cells).[60, 114] In parallel, the thieno[3,4-c]pyrrole-4,6-dione (TPD) unit has been reported by Tour and Zhang in the late 1990s,[238, 239] and was recently rediscovered as a new building block for optoelectronic applications. Power conversion efficiencies as high as 8.1 % (certified 7.4 %) have recently been obtained.[198] Indeed, the TPD is now one of the most promising units in the organic photovoltaic field. However, the understanding of the TPD chemistry is still in progress.

Only a few studies have focused on the modification of the carbonyl groups on either the DPP or the TPD units.[176] More precisely, Mizuguchi has reported a series of papers on the 1,4-dithioketo-3,6-diphenylpyrrolo-[3,4-c]-pyrrole, a thiocarbonyl derivative.[154–156] While using a vapor treatment, a red-shift of the absorption maxima was observed on models compounds, caused by a better packing in the solid state. This molecular reorganization allows a stabilization of the system by an overlapping of the thiocarbonyl orbitals. In parallel, the study of the photophysics of thiocarbonyls has allowed a better understanding of the electronic states present in those compounds and a development of the synthesis of new chromophores with unique optical properties. In this regard, the photophysics of the thiocarbonyl compounds have already been reviewed in the literature.[144, 179, 202]

In this article, we have focused our attention on the synthesis and characterization

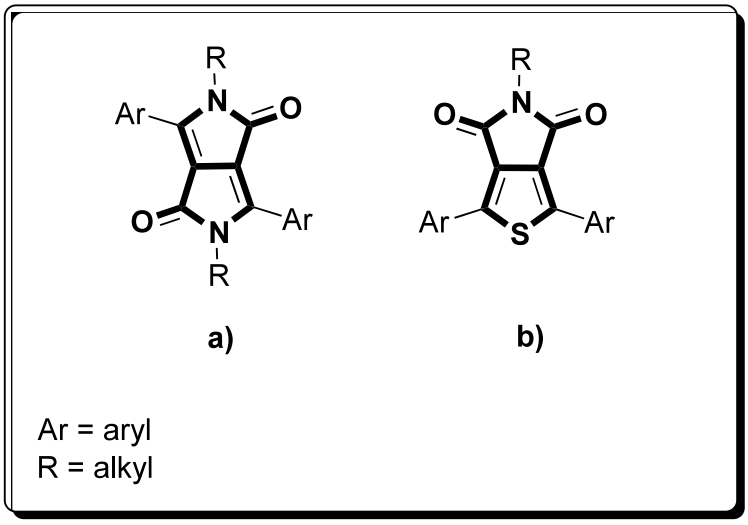

Figure 2.1: (a) Structure of the 1,4-diketopyrrolopyrrole (DPP) unit, and (b) structure of the thieno[3,4-c]pyrrole-4,6-dione (TPD) unit. In both structures, Ar stands for aryl while R stands for alkyl.

of new DPP and TPD derivatives. Their optical and electronic properties were experimentally investigated by UV-visible absorption spectra and cyclic voltammetry measurements (CV), respectively. To further understand the effects of the substitution of a carbonyl by a thiocarbonyl, such as the modification of the optical gap and the relative stability, density functional theory (DFT) and time-dependent density functional theory (TDDFT) calculations have been carried on. DFT and TDDFT are theoretical methods that have been and are still used extensively in an effort to design, understand, and predict the properties of actual and future organic solar cells.[9, 19, 23, 131, 158, 206]

2.2.2 Experimental and Theoretical Methods

All chemicals were purchased from commercial sources (Aldrich, TCI America, or Alfa Aesar) and used without further purification unless stated otherwise. The compounds shown in Figure 2.2 were synthesized according to already reported procedures in the literature[26, 134, 161, 243, 244] or as described in the Supporting Information section (Schemes S1 and S2).[138] More specifically, Lawesson's reagent was used

as the sulfuring reagent to supply the thiocarbonyl corresponding compounds. The reaction must be carried out at high temperature (100-120 °C), in *m*-xylene or 1,2-dichlorobenzene, and in the dark to avoid any early decomposition of the compounds. The UV-visible absorption spectra were recorded on a Varian Cary 50 UV-vis spectrophotometer in CH_2Cl_2. The ionization potential (IP) and electron affinity (EA) energies were determined from the onsets of the oxidation and reduction potentials respectively. To do so, cyclic voltammetry measurements (Solartron 1287 Potentiostat) were carried out using platinum electrodes at a scan rate of 50 mV/s with the desired compound in a solution of Bu_4NClO_4 (0.1 M in CH_2Cl_2) with a Ag wire as the pseudoreference. Potentials are referenced to the standard calomel electrode (SCE), assuming that SCE electrode is -4.71 eV from vacuum.[42, 211]

The theoretical electronic properties of the molecules have been obtained with the Gaussian 03 package.[71] All calculations were done with the B3LYP[20] functional and the 6-311g(d,p) basis set.[128][1] The B3LYP functional is well-known for an accurate description of organic materials because it contains a certain percentage of exact-exchange fitted on empirical data.[4, 111] The *n*-octyl alkyl chains have also been approximated by methyl groups to reduce computational time. The alkyl chains affect mostly the molecular packing, which is not considered here because all molecular calculations were done on single molecules in vacuum. The electronic properties should not be affected by this approximation because the wave function is mostly located on the molecular core, and not in the alkyls chains.

The theoretical molecular orbital energies shown in Tables 2.I and 2.II are the Kohn-Sham energy levels obtained from ground-state calculations. The optical gaps were calculated with TDDFT, which can accurately account for the optical excitations of molecules.[146, 164] In our theoretical stability study (Table 2.III, Figures 2.4 and 2.5), all of the total energies and natural bond orbital charges (NBO) were calculated within the DFT approach.[41]

[1] The molecular structures were relaxed with the tight convergence criteria, which means a maximum force threshold of 1.5×10^{-5} hartree with a residual mean square threshold of 1.0×10^{-5} hartree.

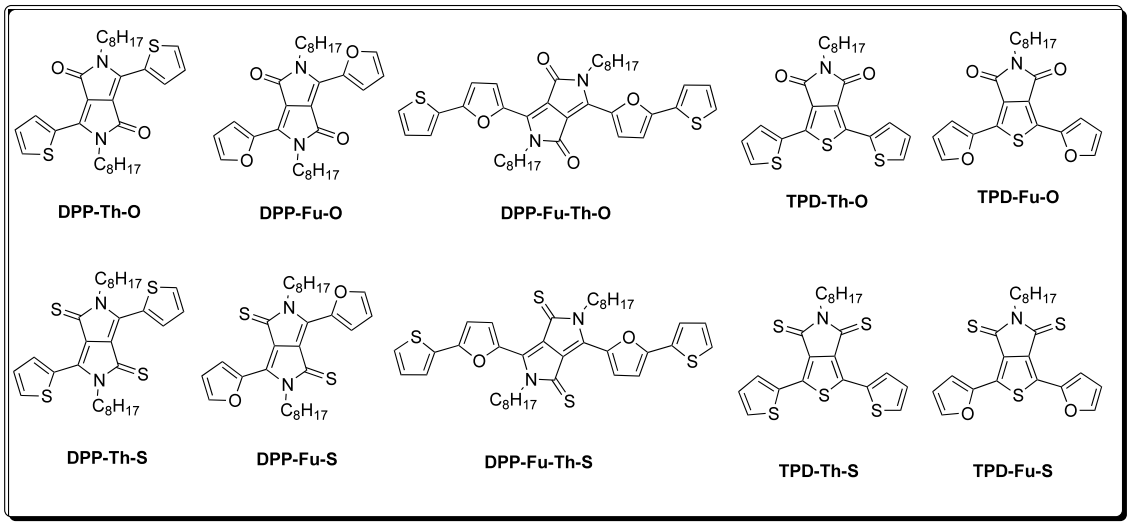

Figure 2.2: Chemical structures of DPP and TPD carbonyls and thiocarbonyls compounds.

2.2.3 Results and Discussion

2.2.3.1 DPP Compounds

The UV-vis absorption spectra of the DPP compounds are shown in Figure 2.3, and the optical gaps are reported in Table 2.I. First, we note that the carbonyl compounds show two principal absorption bands, one strong at 2.27 eV (546 nm) for DPP-Th-O, 2.31 eV (537 nm) for DPP-Fu-O, and 2.04 eV (608 nm) for DPP-Fu-Th-O, together with a weaker band at 3.65 eV (340 nm), 3.54 eV (350 nm) and 3.54 eV (350 nm), respectively. We have also identified small peaks at 511 nm, 496 nm, and 561 nm for each molecule, respectively, that we assign to vibration replica of the main absorption peak. Consequently, we can estimate the optical gaps (from the absorption onset) at 2.12 eV, 2.20 eV, and 1.81 eV for DPP-Th-O, DPP-Fu-O, and DPP-Fu-Th-O, respectively. It is quite normal that the DPP-Fu-Th-O compound possesses a lower optical gap because the conjugation length has been extended by the addition of a thiophene ring on both sides of the molecule.

The DPP-thiocarbonyl compounds show an interesting absorption spectrum. First,

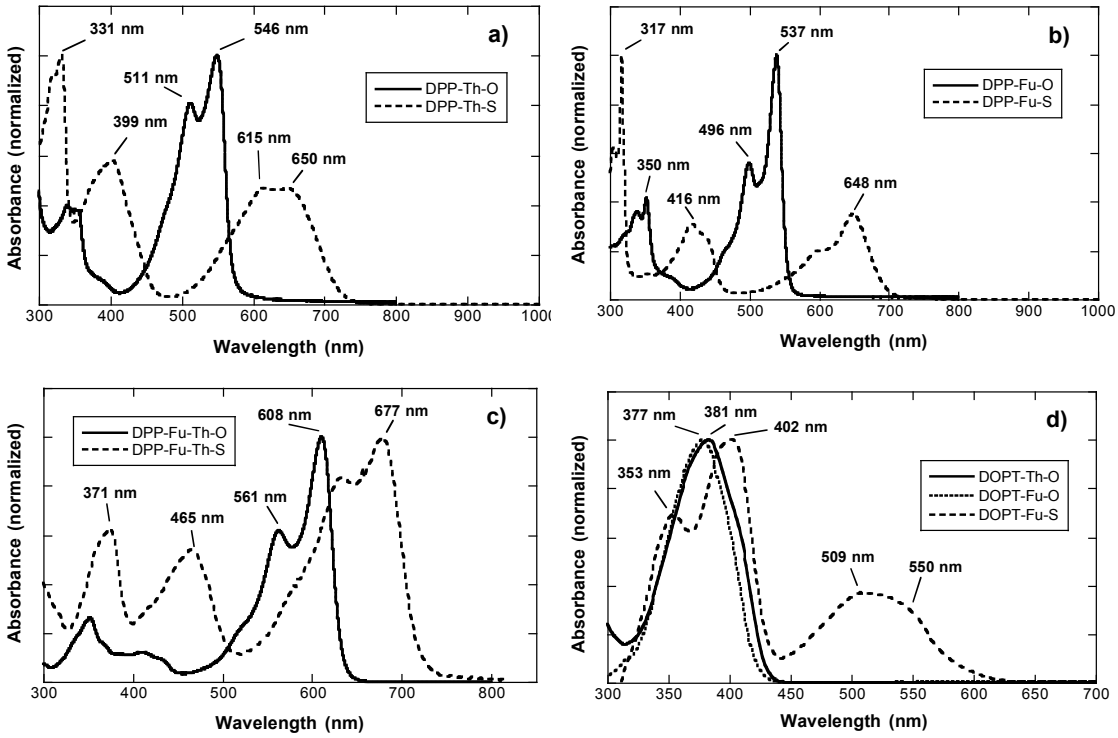

Figure 2.3: UV-vis absorption spectra of (a) DPP-Th-O and DPP-Th-S, (b) DPP-Fu-O and DPP-Fu-S, (c) DPP-Fu-Th-O and DPP-Fu-Th-S, and (d) TPD-Th-O, TPD-Fu-O and TPD-Fu-S in CH_2Cl_2.

upon close inspection, although the DPP-Th-S first peak has its maximum at 615 nm, the shape of the peak suggests that it is indeed the first vibration replica. The pure optical transition would be close to 650 nm or 1.91 eV as indicated in Figure 2.3. If we now compare the absorption spectra of the thiocarbonyl to the carbonyl compounds, we notice that the values of the absorption maxima are red-shifted by 0.36 at 1.91 eV (650 nm) for DPP-Th-S, by 0.40 eV at 1.91 eV (648 nm) for DPP-Fu-S, and by 0.21 at 1.83 eV (677 nm) for DPP-Fu-Th-S. Also, there is an increase of the intensity of the bands at 3.75 eV (331 nm), 3.91 eV (317 nm), and 3.34 eV (371 nm) along with the apparition of a third band at 3.11 eV (399 nm), 2.98 eV (416 nm), and 2.67 eV (465 nm) for compounds DPP-Th-S, DPP-Fu-S and DPP-Fu-Th-S respectively. The optical gap is also reduced to about 1.70 eV for all of the thiocarbonyl compounds (see Table 2.I).

Table 2.I: **Optical, Electronical and Theoretical Properties of the DPP Derivatives**[†]

compound	method	IP (eV)	EA (ev)	E_g^{elec} (eV)	E_g^{opt} (eV)
DPP-Th-O	exp.	5.70	3.92	1.78	2.12 / 2.27
	theor.	5.18	2.72	2.46	2.41
DPP-Th-S	exp.	5.45	4.06	1.39	1.68 / 1.91
	theor.	5.35	3.24	2.11	1.84
DPP-Fu-O	exp.	5.61	3.89	1.72	2.20 / 2.31
	theor.	5.11	2.61	2.50	2.48
DPP-Fu-S	exp.	5.46	4.14	1.32	1.70 / 1.91
	theor.	5.27	3.17	2.10	2.00
DPP-Fu-Th-O	exp.	5.39	4.01	1.38	1.81 / 2.04
	theor.	5.00	2.87	2.14	2.06
DPP-Fu-Th-S	exp.	5.34	4.08	1.26	1.70 / 1.83
	theor.	5.19	3.25	1.94	1.77

[†] The experimental electronic band gap is calculated from the difference between the IP and EA, two values obtained experimentally by cyclic voltammetry. The theoretical determinations of the EA and IP energies are simply taken to be the energy levels of the LUMO and HOMO electronic states, respectively, of the DFT calculations. For the experimental optical band gap, two numbers are reported, the first corresponding to the onset of the UV-vis absorption spectrum and the second taken for the maximum of the first absorption peak. The theoretical optical gaps are from TDDFT calculations.

The IP and EA energies of all of the compounds were determined by CV. As shown in Table 2.I, we observe that compounds DPP-Th-O, DPP-Fu-O, and DPP-Fu-Th-O possess a greater IP energy of about 0.2 eV than their corresponding thiocarbonyl compounds. More precisely, IP energies of 5.70, 5.61 and 5.39 eV are obtained, respectively, for DPP-Th-O, DPP-Fu-O and DPP-Fu-Th-O. For the thiocarbonyl compounds, IP energies of 5.45, 5.46, and 5.34 eV are obtained for DPP-Th-S, DPP-Fu-S and DPP-Fu-Th-S, respectively. Also, on the basis of their IP energies, all of these compounds should be stable to the air oxidation.[31, 58] Finally, if we compare the EA energies, we only observe a slight difference (around 0.1-0.2 eV) between the carbonyl and thiocarbonyl DPP compounds. Indeed, in this case, the carbonyl compounds DPP-Th-O, DPP-Fu-O and DPP-Fu-Th-O possess EA energies of 3.92, 3.89, and 4.01 eV, respectively, which is slightly lower and in the experimental error as compared to the following thiocarbonyls

compounds, DPP-Th-S (4.06 eV), DPP-Fu-S (4.14 eV), and DPP-Fu-Th-S (4.08 eV).

Also shown in Table 2.I are the results of our theoretical analysis. We notice that the reduction in the optical gap is well reproduced by the calculations. In fact, we see that the calculated TDDFT optical excitations are in very good agreement with the maximum energy of the first absorption peak, all theoretical values being within 0.2 eV of the experimental ones. This difference between experiment and theory can be attributed to many different factors such as solvent effects that have not been considered in the calculated values and the precision of the functional used. From the experimental CV energy levels, the reduction of the optical gap on the thiocarbonyl compounds as compared to the carbonyl ones can be attributed to both a larger EA energy and a lower IP energy. Theoretical data show a different behavior where both the IP and EA energies are increased, although the gain is more pronounced for the EA energy, which results in a net decrease of the energy gap. The discrepancy between the experimental results and theoretical calculations on how the IP energies are affected by the substitution of carbonyl groups by thiocarbonyl groups is unclear. Still, we should not pay too much attention to this difference because the Kohn-Sham eigenvalues, used to estimate the IP energies, are not truly simulations of the process that is going on in a CV measurement.

However, the theoretical calculations do offer an important and reliable trend for the optical gaps. The lowering of the optical gaps for each component is accurate to tenths of an electronvolt. For example, if we take DPP-Fu, which, as opposed to DPP-Th, remains stable with the thiocarbonyl compound, the experimental difference between the DPP-Fu-O and the DPP-Fu-S optical gaps is 0.40 eV (cyclic voltammetry) and 0.50 eV (optical). The theoretical counterparts of both of these values are, respectively, 0.40 eV (Kohn-Sham energy levels) and 0.48 eV (TDDFT). This means that the lowering of the optical gap with the presence of thiocarbonyl group is an effect that we can confirm with theoretical calculations.

2.2.3.2 TPD Compounds

Concerning the TPD derivatives (Figure 2.3d), we note the presence of an absorption band at 3.25 eV (381 nm) for TPD-Th-O and at 3.29 eV (377 nm) for TPD-Fu-O. Both

carbonyl compounds (TPD-Th-O and TPD-Fu-O) have similar gaps of 2.90 and 2.95 eV, respectively, obtained from the onset of absorption spectrum. The sulfuration reaction only worked for compound TPD-Fu-S as we were not able to successfully isolate the TPD-Th-S. In this regard, only the TPD-Fu-S is presented in Figure 2.3. We notice the apparition as a major absorption band with its maximum at 2.44 eV (509 nm) and other absorption bands at higher energies, 3.08 eV (402 nm) and 3.51 eV (353 nm). Again, considering the shape of the first absorption peak, its maximum is probably located at its first vibrational replica, and therefore we can estimate the absorption peak at 2.26 eV (550 nm). The estimated optical gap for the TPD-Fu-S is 2.16 eV, a stunning difference of 0.8 eV as compared to the carbonyl compounds.

As shown in Table 2.II, the energy levels of TPD-Th-O and TPD-Fu-O are quite similar. Changing the thiophene of TPD-Th-O for a furan has little impact on the IP energy (6.07 eV vs 6.09 eV) and increases the EA energy by 0.11 eV (3.11 eV vs 3.22 eV). Changing the carbonyls of TPD-Fu-O for thiocarbonyls produces a much more dramatic change to the electronic properties. The modulation of the IP energy is small, TPD-Fu-S (5.94 eV) having an IP energy only 0.15 eV lower than that of TPD-Fu-O (6.09 eV). The increase of the EA energy is a lot more significant as it is increased by a staggering 0.79 eV, going from 3.22 to 4.01 eV.

If we now look at the theoretical results for TPD from Table 2.II, we can draw the same conclusions as for the DPP compounds, and we find that the calculated TDDFT optical transition matches well the maximum of the first absorption peak for each molecule. Indeed, the experimental difference between the TPD-Fu-O and the TPD-Fu-S optical gaps is 0.94 eV (cyclic voltammetry) and 0.79 eV (optical), and the theory predicts, respectively, 0.75 eV (Kohn-Sham energy levels) and 1.06 eV (TDDFT). However, the lowering of the optical gap for the TPD compounds is mostly due to an important increase of the EA energy and a more-or-less constant IP energy, a fact that DFT calculations reproduce adequately.

Table 2.II: **Optical, Electronical and Theoretical Properties of the TPD Derivatives**[†]

Compound	Method	IP (eV)	EA (ev)	E_g^{elec} (eV)	E_g^{opt} (eV)
TPD-Th-O	exp.	6.07	3.12	2.95	2.95 / 3.25
	theor.	5.82	2.44	3.38	3.11
TPD-Th-S	exp.[††]	-	-	-	-
	theor.	5.91	3.15	2.76	2.03
TPD-Fu-O	exp.	6.09	3.22	2.87	2.90 / 3.29
	theor.	5.69	2.22	3.47	3.24
TPD-Fu-S	exp.	5.94	4.01	1.93	2.16 / 2.26
	theor.	5.81	3.09	2.72	2.18

[†] The experimental electronic band gap is calculated from the difference of the IP and EA, two values obtained experimentally by cyclic voltammetry. The theoretical determinations of the EA and IP energies are simply taken to be the energy levels of the LUMO and HOMO electronic states, respectively, of the DFT calculations. For the experimental optical band gap, two numbers are reported, the first corresponding to the onset of the UV-vis absorption spectrum and the second taken for the maximum of the first absorption peak. The theoretical optical gaps are from TDDFT calculations.

[††] Unable to successfully isolate compound TPD-Th-S.

2.2.3.3 Stability Analysis

It is important to note that thiocarbonyl compounds of DPP derivatives (DPP-Th-S, DPP-Fu-S, and DPP-Fu-Th-S) are not stable under ambient light condition. They decompose in a matter of hours if exposed to light. To avoid any fast decomposition of the products, all of the manipulations were carefully done in the dark. However, even if kept in the dark, compounds DPP-Fu-S and DPP-Fu-Th-S have proven to be relatively stable as we obtain the same UV-vis spectra after a few hours. DPP-Th-S, on the other hand, suffers from a rapid decomposition whether it was kept in the dark or not. As for the TPD compounds, TPD-Fu-O and TPD-Fu-S are unstable when exposed to air and light for extended periods of time. It is worth noting that extensive stability tests were not carried out on over an extended period of time.

We now assess the cause of the instability with the help of the DFT calculations. Table 2.III shows the depths of the energy wells according to modification of the dihedral

angles between the central DPP or TPD central unit and the thiophene or furane side unit next to it, as illustrated in Figures 2.4 and 2.5. Such a study has previously been done for molecules to characterize the interaction between the oxygen-sulfur atoms of different units.[108] For DPP derivatives (Figure 2.4) the substitution of the oxygen atom by sulfur in DPP-Th-O (dotted line) leads to nonplanar conformation as the lowest energy state (dashed line). The substitution of thiophene by a furan ring recovers the planar conformation as the ground state for DPP-Fu-O and DPP-Fu-S (plain and dotted-dashed lines, respectively). For TPD derivatives, the substitution of the oxygen atom by sulfur in TPD-Th-O (dotted line) leads to a molecule that has not been successfully isolated, and, in this case again, the torsional energy curve indicates a nonplanar conformation for this molecule (dashed line). The substitution of thiophene by a furan ring leads to two planar molecules, TPD-Fu-O and TPD-Fu-S (plain and dotted-dashed lines, respectively).

NBO charges shown in Figures 2.6 and 2.7 can help us understand the shapes of these torsional energy curves, which seems to be governed by interactions between the side units (thiophene, furan) and the central DPP unit. For the DPP-Th-O and DPP-Th-S compounds (Figure 2.6), the sulfur atoms of the thiophenes, which are positively charged, are repelled by the positively charged hydrogens of the side chains. In DPP-Th-O, a strong attraction between the positively charged hydrogens of the thiophene (0.3 e) and the negatively charged oxygens of the central unit (-0.6 e) compensates to give a planar molecule. In DPP-Th-S, which is neither planar nor stable, the charge on the sulfur is only -0.2 e, which leads to a much smaller attraction with the thiophenes. The molecular conformation can also be hampered by a steric effect between the sulfur atom and the thiophene unit next to it. If we substitute the sulfur atoms of the thiophenes by oxygen atoms to get DPP-Fu-O and DPP-Fu-S (Figure 2.7), the repulsion with the side chains is transformed into a strong attraction leading to planar and stable molecules, at least in the dark.

We would like to point out that similar nonplanar molecular conformations due to sulfur-sulfur interaction have been reported before in bithiophenedicarboxylates,[172] but light sensitivity was not addressed in that study. On the other hand, another *ab initio* study[87] has demonstrated that the C=O bonds are stronger than the C=S bonds,

Table 2.III: **Values of the Dihedral Angle for the Minimum Energy Configurations (θ_{stable}) and Height of the Potential Well (ΔE)**[†]

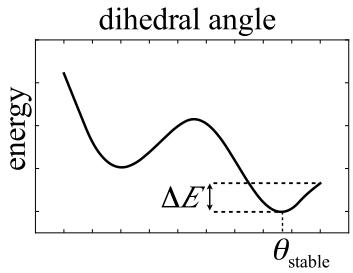

compound	θ_{stable} (deg)	ΔE (eV)	state
DPP-Th-O	180	0.57	stable
DPP-Th-S	150	0.07	unstable
DPP-Fu-O	180	0.89	stable
DPP-Fu-S	180	0.67	stable
DPP-Fu-Th-O	180	0.98	stable
DPP-Fu-Th-S	180	0.78	stable
TPD-Th-O	180	0.43	stable
TPD-Th-S	150	0.05	unable to isolate
TPD-FU-O	180	0.73	stable
TPD-Fu-S	180	0.57	stable

[†] The last column presents the experimental stability of the molecules under dark.

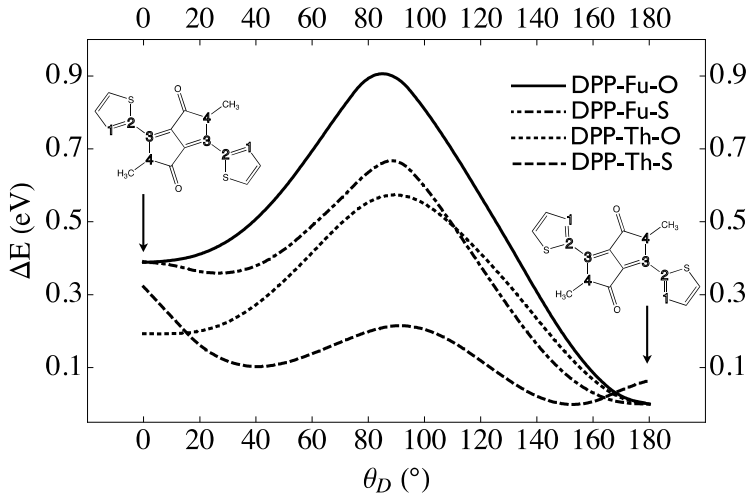

Figure 2.4: Energy as a function of the dihedral angle for the DPP derivatives. The geometries of DPP-Th-O for dihedral angles (between atoms 1 through 4) of 0° and 180° are shown on the left and right part of the graph, respectively.

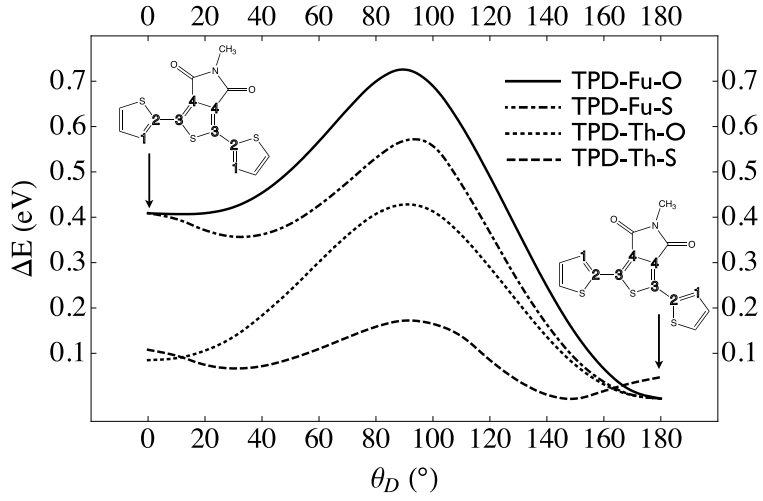

Figure 2.5: Energy as a function of the dihedral angle for the TPD derivatives. The geometries of TPD-Th-O for dihedral angles (between atoms 1 through 4) of 0° and 180° are shown on the left and right part of the graph, respectively.

which can help to explain why some of the thiocarbonyl substitutions are unstable, but it would not explain why others are stable. It would seem that in the present cases, the unstable molecules are also those that have a nonplanar conformation. However, this structural property by itself cannot explain the molecule instability to light exposure. More elaborate quantum simulations such as the calculations of the excited-state potential energy surface would be required to fully address the question of light sensibility of these molecules.

DPP-Th-O

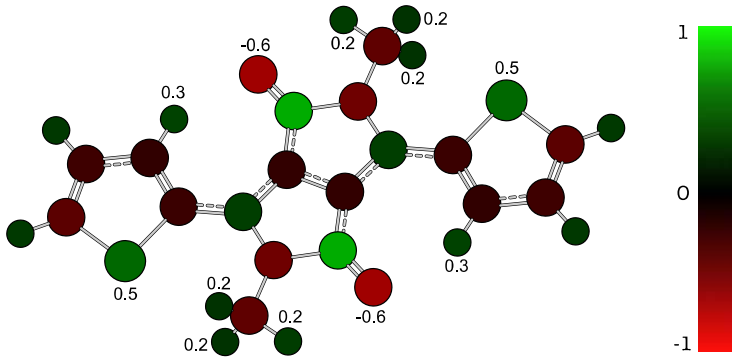

DPP-Th-S

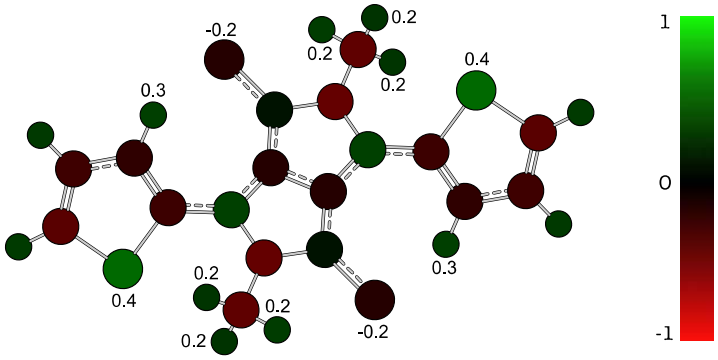

Figure 2.6: NBO charges of DPP-Th molecules before and after the substitution of a carbonyl by a thiocarbonyl, in units of the elementary positive charge.

DPP-Fu-O

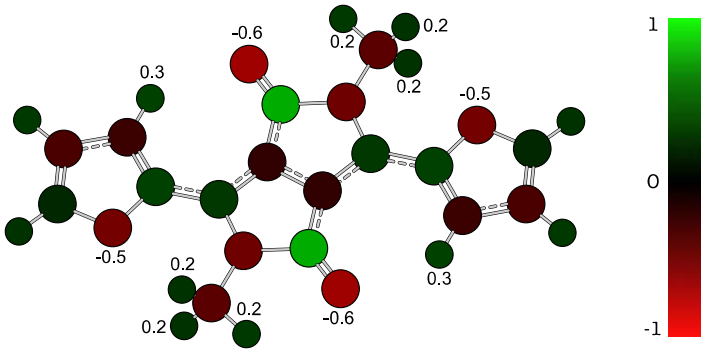

DPP-Fu-S

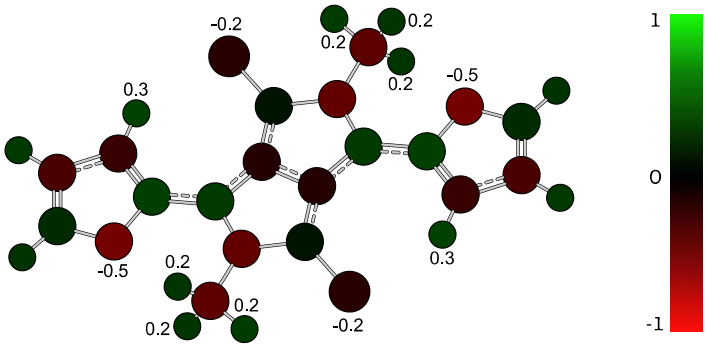

Figure 2.7: NBO charges of DPP-Fu molecules before and after the substitution of a ketone by a thioketone, in units of the elementary positive charge.

2.2.4 Conclusion

In this article, we have reported the preparation and characterization of nine 1,4-diketopyrrolopyrrole and thienopyrroledione derivatives. Their optical and electronical properties have been investigated by UV-vis absorption spectroscopy, cyclic voltammetry, and DFT and TDDFT calculations. To sum, we have found that the thiocarbonyl derivatives (DPP-Th-S, DPP-Fu-S, DPP-Fu-Th-S, TPD-Fu-S) show an extended absorption at lower energy (< 2 eV) due to the red-shift of the absorption band. For the DPP compounds, an increase of the HOMO by 0.2 eV is observed while the LUMO is relatively unchanged. Theoretical calculations show that the Kohn-Sham energy levels are not always a reliable guide for the HOMO and LUMO levels as determinated by CV measurements as they predicted a lowering of the HOMO levels for all compounds with the thiocarbonyl substitution. A completely different observation can be made for the TPD thiocarbonyl compound. The HOMO presented only a small increase of 0.15 eV, while the LUMO level decreased by 0.79 eV. Theoretical Kohn-Sham energy levels corroborate this fact, as they predicted a lowering of the LUMO by 0.87 eV. On the other hand, DFT and TDDFT calculations accurately predict the effects of the substitution on the optical gaps. The decrease of the optical gaps has been predicted for DPP-Fu, the stable DPP compound, with a precision to the tenth of an electronvolt. The value of this decrease was 0.4 eV for the cyclic voltammetry gap, and 0.5 eV for the optical gap. The optical gap lowering for the TPD compounds, situated around 0.8-1.0 eV, was also predicted by theoretical calculations.

Unfortunately, all of the thiocarbonyl compounds reported here show different degrees of light sensitivity. The thiocarbonyl derivatives containing furan aromatic substituents surprisingly appeared to be the most stable. Theoretical calculations show that stable molecules adopt a planar conformation, whereas the unstable molecules would be nonplanar. Further calculations will be require to fully address the instability of these molecules.

Acknowledgements. We thank the funding support of NSERC and the PV Innovation Network for funding support. N.B. acknowledges the Vanier Scholarship pro-

gram. The calculations were done on the computational infrastructure provided by Calcul Québec and Compute Canada. We would also like to acknowledge the support of the Regroupement québécois sur les matériaux de pointe (RQMP) and the Centre québécois sur les matériaux fonctionnels (CQMF).

Supporting information. Synthesis of the different compounds studied in this research as well as the cyclovoltammetry curves used to determine the energies of the different levels are. This material is available free of charge via the Internet at http://pubs.acs.org.[138] The authors declare no competing financial interest.

CHAPITRE 3

DYNAMIQUE ÉLECTRONIQUE DU POLYCARBAZOLE

3.1 Mise en contexte

En plus des propriétés électroniques des composantes comme les niveaux électroniques et le band gap, il est important de considérer le fonctionnement global d'un panneau solaire. Bien que la quête vers des band gaps de plus en plus petits est nécessaire pour absorber la lumière autant que les technologies inorganiques existantes, il est utile de se demander comment les dispositifs organiques doivent évoluer une fois que les molécules aux propriétés électroniques appropriées seront découvertes.

La différence majeure entre l'efficacité des dispositifs organiques et inorganiques provient principalement de la présence de pertes empiriquement mesurées lors de la séparation des porteurs de charge chez les organiques. Ces pertes empiriques sont souvent assumées comme obligatoires à cause du modèle du Scharber, que nous explorerons plus en détail au Chapitre 4, mais la valeur et l'origine de ces pertes sont très loin de faire l'unanimité dans la communauté scientifique.[18, 37, 90]

Il est clair que ces pertes ont lieu entre l'absorption de la lumière contribuant à la création de l'exciton, un processus typiquement situé entre 1,3 et 2,0 eV, et la présence des polarons à l'interface dont l'énergie est autour de 0,6-1,0 eV.[221] Les processus de dynamique électronique entre l'état excitonique et l'état polaronique sont particulièrement mal compris dans les composants organiques, spécialement dans les polymères.

La technique de *femtosecond stimulated Raman spectroscopy* (FSRS) est utilisée pour obtenir des données sur les vibrations d'un composé sur une échelle de temps de la femtoseconde. Puisque chaque état possède un spectre de vibration très particulier, l'évolution de ce spectre donne des informations sur l'évolution de l'état de nos porteurs de charges. Cette technique n'avait encore jamais été utilisée sur un polymère avant cette étude et est donc cruciale pour démystifier la dynamique électronique.

Les résultats de l'étude expérimentale montrent que la séparation des porteurs a lieu

sur une échelle de temps plus courte que 300 fs, un processus beaucoup trop rapide qui contredit plusieurs autres théories de séparation de charge. La compréhension des mécanismes derrière ce processus est cruciale pour comprendre et éventuellement éliminer les pertes énergétiques qui en émanent. Puisque cette étude est sans précédent et touche un domaine très controversé, la présence de calculs théoriques pour corroborer les données expérimentales est très utile. De plus, les calculs théoriques permettent de relier les pics expérimentaux de vibration à leurs mouvements atomiques et ainsi aider à identifier l'état électronique du spectre. Des calculs sur les états excités permettent également d'expliquer en partie la variation d'intensité de certains pics en considérant l'effet de réorganisation de la charge dans le polymère.

L'article a été écrit par Françoise Provencher, à l'exception de la Section 3.2.5.3 qui a été écrite par moi-même. J'ai également obtenu les résultats théoriques de l'article incluant les calculs de DFT et de TDDFT ainsi que créé les Figures 3.3e et 3.3f ainsi que I.2, I.10, I.11, I.12, I.13, I.14 et I.15 de l'Annexe I.

3.2 Direct Observation of Ultrafast Long-range Charge Separation at Polymer:fullerene Heterojunctions

Françoise Provencher,[1] Nicolas Bérubé,[1] Anthony W. Parker,[2] Gregory M. Greetham,[2] Michael Towrie,[2] Christoph Hellmann,[3] Michel Côté,[1] Natalie Stingelin,[3] Carlos Silva,[1,4]and Sophia C. Hayes[5]

[1] *Département de physique et Regroupement québécois sur les matériaux de pointe (RQMP), Université de Montréal, C. P. 6128 Succursale Centre-ville, Montréal (Québec) H3C 3J7, Canada*

[2] *Central Laser Facility, Research Complex at Harwell, Science and Technology Facilities Council, Rutherford Appleton Laboratory, Harwell Oxford, Didcot, Oxfordshire OX11 0QX, United Kingdom*

[3] *Department of Materials and Centre for Plastic Electronics, Imperial College London, South Kensington Campus, London SW7 2AZ, United Kingdom*

[4] *Visiting Professor (Experimental Solid State Physics), Department of Physics, Imperial College London, South Kensington Campus, London SW7 2AZ, United Kingdom*

[5] *Department of Chemistry, University of Cyprus, P.O. Box 20537, 1678 Nicosia, Cyprus*

In polymeric semiconductors, charge carriers are polarons, which means that the excess charge deforms the molecular structure of the polymer chain that hosts it. This effect results in distinctive signatures in the vibrational modes of the polymer. We probe polaron photogeneration dynamics at polymer:fullerene heterojunctions by monitoring its time-resolved resonance-Raman spectrum following ultrafast photoexcitation. We conclude that polarons emerge within 300 fs. Surprisingly, further structural evolution on $\lesssim$ 50-ps timescales is modest, indicating that the polymer conformation hosting nascent polarons is not significantly different from that in equilibrium. This suggests that charges are free from their mutual Coulomb potential, under which vibrational dynamics would report charge-pair relaxation. Our work addresses current debates on the photocarrier generation mechanism at organic semiconductor heterojunctions, and is, to our knowledge, the first direct probe of molecular conformation dynamics during this fundamentally important process in these materials.

3.2.1 Introduction

In photovoltaic diodes based on blends of polymeric semiconductors and fullerene derivatives, photocurrent generation requires charge separation, with photoinduced electron transfer as an early step. From a semiconductor perspective, the electronic structure of the two materials define a type-II heterojunction, providing sufficient driving force to dissociate highly-bound excitons on the polymer.[53] In spite of important progress to optimise the solar power conversion efficiency in polymer solar cells, the mechanism for the evolution from the non-equilibrium primary photoexcitation (the unrelaxed exciton on a polymer chain immediately after light absorption) to photocarriers (unbound charges) is not resolved and is currently the subject of vivid debate.[174] Earlier studies of all-polymer donor:acceptor blends by Morteani *et al*. concluded that an intermediate step between intrachain excitons and free charges is charge separation into Coulomb-bound electron-hole pairs,[157] which we will refer to as charge-tranfer states (CT), emphasising that the electron and hole are mutually bound across the interface. After this initial step, the CT state can either branch directly to free charges or relax to an excitonic state bound at the interface between the donor and acceptor materials, a state termed charge-transfer excitons (CTX). Others also reported this branching behaviour in polymer:fullerene blends.[13, 88] Later reports indicated that initial charge separation to CT states occurs on $\leq$ 100-fs timescales.[82, 212] Furthermore, Jailaubekov *et al*. concluded that at molecular-semiconductor heterojunctions, CT states must produce photocarriers on timescales faster than $\sim 1\,\mathrm{ps}$ if this process is to be competitive against relaxation to the CTX state,[109] as the binding energy of CTX is typically $\sim 10 k_B T$ at room temperature,[77, 89] rendering photocarrier generation from those states energetically unlikely in principle. Nevertheless, these relaxed CTX can be 'pushed' with an infrared optical pulse resonant with an intraband polaronic optical transition to promote them to a delocalised, near-conduction-edge state that can then dissociate into charge carriers, thus enhancing photocurrent.[12] However, Lee *et al*.[135] and more recently Vandewal *et al*.[219] have argued that relaxed CTX states, when excited directly, are in fact the photocurrent precursors in many if not most polymer:fullerene systems. The

contemporary literature therefore reflects disagreement on whether rapid dissociation of non-equilibrium intrachain excitons or charge-transfer excitons is a significant pathway towards photocurrent generation in polymer diodes.

The seemingly conflicting scenarios are all based on probing population dynamics by time-resolved spectroscopies, or directly probing photocurrent internal quantum efficiency spectra in conjunction with steady-state absorption and luminescence measurements, both of which provide limited direct mechanistic insight into photocarrier generation dynamics. In this work, we exploit an ultrafast optical probe that is simultaneously sensitive to molecular-structure and electronic-population (excitons, polarons) dynamics. It is therefore an intricate probe of charge photogeneration dynamics since charges in polymeric semiconductors are polaronic, in which the charge distorts the polymer backbone surrounding it, producing unambiguous molecular vibrational signatures. Although ultrafast solvatochromism-assisted vibrational spectroscopy has been used to study charge dynamics in fullerene aggregates,[170] our work is to our knowledge the first direct time-resolved vibrational probe of polaron formation dynamics on polymers at polymer:fullerene heterojunctions.

We find that by optical excitation of the lowest (π, π^*) optical transition in the polymer, clear polaronic signatures are present within the early-time evolution of the photoexcitation, on $\lesssim$ 300-fs timescales, in a benchmark polymer:fullerene blend. Surprisingly, we observe limited vibrational relaxation following this ultrafast process, indicating little structural changes occuring on time windows spanning up to 50 ps, which we interpret as indicative of holes on the polymer that are sufficiently far from their electron counterparts such that they are free of their Coulomb potential. Our results suggest that in this system, which produces amongst the highest efficiency solar cells, intermediate charge-transfer states (Coulomb-bound electron-hole) pairs are not prerequisite species for photocarriers. Moreover, because vibrational signatures of polarons emerge at a faster rate than exciton relaxation by at least one order of magnitude, we conclude that ultrafast dissociation of non-equilibrium photoexcitations is a significant process in this system.

3.2.2 Results

We implement femtosecond stimulated Raman spectroscopy (FSRS) to characterise the molecular structural dynamics in a model semiconductor copolymer used in efficient solar cells during charge transfer to a fullerene acceptor in the solid state.[150] FSRS measures the transient resonance stimulated Raman spectrum of the photoexcited species by preparing the polymer in its excited state with a short actinic pulse ($\sim$ 50 fs, 560 nm), and then probing the evolution of the stimulated Raman spectrum with a pair of pulses: a Raman pump pulse resonant with a photoinduced absorption of interest (1.5 ps, 900 nm) and a short ($\sim$ 50 fs) broadband probe pulse to generate the excited-state stimulated Raman spectrum of the transient species at various delay times between the actinic and Raman-pump/probe pulses. FSRS thus permits measurement of the time-resolved, excited-state resonance-Raman spectrum with ultrafast time resolution. We collect concomitantly transient absorption spectra by monitoring the differential transmission of the broadband probe pulse induced by the actinic pulse (i.e. by measuring the signal without the Raman pump pulse). In our studies, we apply this technique on poly(N-9′-heptadecanyl-2,7-carbazole-alt-5,5-(4′,7′-di-2-thienyl-2′,1′,3′-benzothiadiazole) (PCDTBT, see Figure 3.1a), which is a carefully engineered 'push-pull' material system for solar cells, with reported solar power conversion efficiency of 6[167] – 7.2%,[207] unusually high internal quantum efficiency approaching 100%,[167] and reported ultrafast charge separation in fullerene blends,[64, 212] such as fullerene derivative [6,6]-phenyl-C_{61} butyric acid methyl ester (PCBM, see Figure 3.1a).

Unequivocal identification of polarons in PCDTBT (see Figure 3.1a) requires knowledge of the spectral signatures of its cations. To measure them, we oxidised a neat polymer film, that is a film composed only of the polymer donor material, with $FeCl_3$, which is known to dope polycarbazoles.[11] The ground-state absorption spectrum of the doped film (Figure 3.1b) features a low-energy absorption band centred around 1.7 eV, which has been assigned to cations in previous doping studies.[11] This absorption band in the doped film corresponds to the 'interband' polaronic transition.[230] It matches closely the transient absorption band of the PCDTBT:PCBM blend in the 1.2–2.0-eV

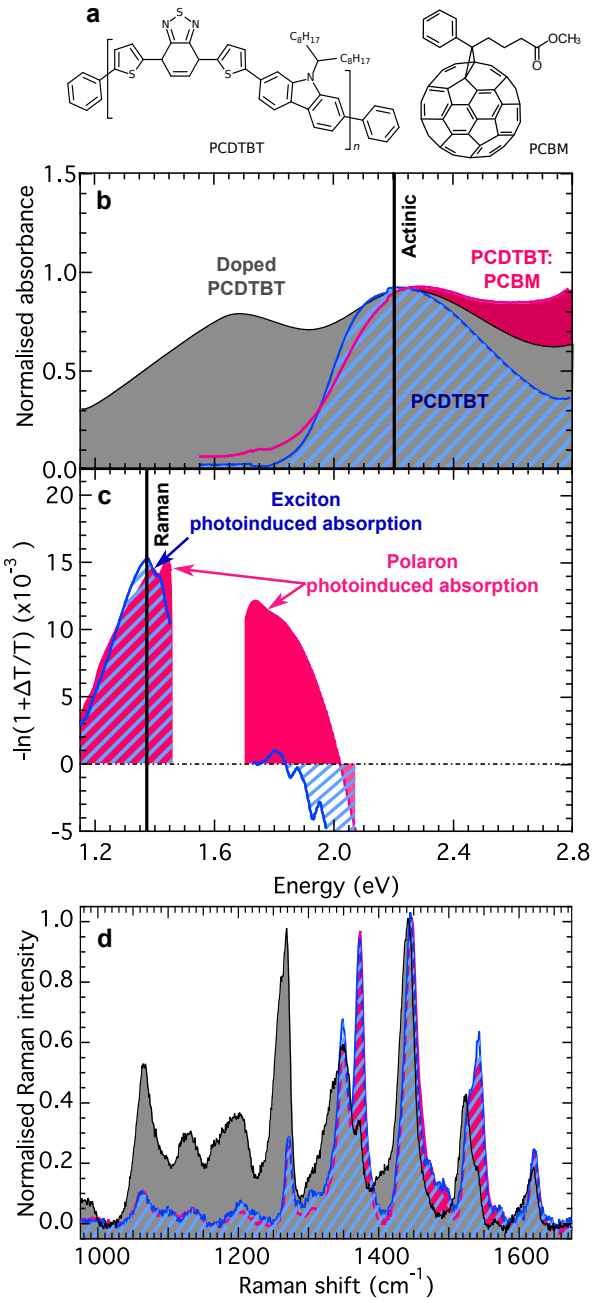

Figure 3.1: **Steady-state absorption, transient absorption, and Raman spectra of films of neat PCDTBT and PCDTBT:PCBM.** (**a**) Structure of PCDTBT (left) and PCBM (right). (**b**) Absorption spectra of neat PCDTBT (blue), PCDTBT:PCBM (pink) and doped PCDTBT (grey) films. (**c**) Transient absorption spectra of the same samples as in part (a). (**d**) Resonance Raman spectra of the same samples as in part (a). The wavelength of the actinic (the femtosecond pump) and Raman (picosecond pump) pulses are indicated by vertical lines in part (b).

region (Figure 3.1c), which reinforces previous assignment of this photoinduced absorption band to polarons.[64, 212] Excitation of the doped PCDTBT film within the low-energy band at 830 nm (1.49 eV) provides thus the resonance-Raman spectrum of the polaron (Figure 3.1d, grey), which is the vibrational fingerprint of that photoexcitation on PCDTBT. Figure 3.1d also shows the resonance-Raman spectra of neat PCDTBT and PCDTBT:PCBM, excited at 514 nm (2.30 eV). To aid with assignment of these peaks, we have calculated Raman frequencies of the ground, excited and cationic states of the PCDTBT dimer in vacuum using density-functional theory (DFT) and time-dependent density-functional theory (TDDFT) utilizing the B3LYP functional. We then identified the modes of the measured Raman peaks by comparing them to the frequency and intensity of the bands in the theoretical Raman spectrum (see Figure I.2 of Section I) and to a published resonance-Raman study of PCDTBT.[180] These assignments are summarized in Tables 3.2.2 and 3.2.2.

The difference in intensities of the cation resonance-Raman spectrum with respect to that of the pristine (as-cast) film, consisting of neutral polymer chains, reveal differences in the geometric distortion between the ground and the resonant-electronic states along the normal coordinate for each mode. In particular, the Raman spectrum on resonance with the polaronic transition shows a marked enhancement of bands corresponding to carbazole and thiophene local modes between 1000 and 1200 cm^{-1}, as well as in benzothiadiazole and carbazole bands at 1268 and 1349 cm^{-1}, which are more delocalised (see Figure I.3 of Section I). This is consistent with the electronic density shift between the highest occupied molecular orbital (HOMO) and the lowest unoccupied molecular orbital (LUMO) of the charged polymer, which affects mainly the carbazole and the thiophene units (see Figure I.10 in Section I). On the other hand, the resonance-Raman spectra of PCDTBT and PCDTBT:PCBM exhibit strong enhancement of modes predominantly involving motion of the benzothiadiazole unit at 1370 cm^{-1} and 1540 cm^{-1}. This is consistent with the electronic density shift between the HOMO and the LUMO of the neutral polymer, which involves the localisation of the wavefunction on the thiophene–benzothiadiazole–thiophene unit (see Figure I.15 in Section I).

The temporal evolution of the FSRS spectrum of a PCDTBT:PCBM film is illus-

Spontaneous pristine (cm^{-1})	0.5 ps pristine (cm^{-1})	100 ps pristine (cm^{-1})	DFT ground state (cm^{-1})	TDDFT excited state (cm^{-1})	Qualitative assignment
1062	1057	1067	1096	1082	L : Th CH ip δ + $\nu_{C=C}$
1135	1124	1122	1153	1152	L: Cz CH ip δ + ring def.
1205	—	—	1231	1238	L : BT +Th CH ip δ, BT ring def.
1270	1260	1256*	1325+1327	1319+1308	D: BT ν_{C-N} + $\nu_{C=C}$+ CH ip δ, Cz +Th CH ip δ + $\nu_{C=C}$
1348	—	—	1384	1377	D: BT+ Th CH δ, Cz+ BT ν_{C-C}
1370	—	—	1405	1416	D : BT + Th + Cz $\nu_{C=C}$ + CH ip δ, Cz ν_{C-N}
1444	1423	1429	1471+1485	1470	L: Cz, Th $\nu_{C=C}$ + CH ip δ, Cz ν_{C-N}
1490	1473	1457	1522+1527	1521	L: Cz sym. $\nu_{C=C}$, CH ip δ
—	1508	—	1543	1540	L : Cz asym. $\nu_{C=C}$, CH ip δ
1525	—	—	1569	1563	L: Cz asym. $\nu_{C=C}$+ CH ip δ + ν_{C-N}
1540	—	—	1570+1572	1560+1556	L: BT + Th sym. $\nu_{C=C}$, CH ip δ
1570	1571	1555	1605	1590	L: Cz $\nu_{C=C}$ + CH ip δ
1622	1608	1612	1664	1638	L: Cz $\nu_{C=C}$ + CH ip δ

Table 3.I: Neat and pristine (undoped, as cast) PCDTBT film spontaneous Raman and FSRS shifts. Mode abbreviations: ip = in plane, ν_{a-b} = stretch of *a*—*b* bond, δ = bend, sym. = symmetric, asym. = asymmetric, def. = deformation, BT: benzothiadiazole, Cz: carbazole, Th: thiophene, L: localised, D: delocalised. *The peak at 1256 cm^{-1} is asymmetric (See Figure I.13 in Section I for vector graphics of the vibrational modes.)

Spontaneous doped (cm^{-1})	0.5 ps blend (cm^{-1})	100 ps blend (cm^{-1})	DFT cation (cm^{-1})	Qualitative assignment
1064	1083	1083	1104	L: Th CH ip δ + $\nu_{C=C}$
1130	1129	1146	1153	L: Cz CH ip δ + $\nu_{C=C}$
1200	1192	1190*	1182	L: Cz CH ip δ
1268	1262	1260	1303	D: BT ν_{C-N} + CH ip δ + $\nu_{C=C}$, Cz +Th CH ip δ
1334	—	—	1344	L: Cz ring deformation, Cz + Th CH ip δ
1349	1357	1354	1371	D: Cz + BT $\nu_{C=C}$ + CH ip δ
1371	—	—	1397	D: BT + Cz + Th $\nu_{C=C}$
1442	1429	1434	1464	L: Th $\nu_{C=C}$, Cz ν_{C-N} + $\nu_{C=C}$ + CH ip δ
1522	1513	1513**	1540+1547	L: Cz+Th asym. ring deformation, + CH ip δ
1538	—	—	1560	L: BT sym. ν_{C-C} + CH ip δ , Th. asym. $\nu_{C=C}$, CH ip δ
1620	—	—	1648	L: Cz sym. ring deformation + ip CH δ

Table 3.II: Doped PCDTBT film spontaneous resonance Raman at 830 nm (resonant with a positive polaron optical transition) and PCDTBT:PCBM (as-cast) film transient Raman shifts. Mode abbreviations: ip = in plane, ν_{a-b} = stretch of *a*—*b* bond, δ = bend, sym. = symmetric, asym = asymmetric, BT: benzothiadiazole, Cz: carbazole, Th: thiophene, L: localised,D: delocalised. *1190 cm^{-1} at 20 ps, **1513 cm^{-1} at 50 ps. (See Figure I.14 in Section I for vector graphics of the vibrational modes.)

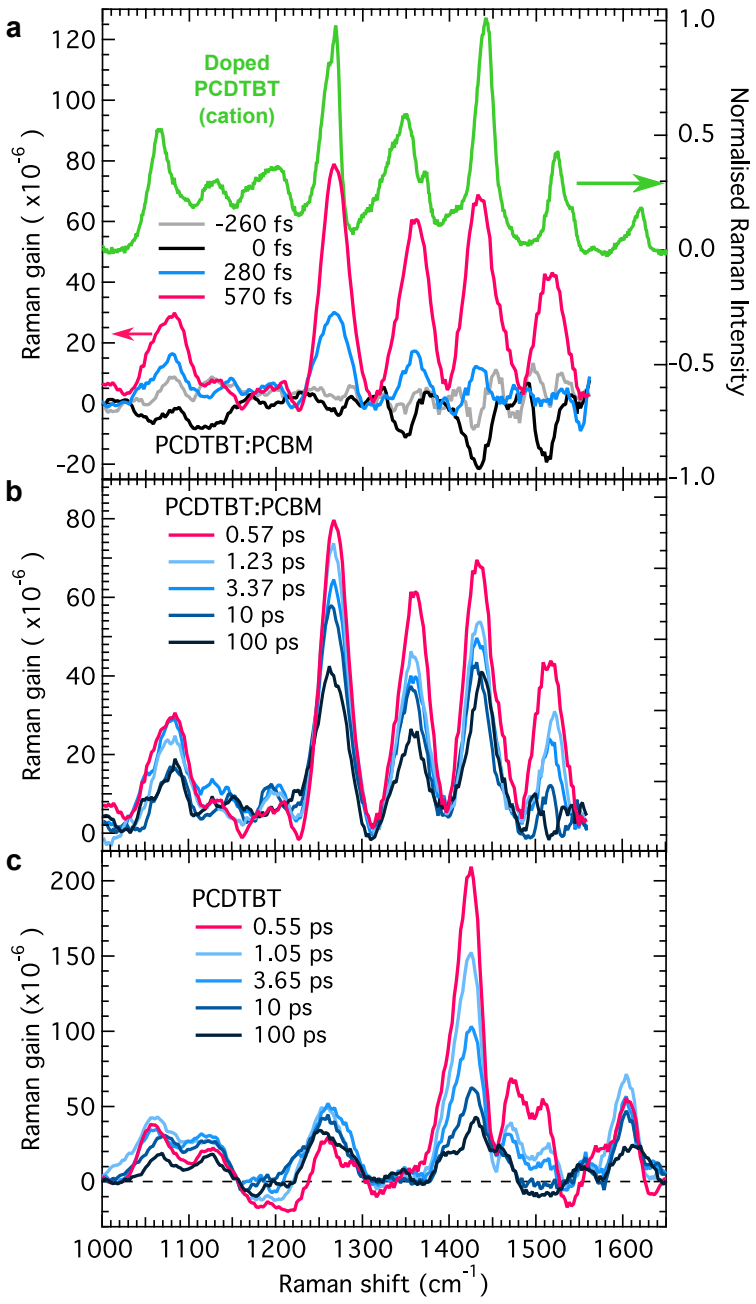

Figure 3.2: **Excited-state transient resonance-Raman spectra of PCDTBT:PCBM and neat PCDTBT.** Shown are femtosecond stimulated Raman spectra of (**a**, **b**) PCDTBT:PCBM and (**c**) neat PCDTBT films to illustrate structural relaxation over a 100-ps time window. Spontaneous resonance Raman of doped PCDTBT (green) is also shown in parts (a) for comparison.

trated in Figures 3.2a and 3.2b (see Figure I.8 and I.9 of Section I for FSRS spectra at all recorded time delays). We use a Raman pump pulse at 900 nm (1.38 eV) to be on resonance with the low-energy part of the polaron optical absorption spectrum, and thus these figures represent the temporal evolution of the stimulated resonance-Raman spectrum of the photoinduced polarons in PCDTBT:PCBM heterojunctions. We note the striking similarity of the transient FSRS spectra with the steady-state, spontaneous resonance-Raman spectrum of the doped PCDTBT film, confirming that we are probing hole polarons directly on the PCDTBT backbone. The characteristic bands of this polaronic signature readily follow the ultrashort actinic pulse (see also Figure I.1 of Section I), in particular the 1357 cm^{-1} band that is absent from the FSRS neat-PCDTBT spectrum at any delay time (see Figure 3.2c) and the 1260 cm^{-1} band that is present in the FSRS neat-PCDTBT spectrum with a low intensity.

The nature and timescale of molecular changes that FSRS is able to follow has been the subject of a recent comment by Mukamel and Biggs suggesting that the FSRS spectra at very early times may not truly represent vibrational spectra but rather a capturing of polarisation changes within the molecule following photoexcitation as at these early times the system may not be yet equilibrated to establish its vibrational modes.[160] However, the FSRS signal does not represent the instantaneous frequencies present at the sample only at the moment the probe pulse (the white-light) arrives to initiate a vibrational coherence upon interaction with the Raman pump, but the vibrational frequencies that develop over the vibrational dephasing time.[149] The ability of FSRS to capture frequency changes occurring on timescales faster than the dephasing time is due to the heterodyned detection system, where interference of the two optical fields causes negative signals, leading to 'derivative' type spectral features. These can be deconvoluted to reveal time-dependent molecular frequencies as in the case of rhodopsin recently carried out by McCamant.[149] There, an analysis of the early time FSRS line shapes and the spectral kinetics of the C10 hydrogen-out-of-plane (HOOP) mode during the ultrafast isomerisation of rhodopsincorrelated the early (< 1 ps) line shapes with frequency changes during the Raman vibrational free induction decay showing the HOOP mode relaxing with a 140-fs decay time.

Now, in the case of a molecule in which the vibrational frequencies do not change during the dephasing of the vibration, the time resolution can be instrument limited,[74] here 200 fs. Our FSRS observations at very early subpicosecond times following excitation represent the changing molecular system undergoing initial free induction decay following photoexciation but here the fact we observe Raman spectra that do not change from such early times and are extremely similar to those of the product states has to be taken as evidence that we are observing a molecular state that is representative of the product state. Thus, the molecular dynamics leading to the formation of the cation can be followed via changes in femtosecond Raman spectra that occur during its formation. At very early times, as coherences between the optically applied field and the molecular eigenstates are lost due to both electronic and nuclear changes, the FSRS spectra show 'derivative' line shapes are portrayed in our FSRS spectra only at the earliest time delay, indicating that free-induction decay following the electronic excitation and charge transfer is extremely rapid.

The fact that we see clear signals of the cation forming at early times confirms the charge transfer reaction is occurring well within the few-hundred-femtosecond timescale. This structurally sensitive measurement thus establishes unambiguously that polarons in PCDTBT:PCBM blends are created over one order of magnitude faster than transfer of electronic density in the neat polymer film (see below).

The structural distortion imposed on the polymer through the generation of the radical cation can be characterized through the frequency shifts in the FSRS bands in the spectrum of the blend film. A significant upshift of $\sim$20 cm^{-1} is observed for the 1064 cm^{-1} mode involving the thiophene C—H bend and C=C stretch, implying an increase in bond order of the latter bond associated with the transition to a quinoidal state. This is supported by the 13 cm^{-1} decrease in the frequency of the 1444 cm^{-1} band associated with the other two C=C bonds in thiophene, as well as increase in the frequency of C=C stretching carbazole modes, demonstrating the alternation of single double bonds. Whilst the differences in the Raman spectrum between the ground and excited states reflect differences in structure between the ground and excited electronic states, the small changes in the Raman spectrum of the excited state observed as a function of time in-

dicate that any structural changes occurring during electronic and vibrational relaxation are small.

Indeed, the overall shape of the FSRS spectrum of PCDTBT:PCBM at $<$ 500-fs timescales is essentially constant and decays with the population dynamics (see Figure 3.3a and Section I Figure I.1), with the exception of the carbazole mode at 1513 cm^{-1} whose dynamics will be discussed later in this article. Since the spectral signature of polarons emerges in the relaxed structure form at timescales earlier than what we would expect from structural reorganisation, this hints that the conformation of the polymer emerging from the Franck-Condon region is already close to the relaxed hole conformation.

Having established that polarons appear on ultrafast timescales in PCDTBT:PCBM blends, we address whether they are readily observable in the neat polymer as well. The FSRS spectra of neat PCDTBT, reported in Figure 3.2c, do not display polaronic signatures, excluding that species as a direct photoexcitation on the neat polymer on timescales shorter than 100 ps. In particular, the 1357 cm^{-1} band is absent, and the relative intensity of the 1260 cm^{-1} band with respect to the 1429 cm^{-1} band is at least four times lower at 0.5 ps. As the excitation decays, we do not observe the rise of the characteristic 1367 cm^{-1} band, indicating that there is no conversion of the initial excitation into polarons at later times. Therefore, polarons are not a dominant primary photoexcitation in neat PCDTBT. We thus assign the observed FSRS spectra in the neat PCDTBT film to intrachain singlet exciton as the primary photoexcitation. Indeed, Etzold *et al*. assigned the photoinduced transient absorption band in neat PCDTBT, centred at the energy we use for our Raman pump (1.38 eV), to singlet excitons,[64] while triplets were argued to form on timescales much longer than those explored in the present experiment.[180] In addition, the calculated exciton Raman spectral line shape in PCDTBT from our TDDFT calculations is in remarkable agreement with the experimental data (see Figure I.2 of Section I), which further supports our assignments.

These direct structural measurements have important implications on our understanding of 'push-pull' co-polymers, which comprise electron-rich and electron-poor moieties within the polymer repeat unit. Indeed, a hypothesis to rationalise the gener-

ally high solar power-conversion efficiency of this class of co-polymers would be that they readily form loosely-bound polaron-pairs upon photoexcitation, without the aid of a fullerene acceptor.[210, 230] The evidence presented here in favour of the singlet exciton contradict this hypothesis. We underline that according to our calculations and other work,[16, 180] the singlet exciton exhibits some degree of charge-transfer-like character. However, we insist that this picture is distinct from the loosely bound polaron pairs hypothetised for similar 'push-pull' co-polymers as noted above.

The evolution of the FSRS spectral line shape in neat PCDTBT is complex, but is consistent with transfer of electron density to the acceptor unit on the polymer (TBT) on a picosecond timescale. To appreciate the evolution of individual modes, we extract their kinetics by fitting FSRS peaks with a Gaussian curve and report their area as a function of time on Figure 3.3c, comparing them with population dynamics extracted from transient absorption measurements probed at 1.2 eV (1035 nm). The most intense FSRS peak at 1429 cm^{-1}, comprising mainly thiophene C=C stretching and carbazole C—N—C bending/C—C stretching, follows the exciton population dynamics after 1 ps. However, other bands deviate significantly from population dynamics. Specifically, the 1507-cm^{-1} peak decays to 25% of its initial intensity within 3 ps, while the 1260-cm^{-1} band grows on a similar timescale. The 1507-cm^{-1} band is a carbazole mode not visible in the ground state of neutral PCDTBT. However, our TDDFT calculations reveal that coupling with neighbouring thiophenes activates this mode. The 1260-cm^{-1} band is a delocalised mode characterised by C—H in-plane bending and C=C stretching in the BT phenyl ring along with C—N stretching in the thiadiazole ring in addition to carbazole and thiophene motion, and hence is sensitive to changes in electronic density on the acceptor unit. A slow increase in intensity is also observed in other modes, such as the 1057 cm^{-1} thiophene C—H bending mode. The evidence provided by FSRS thus helps draw a picture of the exciton evolution following photoexcitation to the Franck-Condon region, where the wavefunction is initially delocalized along the polymer chain.[14] The rapid decay of the 1507-cm^{-1} mode indicates that initial enhancement is lost either due to the loss of coupling as predicted by the TDDFT calculations and/or changes to the Raman cross section upon shifting of electron density from carbazole to the benzothiadazole

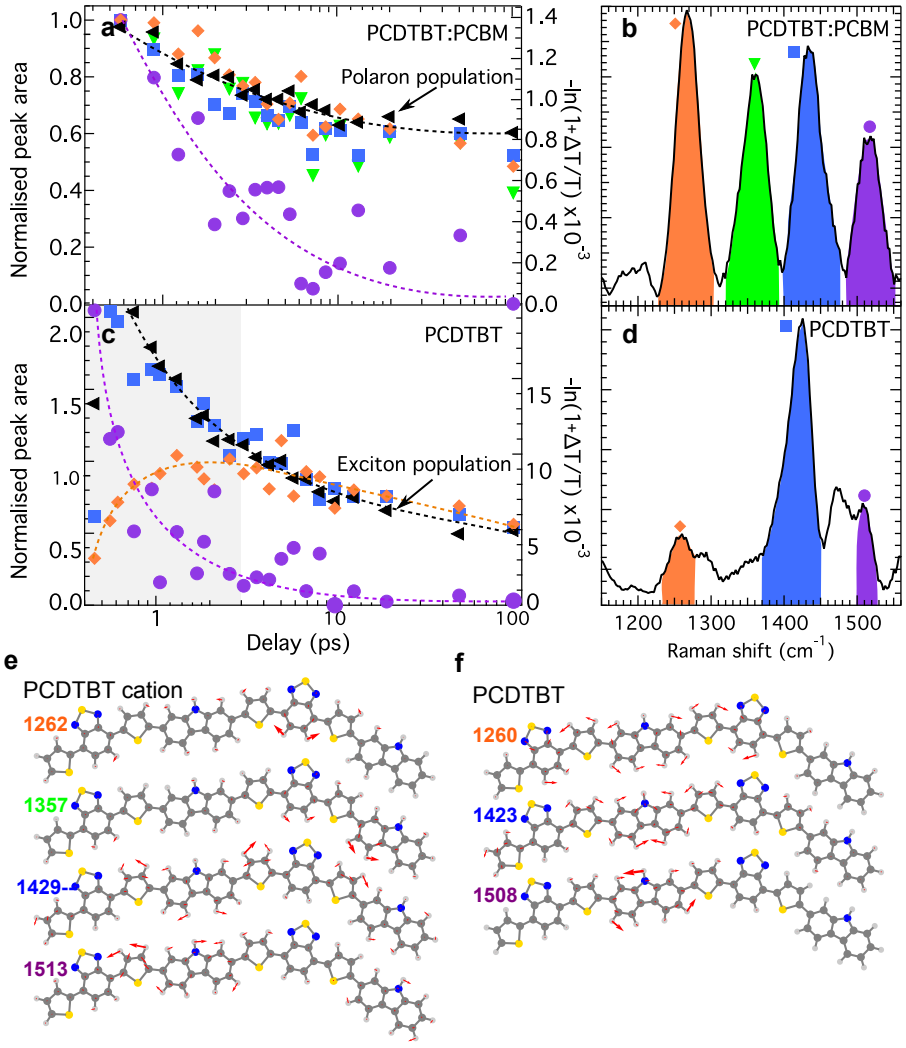

Figure 3.3: **Comparison of femtosecond stimulated Raman and transient absorption dynamics.** Shown are the dynamics of the stimulated Raman peak areas (extracted by Gaussian curve fit) and the excited species population in (**a**) PCDTBT:PCBM and (**c**) PCDTBT films. The analyzed FSRS peaks for the neat material and the blend, along with the symbol key for the time-resolved data shown in panels (a) and (c), are shown in panels (**b**) and (**d**), respectively. The data are normalised at 4 ps for panel (a) and at 0.6 ps in panel (c). The dotted lines in panels (a) and (c) are meant as a guide to the eye. Vector diagrams showing vibrational motion associated with the corresponding analysed peaks in a dimer of PCDTBT, determined by ab-initio calculations, are displayed for the cation (**e**) and the neutral molecule (**f**). Animations of those vibrational modes can be viewed as supplementary information on the Nature Communications website.

acceptor. This shift in electronic density is evidenced by the growing intensity of the 1260-cm^{-1} band.

Transfer of the electronic density to the benzothiadiazole and thiophenes on a few-picosecond timescale is consistent with the calculated localisation of the electronic density in the LUMO (see Figure I.15 of Section I), and is in general agreement with the 1–10-ps timescale reported for exciton dynamics in conjugated polymers.[57, 123] Therefore, the rich dynamics that develop in this excitonic system probed by FSRS reflect the dynamics of electron density flow in the polymer on a much slower timescale than the observed charge separation process in the blend system.

We now return to a discussion of the FSRS dynamics displayed in Figures 3.2a and 3.2b, in which we had pointed out that the overall shape of the FSRS spectrum of PCDTBT:PCBM at early times is comparable to that of the relaxed structure (100 ps and beyond) and decays with the population dynamics (see Figure 3.3a and Section I Figures I.1 and I.4).

As noted above, the only rapid FSRS dynamics that we observe involve the decay of the mode at 1513 cm^{-1}. In fact, the 1200 cm^{-1} mode displays similar behaviour, though its modest intensity makes quantitative analysis challenging. Interestingly, what these two modes have in common is that their band intensity depends on the extent of the coupling between carbazole and its neighbouring thiophene.

We can rationalise the decay dynamics of these modes by a dynamic decoupling of carbazole and thiophene, possibly arising from evolution of the dihedral angle between these moieties. We also note that although the 1513-cm^{-1} mode decays rapidly, this decay is slower in the blend than for the 1507 cm^{-1} mode in the neat film (Figure 3.2c). This suggests that the mechanism in the blend is distinct from the excitonic behaviour in the neat film.

Insight on the significance of those dynamics can be gained by considering previous work by Pensack *et al*. focusing on a carboxyl spectator mode in PCBM using ultrafast solvatochromism assisted vibrational spectroscopy.[170] These authors proposed that vibrational energy originally in Franck-Condon active modes in a polymer:PCBM electron transfer reaction redistributes on a few-picosecond timescale into a distribu-

tion of vibrational modes including those involved in electron transport between PCBM molecules.[170] We speculate that the rapid relaxation of the 1513 cm^{-1} mode could be related to mobile hole polarons as they move away from the interface.

In contrast to the modest relaxation of the polymer backbone in the presence of nascent hole-polarons, the overall spectral shape of the FSRS spectrum of neat PCDTBT, hosting excitons as the dominant photoexcitation, evolves continuously during the first 100 ps after photoexcitation and probably beyond, which indicates that after the initial fast electron-density redistribution, a slower structural relaxation takes place. This indication would explain fluorescence up-conversion measurements on PCDTBT thin films, which show that the photoluminescence spectrum red shifts to its relaxed state within 200 ps.[15] In particular, we observe red-shifting of the 1260 and 1471-cm^{-1} bands that correspond to benzothiadazole and carbazole motion likely due to change in the bond order of the backbone in the thiophene-benzothiadiazole-thiophene unit, and shift of the electron density from the carbazole to the acceptor moiety, lengthening thus the carbazole C—C bonds (see Figure I.15 of Section I). On the other hand, the 1429-cm^{-1} thiophene and carbazole band blue-shifts significantly between 50 and 100 ps, reflecting structural reorganisation accompanied by vibrational relaxation on those timescales, involving possibly dihedral angle changes between the two units.

3.2.3 Discussion

The two key observations presented in this paper are that (*i*) in PCDTBT:PCBM, ultrafast charge transfer happens prior to exciton relaxation dynamics on the few-picosecond timescale, as determined by the emergence of polaron resonance-Raman signatures on PCDTBT on timescales well within a few hundred femtoseconds; (*ii*) once formed on sub-picosecond timescales, polaron resonance-Raman signatures do not undergo significant spectral shifts or changes in linewidth during the first 50 ps.

Result (*i*) is strongly indicative that electron transfer occurs before exciton relaxation following photoexcitation of PCDTBT blended with PCBM. We consider the nature of this prompt charge separated excitation — Coulomb-bound electron-hole pair versus unbound charges with correspondingly large separation — by comparing to pre-

vious Raman studies on charge separation in solution as follows. In a previous FSRS study employed to follow the charge separation process of a non-covalent charge transfer complex in solution, Fujisawa *et al*. observed that the frequencies of Raman modes remained constant throughout the process, and concluded that the Franck-Condon state had significant charge separated character,[75] which is a very similar scenario as presented here. Earlier work by Vauthey *et al*. utilised time-resolved resonance-Raman spectroscopy with nanosecond resolution to follow the separation of a geminate ion pair into free ions in solution, and the authors distinguished between loosely-bound charge pairs and separated ions invoking changes in the band frequencies.[220] We thus expect that the FSRS spectrum of PCDTBT:PCBM is a very sensitive probe of the nature of the charged photoexcitation following initial charge separation and conclude that polarons, not charge-transfer excitons, are the photoproduct of such rapid dynamics, as we do not observe the dynamic signatures of separation of geminate pairs as observed by Vauthey *et al*. This implies that the corresponding electron on a PCBM phase, not detected by our FSRS measurements, must be separated over a sufficiently large distance on average in order for the polaron on the polymer backbone to not evolve under the resulting Coulomb potential on subnanosecond timescales, as evolution within such potential would result in evolution of the FSRS spectral line shape. In the dielectric environment defined by this class of materials, this separation must be in the order of several nanometers. In fact, Gélinas *et al.* have analysed signatures of a transient Stark effect in the photobleach component of a transient absorption measurement in molecular donor blends with PCBM, and have concluded that over ~ 40 fs the average electron-hole separation evolves to several nanometers,[78] supporting our conclusion. Such rapid, long-range charge transfer can be rationalised by exciton delocalisation phenomena,[14, 159] which can generally persist over sufficiently long timescales to play a role in the charge separation dynamics of interest in this work.

Understanding the mechanism of ultrafast charge separation is important, as it was demonstrated that even when electronic alignments are unfavourable to charge separation (e.g. in the presence of triplets), ultrafast kinetics can dominate and lead to very high internal quantum efficiencies.[190] Golden-rule formalisms applied to molecular elec-

tron transfer between localised asymptotic states cannot generally describe such rapid dynamics; however, when formulated in a delocalised basis set, such rapid dynamics can be readily described.[240] Another possible mechanism under which ultrafast electron transfer can occur is bath-induced coupling of asymptotic eigenstates of the system.[29] In this mechanism, the vertical, non-equilibrium exciton state transfers by resonant tunnelling to a delocalised charge-transfer state induced by a dynamic coupling due to common zero-point fluctuations within a vibrational noise spectrum of the system. Indeed, such spectacularly rapid charge separation points strongly to quantum coherence dynamics which are correlated to the dynamics of the molecular lattice,[186] and has been argued to play a key role in energy transfer dynamics in biological systems.[192] Either of these two mechanisms permit exciton separation over timescales that are much shorter than those in which a Marcus-theory description of ultrafast electron transfer is valid.

Observation (*ii*) concerning the limited evolution of the Raman spectrum after polaron formation is surprising, since polaronic relaxation following ultrafast charge transfer is generally expected in these polymers composed of such complex repeat units. We observe clearly from the change in the excited state frequencies compared to the ground state that the polymer structure changes upon polaron formation within 300 fs in PCDTBT:PCBM, but the subsequent structural evolution over 50 ps is very modest, which implies once more that the nascent hole is sufficiently far from the electron counterpart such that they are free from their mutual Coulomb potential. If the charge pair was Coulomb-bound, we would expect evolution of the polaron vibrational signatures as the two charges relax within their attractive potential. Similar to our findings, another FSRS study concerning a coumarin:TiO_2 system also observed the absence of significant reorganisation after charge formation.[73] Rapid charge separation is expected in that organic:inorganic hybrid system, since electron injection occurs into delocalised states in a conduction band of the inorganic nanostructure. The remaining positive charge on the dye therefore does not evolve under the influence of the electron potential. It is surprising that this seems to occur in PCDTBT:PCBM as well, given that such delocalised states in acceptor molecular aggregates are not expected *a priori*. These modes, that do not evolve after the initial charge transfer, are sensitive to the structure of the polymer, as

exemplified by the frequency shifts of the modes between the ground and the polaronic state, which is of quinoidal structure, and also exemplified by the dynamics of the frequency shift of the main FSRS band in different solvents (see Figure I.16 of Section I). Regarding the modest structural evolution on the polymer, we note that Österbacka *et al*. concluded that an increase in polymer chain stiffness is related to a smaller polaron relaxation energy.[165] In a different vein, Coffey *et al*. have suggested that a key route for improving future excitonic solar cells might be to reduce the reorganisation energy inherent to photoinduced electron transfer.[54] Indeed, we propose that correlating reorganisation dynamics with macroscopic optoelectronic parameters will enable a fundamental understanding of the critical factors that lead to efficient photovoltaic systems at a molecular level. The modest polaron relaxation in PCDTBT:PCBM is an intriguing result, and one that opens a new door to understanding of the differences between material systems that produce efficient solar cells and those that should but do not perform as well, even if they obey the same 'rational design' principles based on empirical design rules relating device parameters (e.g. open-circuit voltage, short-circuit photocurrent) to materials properties (e.g. absorption spectral range, reduction potentials with respect to PCBM, etc.).

Finally, we discuss that observations (*i*) and (*ii*) indicate the possibility of parallel pathways for polaron formation in organic solar cells, as was also highlighted in the literature for P3HT:PCBM. Sheng *et al*. demonstrated that polarons in P3HT:PCBM are created through two different channels: a direct, ultrafast one-step process and a slower, two-step process involving the creation and the dissociation of charge-transfer states,[195] but Aryanpour *et al*. applied a Coulomb-correlated Hamiltonian to find that fully-separated charge-pairs are not a *direct* photoexcitation in polymer:fullerence heterojunction.[7] These two works would suggest that in some systems the rapid charge separation dynamics argued here are not observed. However, Gao and Grey inferred that the dephasing of the vibronic coherence on ultrafast timescales does not depend on PCBM loading ratio in regiorandom P3HT:PCBM,[76] indicating that ultrafast coupling to charge-transfer states is not significant. Therefore, because photocarriers are generated with high yield in that system, there must be a direct mechanism for their

generation that must bypass charge-transfer intermediates. Similarly, the present work points strongly to direct photogeneration (i.e. no CT intermediate) of unbound polarons in PCDTBT:PCBM, although it is also clear that CTX must form eventually in this system since in a previous publication we observed geminate recombination through CTX emission on nanosecond to microsecond timescales.[175] We note from this work, however, that the direct polaron generation mechanism is operative on ultrafast timescales in PCDTBT:PCBM, with no forthright evidence of early involvement of intermediate charge-transfer states, while both channels may contribute to photocurrent in P3HT:PCBM. The degree of importance of the charge-transfer-state-mediated mechanism appears to be highly system dependent.

In ultrafast pump-push photocurrent measurements in polymer:PCBM photodiodes, Bakulin *et al*. pumped the polymer with femtosecond pulses and then 'pushed' any Coulomb-bound charge pairs across the heterojunction with mid-infrared pulses resonant with sub-gap polaronic transitions.[12] This promoted the charge pairs towards a delocalised state in which the charge pair could overcome their Coulomb binding and produce additional photocurrent. The degree to which Coulomb-bound charge pairs form following initial charge separation correlated with the degree to which additional photocurrent could be produced by pushing charges away from each other. Intriguingly, *no* additional photocurrent could be gained by application of the infrared push pulse in PCDTBT:PC_{70}BM. This implies that a direct photocarrier mechanism is favoured in this system, which is in agreement with our conclusions that are based on a direct structural probe of polarons.

If direct photocarrier generation is dominant in PCDTBT:PCBM and related efficient polymer systems,[82] avoiding the two-step process as is found in P3HT:PCBM[195] might be key in driving up efficiencies in solar cells by avoiding highly-bound CTX states,[77] even if it is the case that these states are photocurrent precursors.[219] The conclusion that relaxation to bound charge pairs is limited in PCDTBT blends is the key observation that must be understood in order to better engineer polymers for solar-cell applications.

3.2.4 Conclusion

We have implemented stimulated Raman spectroscopy on thin films of a photovoltaic-relevant polymer:fullerene heterostructure to reveal the structural dynamics of the polymer after photoexcitation, and assign the molecular origin of the observed features in transient absorption[212] and time-resolved photoluminescence[15] spectroscopies. Upon absorption in the lowest (π, π^*) band at 2.21 eV (560 nm), ultrafast charge generation occurs within 200 fs to form a hole polaron on the polymer. The charge separation takes place before exciton localisation (within 3 ps) in the neat film, while the exciton is far from vibrational equilibrium. Furthermore, vibrational relaxation of the resulting polaron on the polymer is modest over the first 100 ps, which suggests that the hole is free from the Coulomb potential that the twin negative charge would impart. This mechanistic insight is key for future optimization of the efficiency of polymer:fullerene based solar cells as it provides a window into the relationship between electronic dynamics and those of the polymer lattice involved in the conversion of excitons to photocarriers, which is of key importance for fundamental mechanistic understanding with molecular detail. Moreover, these conclusions are generally important in molecular photoexcitation because virtually every photochemical, photophysical, or spectroscopic process in molecular materials involves coupled dynamics of electrons and the structure.

3.2.5 Methods

3.2.5.1 Sample preparation.

PCDTBT ($M_n = 13,000$ kg/mol; $M_w = 30,000$ kg/mol; PDI = 2.3) was synthesised by Serge Beaupré in the group of Mario Leclerc at Université Laval as described elsewhere[30] and used as received. PCBM was purchased from Solenne ($PCBM_{60}$, 99.5%, lot 15-05-12) and used as received. Thin films were wire-bar-coated at 100°C on sapphire substrates (UQG Optics, 15-mm diameter, 1-mm thickness) using a bar with a channel width of 0.05 mm from solutions in 1,2-dichlorobenzene (HPLC grade, Alfa Aesar) of neat PCDTBT at a concentration of 8 mg/mL and PCDTBT:PCBM in a ratio of 1:4 at a concentration of 8 mg of polymer for 32 mg of PCBM in 1 mL. The poly-

mer concentration was kept constant constant to preserve the required viscosity of the solutions to make the films. Morphologicial studies including X-ray, optical and thermal experiments on this material system can be found in Section I, see Figure I.5 and I.6.

3.2.5.2 Spectroscopic methods.

Steady-state spontaneous Raman spectra were acquired with a Raman microscope (Renishaw inVia) with either 830 or 514-nm excitation. Femtosecond stimulated Raman spectroscopy (FSRS) was performed at the Central Laser Facility of the Rutherford-Appleton Laboratory using the ULTRA setup, a 10-kHz synchronized dual-arm femtosecond and picosecond laser system described elsewhere.[84] FSRS requires the generation of three pulses: the actinic pulse (560 nm, $\sim$ 50 fs), the Raman pulse (900 nm, 1.5 ps) and the broadband probe pulse ($\sim$ 50 fs), which yields an experimental time resolution of $\sim$ 70 fs. These were generated using two custom titanium-sapphire amplifiers (Thales Laser) seeded from a single oscillator (20 fs, Femtolasers) to create synchronised femtosecond and picosecond outputs after compression, respectively. The femtosecond beam was split into two: one femtosecond beam pumped an optical parametric amplifier (Light Conversion TOPAS) to generate the actinic pulse, while the other femtosecond beam was focused onto a lead-doped-glass window to create a broadband white light continuum to generate the broad-band probe pulse. The 800-nm fundamental wavelength of the laser was then rejected from the white light continuum by a pair of notch filters (Kaiser Holographic notch plus) to avoid two-photon absorption in the sample. These notch filters are responsible for the gap at 800 nm in the transient absorption spectra presented in Figure 3.1.The picosecond beam was tuned to 900 nm by an optical parametric amplifier (Light Conversion TOPAS) and acted as the Raman pump pulse. The actinic and Raman beams were mechanically chopped at 5 kHz and 2.5 kHz, respectively, while the probe beam was kept at the system repetition rate of 10 kHz. These different repetition rates create four different sequences of pulses, namely actinic-probe (01), Raman-probe (10), actinic-Raman-probe (11) and probe alone (00). The actinic-probe and probe alone sequences are used to obtain the transient absorption spectrum, while the FSRS spectra are obtained using a combination of those four sequences, as ex-

plained by Greetham *et al.*[84] Temporal dispersion of the pulses was minimized using reflective optics to transport beams to the sample. A linear motor drive translation stage (Newport) provided femtosecond to nanosecond pump-probe timing.The beams were focused onto the sample to typical beam diameters of 50 μm (probe beam) and 100 μm (actinic and Raman beams) set in a non-collinear geometry with with an angle of 10° between the Raman and actinic beams and the probe.

Samples were placed in a cold-finger cryostat (Janis Research Company) and kept under a dynamic vacuum (10^{-6} mbar). Low temperatures were achieved by flowing liquid helium, reaching 100 K and 180 K for the PCDTBT:PCBM and the neat PCDTBT films, respectively. The cryostat was rastered by a mecanical stage in the plane perpendicular to the beams to minimize cumulative photo-damage.

After passing through the sample, the probe beam was collimated and focused into a spectrograph (0.25 m f/4 DK240, Spectral Products), then detected shot-by-shot using custom high-rate-readout linear dual detectors (Quantum Detectors). The spectra were averaged using a computer, averaging 216,000 detected shots per spectra for the neat PCDTBT film and 441,000 shots per spectra for the PCDTBT:PCBM film.

The spectra obtained were then smoothed using a feature-preserving Savitzky-Golay filter in MATLAB. The step size of the filter was small to avoid losing spectral accuracy. The FSRS spectra were baseline corrected, using a polynomial fit to the broad background shape, preserving the FSRS peaks (see Figure I.7 of Section I). FSRS peak dynamics (peak area, centre frequency) were extracted by fitting a single Gaussian curve to individual peaks, or multiple Gaussian curves in areas of peak congestion.

3.2.5.3 Computational methods.

All calculations were carried out within the framework of density functional theory (DFT)[148] using Gaussian 03 and Gaussian 09 software[72] with the 6-311g(d) basis set.[128] The functional B3LYP[20] was used, which contains an empirically fitted percentage of exact-exchange for a better description of organic molecules. Other functionals were tested, such as CAM-B3LYP,[234] but the B3LYP was chosen due to a better description of the experimental vibrational spectrum of the ground state. All the opti-

mization calculations were forced in a planar geometry, since the low-frequenecy torsion motion of the excited state threw the system out of the harmonic regime. Therefore, all torsion effects are not described by those calculations.

While the ground-state and cation properties are calculated with DFT, the optically-excited-state properties are obtained by applying time-dependent density functional theory (TDDFT).[146] The new vibrational frequencies of each mode are obtained by fitting a parabola through nine single-point energy calculations around the energy minimum of the first singlet excited state, going from the minimum to the zero-point motion amplitude of the mode. This technique assumes that the effect on the frequency eigenvalues is limited to the first order, and that second-order effects of displacement eigenvectors can be neglected.

The excited state intensities depend on the charge reorganisation of the addition of an electron and a hole in our system, and they are approximated using the cation and anion ground state calculations. The ground-state mode was decomposed in the cation and anion vibrational modes, and a weighted average of all the intensities were done accordingly, with equal weight between the cation and the anion, to obtain the new intensity. This technique neglects the effect of the interaction between the electron and the hole in the excited state. This effect is presumed to be small in PCDTBT's case, since the description of the first singlet excited state after geometrical optimisation is composed of 97% of the HOMO$\rightarrow$LUMO transition. However, the new excited vibrational intensities must only be used to indicate the tendencies of the effects of the charge reorganisation, and their quantitative significance is ambiguous.

Acknowledgements. CS acknowledges funding from the Natural Sciences and Engineering Research Council of Canada, the Canada Research Chair in Organic Semiconductor Materials, the Royal Society, and the Leverhulme Trust. CS, SCH and NS acknowledge funding from Laserlab 2 EC Grant Agreement No. 228334 and STFC ULTRA facility for experimental time. NS and CH acknowledge funding from the UK, Engineering and Physical Sciences Research Council EP/G060738/1 grant, the European Research Council (ERC) Starting Independent Research Fellowship under the grant agreement No. 279587 and King Abdullah University of Science and Technol-

ogy (KAUST CRG). The authors acknowledge the assistance of A. Scaccabarozzi for film deposition and are grateful to Serge Beaupré and Mario Leclerc for providing the PCDTBT.

Authors contribution Samples were prepared by CH and FP. Microstructural characterisation was carried out by CH. Spectroscopic data were collected by FP, SCH, AWP, GMG, and MT, and analysed by FP and SCH. The experiments were conceived by CS, SCH, FP and AWP. Ab-initio calculations were carried out by NB. CS and SCH supervised the spectroscopy activity, MC supervised the theoretical calculations, and NS supervised the processing and characterisation activity. FP, SCH, and CS were primarily responsible for writing the manuscript, but all authors contributed to it.

Competing financial interests The authors declare that they have no competing financial interests.

CHAPITRE 4

THÉORIE DE LA FONCTIONNELLE DE LA DENSITÉ DANS LE MODÈLE DE SCHARBER

4.1 Mise en contexte

En 2006, alors que les cellules solaires organiques atteignaient des records d'efficacité en laboratoire autour de 4-5 %, Scharber et al. ont établi un modèle semi-empirique destiné à évaluer le potentiel de cette nouvelle technologie prometteuse. En effet, Scharber établit un lien entre le potentiel d'ionisation du polymère donneur et le voltage en circuit ouvert du dispositif. Bien que cette relation linéaire témoigne de pertes empiriques totalisant 0,6 eV, qui ont été explorées au Chapitre 3, avec des attentes réalistes des propriétés du dispositif sur la mobilité des charges et l'efficacité de l'absorption des photons, cette étude montrait la possibilité de doubler l'efficacité des cellules jusqu'à 10 % simplement en trouvant un composant dont les niveaux énergétiques étaient situés dans des plages de valeurs définies. Scharber permettait ainsi de guider la voie de la recherche de dispositifs plus efficaces en se concentrant sur l'optimisation des niveaux énergétiques et du band gap du polymère.

Étant alors en train de collaborer avec certains groupes de chimistes de synthèse, principalement le groupe de Mario Leclerc à l'Université Laval, j'ai remarqué que la synthèse de nouveaux polymères est un processus long et ardu, et que les calculs de DFT sont souvent utilisés comme guides pour établir les candidats les plus propices. Cependant, bien que plusieurs études existent sur l'efficacité de la DFT dans les organiques, plus spécifiquement sur la fonctionnelle semi-empirique B3LYP qui est le standard pour la caractérisation des composés organiques, la majorité porte sur les molécules finies. Malgré l'utilisation de la DFT pour caractériser les polymères dans le but d'atteindre de meilleures propriétés électroniques dans le cadre de l'étude décrite au Chapitre 2, très peu d'études existent sur la caractérisation des polymères, et encore moins par rapport aux polymères photovoltaïques. Considérant que la fiabilité de la DFT varie énormément

selon les composants et les propriétés étudiées, il est donc nécessaire de tester cette méthode avant de continuer à l'utiliser dans cette optique.

Les calculs DFT associés à une base de trente polymères photovoltaïques, dont les dispositifs solaires ont été créés et caractérisés dans la littérature, ont ainsi été testés. Bien que les précisions sur les niveaux énergétiques sont plus grandes que prévues, la précision sur le band gap et le voltage du dispositif se situent en dessous de 0,1 eV. Cette précision se traduit par une erreur allant jusqu'à 2,5 % sur l'efficacité totale du dispositif. Considérant la rapidité des calculs DFT, qui prennent quelques heures, par rapport aux processus de synthèse pouvant prendre plusieurs mois, cette précision est plus qu'acceptable pour sonder les candidats potentiels.

Le vrai problème se situe au niveau du courant produit, pour lequel le modèle de Scharber suppose une limite supérieure qui n'est atteinte que si le dispositif possède une bonne morphologie. Malheureusement, puisque la morphologie dépend beaucoup des processus de synthèse et très peu des propriétés électroniques, il est impossible de la prédire adéquatement pour le moment. Le modèle de Scharber nous donne simplement l'efficacité du dispositif en supposant que la morphologie est adéquate.

Suite à ces résultats, la totalité des calculs DFT accomplis au cours de mon doctorat a été répertoriée dans une base de données et analysée dans le but d'établir les candidats prometteurs pouvant atteindre, selon le modèle de Scharber, une efficacité au-delà du 8 %, qui constituait le record du monde d'efficacité au moment de l'étude. Les calculs sur les polymères accomplis au cours des stages d'été de Vincent Gosselin et de Josiane Gaudreau sous ma supervision ont également été incorporés dans la base de données.

Cet article a pu établir l'efficacité des calculs de DFT sur les polymères et offrir un estimé de la précision attendue pour diverses propriétés. À ce jour, cet article possède cinq citations, ce qui témoigne de l'intérêt de cette méthode de calcul dans le domaine des polymères photovoltaïques. En terme de pouvoir prédictif, il faut rappeler que l'efficacité photovoltaïque des candidats proposés par l'article n'est pas garantie, et que le but de cette étude était d'offrir une première sélection avant de procéder à de meilleurs calculs et une meilleure méthode de synthèse.

Plusieurs candidats ont été synthétisés depuis la parution de cet article, dont le poly-

mère P104 de la Figure 4.3. Les calculs de la Table 4.I prédisent un potentiel d'ionisation de 5,32 eV, une affinité électronique de 3,72 eV et un band gap optique de 1,60 eV. Les valeurs expérimentales de ces quantités sont 5,37, 3,85 et 1,43 eV, respectivement.[6] Les calculs sont donc dans l'accord espéré avec l'expérience, sauf pour un écart légèrement trop grand pour le band gap optique. Le polymère P104 est donc un candidat très prometteur pour atteindre l'efficacité prédite de 8,4 %. D'après une discussion avec le groupe de Mario Leclerc, les autres polymères de cette table sont cependant difficiles à synthétiser pour le moment, comme les polymères P102, P111 et P112. Pour cette raison, une attention particulière a été donnée aux candidats du Chapitre 5 pour que la synthèse soit possible avec les techniques expérimentales actuelles de copolymérisation. Nous pouvons toujours espérer que de plus en plus de ces polymères soient synthétisés dans le futur, et que leurs méthodes de synthèse s'améliorent au fil du temps et que leurs performances augmentent, à l'instar du polythiophène.

4.2 Designing Polymers for Photovoltaic Applications Using ab Initio Calculations

Nicolas Bérubé, Vincent Gosselin, Josiane Gaudreau and Michel Côté

Département de physique, Université de Montréal, C. P. 6128 Succursale Centre-Ville, Montréal (Québec) H3C 3J7, Canada

This article evaluates the efficiency of density functional theory calculations when used in conjunction with Scharber's model to predict the power conversion efficiency of organic solar cells. Thirty polymers were investigated, and their calculated electronic properties were assessed against their reported experimental values. The energy level calculations have a relatively small standard deviation of about 0.2 eV after a correction for a systematic overestimation. The optical band gap and the open-circuit voltage are obtained within an accuracy of 0.09 eV and 0.10 V, respectively. Also, the model provides an indication of the maximum value for the short-circuit current and an interesting guiding tool to identify promising suitable polymers to reach high power conversion efficiencies. After validating the present numerical approach against known devices, new polymers that could reach a power conversion efficiency ranging from 8 to 11% are presented.

4.2.1 Introduction

Organic photovoltaic cells have received much attention in recent years as they offer an environmentally friendly and low-cost solution to the world's rising energy needs. Claims for organic solar cells with a 10% power conversion efficiency have already been made.[83, 194] A bulk heterojunction solar cell,[59, 226] which uses a polymer as an electron donor and a fullerene derivative as an electron acceptor blended into an interpenetrating network, is a type of architecture that can be easily produced while providing promising results with power conversion efficiencies now reaching over 7%.[51, 141, 142, 173] This technology is already used with high production volume screen printing processes to provide flexible devices, and this market could develop as soon as it becomes commercially competitive.[127]

For many years, the goal of the scientific community has been to find better polymers that could give high power conversion efficiencies. Since the process of polymer synthesis and device production is a time-consuming one, it would be important to have a guide in searching for these optimal polymers. In 2006, Scharber et al.[189] proposed a simple model that describes how to estimate the power conversion efficiency of bulk heterojunction solar cells, and it is well-known for its claim that those devices can reach power conversion efficiencies of 10%. Scharber's model requires the knowledge of the energy levels to assess the potential of a polymer that will be used in a photovoltaic device. Normally, those energy levels are obtained by cyclic voltammetry experiments after the synthesis of the polymer. This is where modern theoretical tools like density functional theory are helpful. In principle, these tools can predict the properties of the polymer even before it is synthesized.

Scharber's model has been abundantly used in the past with density functional theory in an effort to design, understand, and predict the properties of actual and future organic solar cells.[9, 22, 31, 131, 242] However, even though the model clearly predicts certain particular properties like the open-circuit voltage or the short-circuit current density, one can ask if the model estimates some properties more accurately than others, when used in conjunction with the density functional theory. The reliability of theoretical calculations

is important as they offer the opportunity to understand and to predict the properties of devices. It is worth noting that some very extensive studies have already been made on oligomers[68, 86, 162, 163, 166] or crystals,[199] but the comparison of calculations made on polymers with experimental data remains scarce.

In this article, we will briefly review Sharber's model. Only a few key electronic properties are needed to apply this model. We will then assess the accuracy of density functional theory calculations to predict these values when compared to reported known polymer devices. We will find that the accuracy on most of these properties can be used as a guiding tool to sample the vast chemical space. This approach of combining density functional theory calculated properties with Sharber's model provides indications of the maximum values that can be obtained for the power conversion efficiencies. After establishing the validity of the approach, we will finish by proposing new interesting candidates for donor polymers. As a guiding tool, the present approach should be considered as a gateway toward a more detailed analysis of the promising polymer candidates and cannot be used on its own to obtain exact predictions.

4.2.2 Methodology

Scharber's Model. By convention, the power conversion efficiency (PCE) of a solar cell is equal to the maximum power density output of the device divided by the total incoming power density from the Air Mass 1.5 solar spectrum,[1] which is 1000 $\mathrm{W/m^2}$. The power density output of the device is given by the product of the open-circuit voltage (V_{OC}), the short-circuit current density (J_{SC}), and the fill factor (FF). According to Scharber's model, the V_{OC} is related to the difference between the lowest unoccupied molecular orbital (LUMO) of the acceptor and the highest occupied molecular orbital (HOMO) of the donor. One has to subtract 0.3 eV from the difference between those energy levels to obtain the V_{OC}. This shift was found empirically and is attributed to the residual binding energy between the carriers and various interface effects. However, the exact value of this binding energy is still debated.[18, 37, 90] The J_{SC} is the integral of the external quantum efficiency (EQE) multiplied by the number of photons given by

[1] Air Mass ASTM G-173 data available at http://rredc.nrel.gov/solar/spectra/am1.5/

the Air Mass 1.5 solar spectrum over all frequencies. The EQE is simply taken as a step function, with a value of 0% for energies below the donor's optical band gap (E_{opt}) and 65% for energies above it. The fill factor is approximated as a constant FF = 0.65 for all devices. It is worth noting that other assumptions for the EQE and the FF can be made if desired. For example, the EQE could be obtained by studying the Kohn-Sham joint density of states, which would give us insight into the frequency-dependent behavior of the absorption cross-section. However, in the present case, the assumption is that the polymer layer is thick enough to absorb any photon over the optical band gap and that the EQE is mostly limited by the morphology of the films. Scharber's model[189] can be described according to the following equations

$$\mathrm{PCE} = \frac{V_{OC} J_{SC} \mathrm{FF}}{1000\ \mathrm{W/m^2}} \tag{4.1}$$

$$\mathrm{LUMO_{donor}} > \mathrm{LUMO_{acceptor}} + 0.3\ \mathrm{eV} \tag{4.2}$$

$$\mathrm{e}V_{OC} = \mathrm{LUMO_{acceptor}} - \mathrm{HOMO_{donor}} - 0.3\ \mathrm{eV} \tag{4.3}$$

$$E_{opt} = \mathrm{LUMO_{donor}} - \mathrm{HOMO_{donor}} \tag{4.4}$$

$$\mathrm{EQE}(\omega) = 0.65 \times \Theta(\hbar\omega - E_{opt}) \tag{4.5}$$

$$J_{SC} = \int \mathrm{EQE}(\omega) \times \#\mathrm{photons}_{\mathrm{Air\ Mass\ 1.5}}(\omega)\mathrm{d}\omega \tag{4.6}$$

As Equation (4.2) points out, this model assumes an energy difference between the LUMO of the donor and the LUMO of the acceptor of at least 0.3 eV to ensure an efficient charge transfer between the components. This LUMO offset value must not be confused with the empirical shift of 0.3 eV for the V_{OC} calculation of Equation (4.3). This means that the maximum value for eV_{OC} is $E_{opt} - 0.6$ eV.

Theoretical Methodology. All calculations were done in the framework of density functional theory (DFT)[41] by using the Gaussian 03 and Gaussian 09 packages.[72] The exchange-correlation energy was treated with the B3LYP functional.[20] The B3LYP functional shows an improvement over the local-density approximation (LDA) since the former contains a certain percentage of exact-exchange fit on empirical data.[4]

The addition of exact-exchange in the B3LYP functional approximates the derivative discontinuity in the fractional occupation orbital energies, which improves the band gap description.[55, 147, 193] To this day, no other functional has clearly replaced the B3LYP functional as a standard in the organic photovoltaic domain,[19, 166] and for this reason it will be used in this article. The polymers were calculated in a one-dimensional periodic and isolated system. The number of primitive cells included in the exact-exchange calculation and the k-point sampling was done automatically by the Gaussian software, as they both depend on the primitive cell length. The exchange energy was calculated over a distance ranging from 5 to 15 primitive cells. Each copolymer calculation contains a number of k-point ranging from 9 to 44. Those parameters should be treated more carefully when studying systems with low band gaps, which is not the case here. The atomic positions were relaxed with the 6-311g(d) basis set.[2][128] The electronic properties were then calculated from those positions with the 6-311g(2d) basis set.

The various alkyl chains have been modeled by ethyl or isopropyl groups, depending on the beginning of the chain, to allow for faster calculations and better convergence criteria. The results should not be affected by this approximation since the electronic wave functions of the LUMO and HOMO states are mostly located on the polymer backbone and not on the chains. The alkyl chains mostly influence the molecular packing, which is not considered here since the calculations were done for isolated polymers. Convergence tests on poly(3-hexylthiophene) (P3HT) reveal that an alkyl chain of at least two carbon atoms is required to get electronic energy levels inside 0.1 eV of the converged full alkyl chain value.

There are many different ways to calculate the electronic properties of polymers. In this study, only DFT Kohn-Sham energy levels were investigated. The HOMO energy level can be related to the ionization potential according to Janak's theorem.[110] However, it is important to note that these values strongly depend on the functional used. This choice was made with a design purpose in mind. Since the Kohn-Sham energy levels are

[2]The relaxation was done with the *tight* convergence criteria, which means a maximum force threshold of 1.5×10^{-5} Hartree with a residual mean square threshold of 1.0×10^{-5} Hartree.

rapidly and easily obtainable for almost any polymer, they can be used as guidelines for future experiments by spanning quickly over a large number of possible candidates and reveal which ones are suitable for further, more accurate calculations like the GW calculations and the Bethe-Saltpeter equations.[93, 94, 164]

4.2.3 Results and discussion

The calculations were done on 30 different donor polymers, which already have been synthesized.[46, 80] They are labeled from P1 to P30 and illustrated in Figure 4.1. When needed, the primitive cells were doubled to obtain a stress-free configuration. For example, the intermolecular bonds on the first and fourth carbon atom of the aromatic ring of a thiophene unit are not parallel, and forcing them to be parallel would cause virtual stress on the polymer. Since all calculations on polymers must be done on a repeating cell that is linearly periodic, a second thiophene unit has to be added upside down in the repeating cell, effectively doubling the number of atoms in the unit cell.

Band Gaps and Electronic Levels. Cyclic voltammetry probes one-body excitations corresponding to adding or withdrawing an electron to the system, which are associated to the LUMO and the HOMO energy levels, also known as electron affinity and ionization potential, respectively. Because cyclic voltammetry measurements are done for polymers in a solvent, the values obtained can differ from the idealized electron affinity and ionization potential of a polymer in a vacuum. The optical band gap is a two-body excitation where the electron and the hole can interact. Therefore, the optical band gap should be equal to or lower than the difference between the electron affinity and ionization potential. However, Scharber's model assumes that the gap is exactly equal to the difference between the energy levels, as Equation (4.4) shows. To remain within the scope of this model and to keep the PCE limit of 11.1%, we will only consider one single band gap which will be associated to the difference between the HOMO and the LUMO energy levels. Both the optical band gap and the cyclic voltammetry band gap were considered and compared with the Kohn-Sham energy level difference. When attempting to apply a linear fit to the data, one finds that the optical band gap is better described than the cyclic voltammetry one, as the standard deviations for both these values

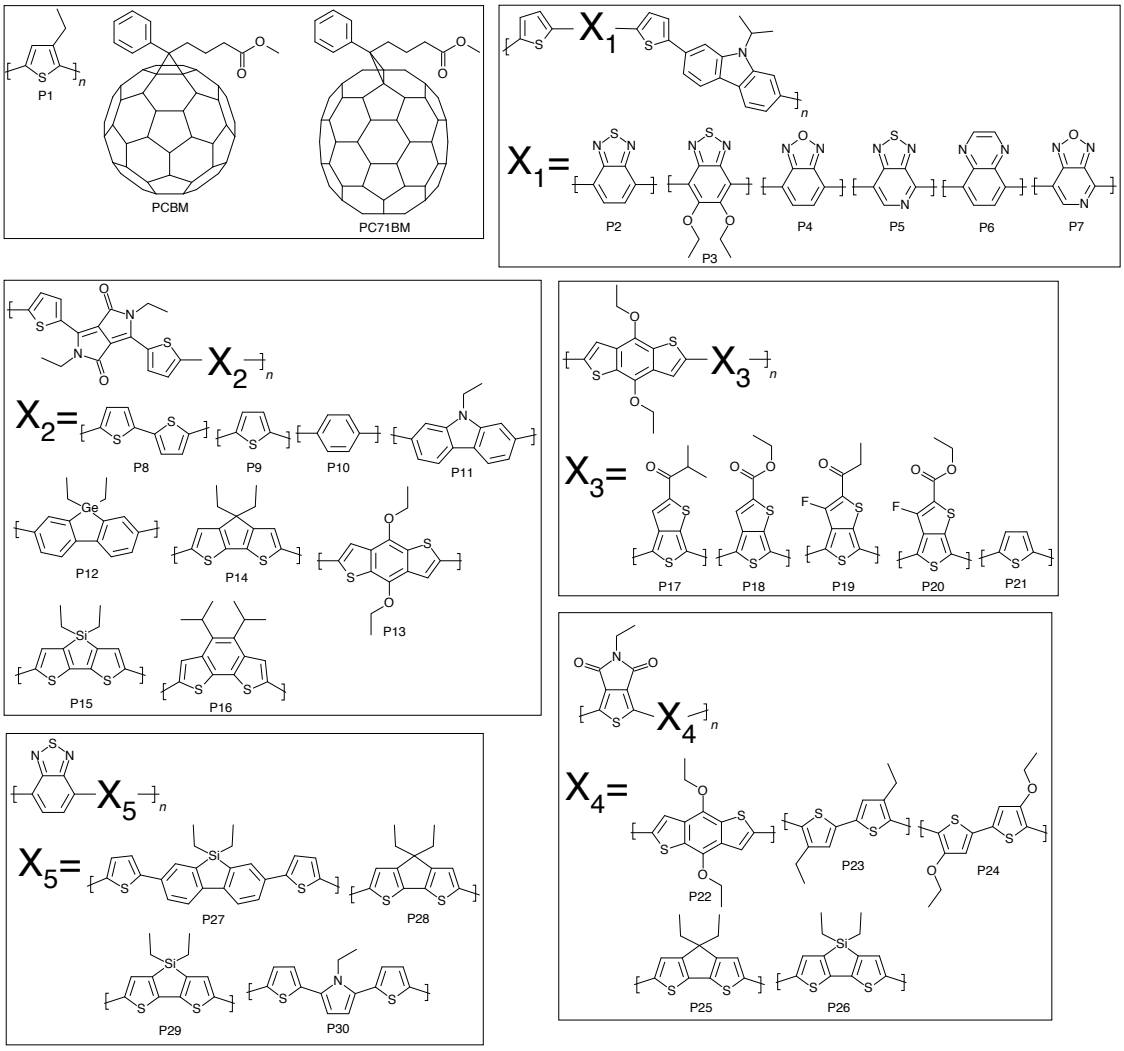

Figure 4.1: Structure of the polymers in this study. The references for the experimental data are the following: P1[102, 118] P2[167] P3[177] P4[31] P5[31] P6[31] P7[31] P8[231] P9[27] P10[25] P11[112] P12[5] P13[116] P14[44] P15[103] P16[103] P17[99] P18[140] P19[99] P20[141] P21[101] P22[171] P23[236] P24[85] P25[85] P26[51] P27[225] P28[168] P29[100] P30[217]

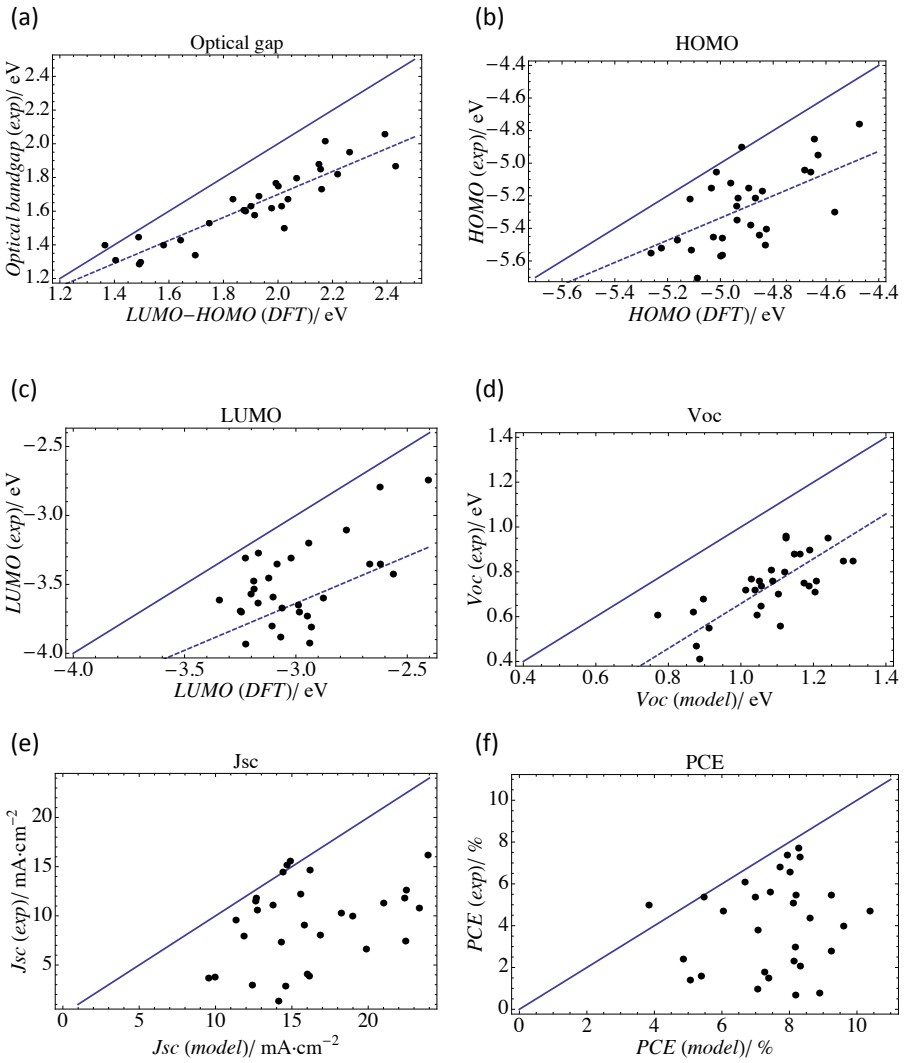

Figure 4.2: (a) Optical band gaps of various polymers used in solar cells. The x-axis is the energy difference between the theoretical HOMO and LUMO levels, while the y-axis is the experimental value. The full line is the $y = x$ line, and the dashed line corresponds to Equation (5.6). (b) HOMO and (c) LUMO energy levels of various polymers used in solar cells. The x-axis is the theoretical DFT value, while the y-axis is the experimental value from cyclic voltammetry. The full line is the $y = x$ line, and the dashed line corresponds to Equations (5.7) and (4.9). (d) Open-circuit voltages of solar cells with various donor polymers used with PCBM or PC71BM. The x-axis is the theoretical value calculated with Equation (4.3), while the y-axis is the experimental value. The full line is the $y = x$ line, and the dashed line corresponds to an overestimation of 0.34 eV according to Equation (4.10). (e) Short-circuit current densities and (f) Power conversion efficiencies of solar cells with various donor polymers used with PCBM or PC71BM. The x-axis is the theoretical value calculated with Equations (4.1)−(4.3), while the y-axis is the experimental value. The full line is the $y = x$ line, which acts as an indication of the maximum value.[5, 25, 27, 31, 44, 51, 85, 99–103, 112, 116, 118, 140, 141, 167, 168, 171, 177, 217, 225, 231, 236, 241]

are 0.09 and 0.17 eV, respectively. The need for linear fits has been observed in previous studies[19, 104, 105] and is not surprising for this type of functional. If we assume the linear fit to be systematic for all polymers, DFT can retain its predictive power as long as the standard deviations remain small. The optical band gap data are reported in Figure 4.2a. The resulting fit for the optical band gap is given by the following equation

$$E_{opt} = 0.68 \times (\mathrm{LUMO}_{\mathrm{DFT/B3LYP}} - \mathrm{HOMO}_{\mathrm{DFT/B3LYP}}) + 0.33\ \mathrm{eV} \tag{4.7}$$

Results for the electronic energy levels are shown in Figure 4.2b and Figure 4.2c. Because of Equation (4.4), the linear fits on the energy levels must be applied with the two following constraints: the slope of the fit must be 0.68, the same as Equation (5.6), and the difference between the intercepts must be equal to 0.33, the intercept of Equation (5.6).[3] We obtained the following expressions for the fitted results of the energy levels

$$\mathrm{HOMO} = 0.68 \times \mathrm{HOMO}_{\mathrm{DFT/B3LYP}} - 1.92\ \mathrm{eV} \tag{4.8}$$

$$\mathrm{LUMO} = 0.68 \times \mathrm{LUMO}_{\mathrm{DFT/B3LYP}} - 1.59\ \mathrm{eV} \tag{4.9}$$

The standard deviations for the HOMO and LUMO levels are 0.18 and 0.24 eV. It is interesting to study how the energy level standard deviations affect the PCE. An error of 0.18 eV in the ideal energy levels, while keeping the band gap constant, would reduce the PCE from 11.1% to 8.6% or prevent charge separation altogether. This is why we will later present polymer candidates with PCE starting from 8% or with LUMO levels close to the charge separation threshold since our accuracy on the energy level alignment is not sufficient to clearly distinguish the best polymers out of these sets. We

[3]The fit parameters from Equation (5.6), namely, the slope of 0.68 and the intercept of 0.33 eV, have been used to impose the constraints on the LUMO and HOMO fits because of their low standard errors compared to independent fits on the energy levels. The standard deviations for the HOMO and LUMO levels are 0.18 and 0.24 eV. Since the standard deviation on the HOMO energy values is smaller than the LUMO one, the intercepts have been fit on the HOMO data. The LUMO intercept will then simply be the sum of the HOMO and the optical band gap ones. This sum is -1.59 eV, whereas the optimal intercept for the LUMO level would be -1.46 eV. Since the difference between those two values is lower than the standard deviation on the LUMO data, the offset could be partially explained by a statistical effect.

would also like to stress that this observation emphasizes the need for the continuing development of better electronic structure methods and more systematic analysis of the experimental data. Presently, we use an approach that is the best compromise between cost in computational resources and accuracy of the results to help the development of new polymers for photovoltaic applications. Precise energy level data should be left for more demanding calculations.

The fact that the prediction of the LUMO level is not as precise as the HOMO level might also be a problem; however, DFT energy levels have to be assessed in the context of the derived quantities of interest. According to Equations (4.4), (4.2), and (4.3), the LUMO level allows us to calculate the optical band gap, the LUMO offset, and the open-circuit voltage. The optical band gap description is not an issue in this case since the LUMO level description has been fit according to the band gap. Since the LUMO offset criteria is necessary to ensure a functioning device, it might cause a problem for donor polymers that have LUMO values near the 0.3 eV limit of Equation (4.2). However, a larger uncertainty on the LUMO level value is not problematic for levels that are far from this offset limit. The open-circuit voltage problem only considers the LUMO level of the acceptor and will be discussed in greater detail in the following section.

Open-Circuit Voltage. In this study, all donors have been experimentally paired with either the [6,6]-phenyl-C60-butyric acid methyl ester (PCBM) fullerene derivative or [6,6]-phenyl C71-butyric acid methyl ester (PC71BM) as the electron acceptor. Given the fact that the calculated difference in LUMO levels between these two compounds is small (0.03 eV), the LUMO level of the acceptor is effectively a constant for all devices. However, there is no guarantee that the fit obtained in Equation (4.9) for donor polymers is applicable to a single, nonperiodic acceptor molecule like PCBM. Indeed, while the experimental value of the LUMO level of the PCBM used by Scharber is -4.3 eV, the value predicted by Equation (4.9) is -3.89 eV.[4]

The experimental open-circuit voltage V_{OC} has been compared to the theoretical one, calculated with Equations (4.3), (5.7), and (4.9). As illustrated in Figure 4.2d, there is an

[4]The DFT LUMO levels of PCBM and PC71BM that were calculated and used in Equation (4.9) were -3.39 and -3.34 eV, respectively.

average overestimation of the V_{OC} of 0.34 V. One notes that this overestimation could be attributed to an erroneous value of the residual binding energy of Equation (4.3). Indeed, one could keep the PCBM's LUMO level around -4.0 eV[3, 126, 137, 152] and change the residual binding energy and the LUMO offset of Equation (4.2) accordingly, and the model would virtually be the same. However, for the sake of simplicity, the overestimation will be entirely attributed to the PCBM's LUMO level. Therefore, the PCBM's LUMO level will be changed to -4.23 eV.[5] Considering that the standard deviation on the V_{OC} data is 0.10 V, it is compatible with Scharber's value of -4.3 eV. This new value of -4.23 eV is the one that is going to be used to determine the LUMO offset in Equation (4.2), meaning that an efficient donor polymer would need a LUMO level over -3.93 eV to ensure an efficient charge transfer.[6] Equation (4.3) can then be rewritten as follows

$$eV_{OC} = 0.68 \times |\mathrm{HOMO}_{\mathrm{DFT/B3LYP(donor)}}| - 2.61 \text{ eV} \tag{4.10}$$

Short-Circuit Current Density. As shown in Figure 4.2e, the principal failure of this model lies in the short-circuit current density J_{SC}, for which the theoretical value, calculated with Equations (4.6) and (5.6), only seems to act as an indication of the maximum value for the experiments. Moreover, if the short-circuit current density is calculated with Equation (4.6), but using the experimental optical band gap E_{opt}, one finds that there is a total lack of correlation between this value and the real experimental J_{SC}. The inaccuracy in the value of J_{SC} is expected, as the model uses very simplistic assumptions for the EQE value in Equation (4.5), whereas the real EQE is a complicated frequency-dependent function that would have to account for transport effects. Experimental values for the quantum efficiency vary by an order of magnitude for essentially the same polymer with various modifications on alkyl side chains, solvent, or thermal annealing.[80, 85, 139] For this reason, a correction to the EQE model would be very hard to find, as it would have to account for a multitude of different effects depending on details of the morphology of the films. Regarding the present study, it is worth not-

[5] This value for devices using PC71BM will be -4.20 eV

[6] For PC71BM, this value is -3.90 eV.

ing that only the experimental J_{SC} of the device obtaining the highest power conversion efficiency was considered.

The J_{SC} values obtained with Scharber's model do not constitute a strict upper bound, and they should only be considered as an indication of a polymer's potential that could be harvested if the device possesses a good EQE. This assumption is taken for granted in the present model, and the only way to know if it is realistic is through a more detailed analysis of the promising candidates. It can be concluded that Scharber's model cannot be used on its own for accurate predictions, but only as a guide toward further research. This limitation is inherent to any model limited to molecular orbitals since the J_{SC} mostly depends on condensed phase behavior.

Fill Factor. Although treating the fill factor as a constant for all devices might seem like a coarse approximation, the error it generates is minimal compared to the problem of the EQE model. Indeed, if one calculates the power conversion efficiency with Equation (4.1), taking the V_{OC} and FF from Scharber's model but the experimental J_{SC}, the correlation between this PCE value and the experimental PCE is very high, showing an absolute standard deviation of 0.8%.[7] On the other hand, if one uses the V_{OC} and J_{SC} from Scharber's model but the experimental FF, the model still lacks predicting powers, showing that the EQE is the main problem of Sharber's model.

Power Conversion Efficiency. Results for PCE are shown in Figure 4.2f. The PCE is calculated with Equation (4.1), with the corrections for overestimations of the optical band gap, the HOMO and the LUMO levels of Equations (5.6), (5.7) and (4.9). One can then draw the same conclusions for the PCE as for the short-circuit current density. Scharber's model provides an indication of a polymer's potential that could only be reached assuming a good charge mobility, a good absorption, and an efficient charge separation process. However, those assumptions cannot always realistically be taken for granted, and a more detailed analysis with further research must be done to assess them. The data point that breaks this upper bound corresponds to the P1 (P3HT) device, and its performances are due to its unusually low residual binding energy in Equation (4.3).

[7] The absolute standard deviation is actually a percentage point since the units for PCE values are percentages.

This is supported by the fact that P3HT devices have an EQE that compares well with our model.[113] Its HOMO level being measured at -4.76 eV,[102] Scharber's model predicts a value of 0.16 V for the V_{OC}. The fact that open-circuit voltages of around 0.65 V are reported in the literature supports our interpretation regarding the low residual binding energy of devices using P3HT.

Promising Polymers. Knowing the limits of the present approach using density functional theory values in conjunction with Scharber's model, it is interesting to use the predicting power of ab initio calculations to evaluate new unsynthesized polymers that can reach the present model's theoretical limit of 11% efficiency. The properties of polymers that have high PCE are shown in Table 4.I and Figure 4.3. The six best ones that have already been synthesized have been identified, as with twelve new ones (P101 to P112) that have not yet been synthesized. New copolymers were mostly designed with the donor-acceptor approach in mind[185] pairing an electron-rich unit with an electron-poor one. All pairings use units that have already been synthesized on their own or closely resemble them.

The predicted PCE of polymer P7 could be hard to reach since its asymmetry means more effort might be needed to make it regioregular. Almost all of the best synthesized polymers (P8 to P16) belong to the diketopyrrolopyrrole (DPP) family, which is already well-known, but could still possess untapped potential provided a better experimental EQE is achieved. The P101 and P102 copolymers also belong to the DPP family but have yet to be synthesized. Copolymers P103 through P107 belong to the thienopyrrole-dione (TPD) family, a recent set of copolymers that still hold a promising future.[244] One can also notice the presence of another new family of copolymers based on a new thiophene-substituted isoindigo unit.[8] Within this new family, copolymers P108 to P110 hold promising potential for photovoltaic applications. We also note that these last three polymers have very low optical band gaps and large electron affinities, characterized by a low LUMO. This low value of the LUMO is comparable to PBCM, which means that they could potentially be used for electron transport. Finally, copolymers P102, P104, P111, and P112 all use the thienothiazole (TTz) monomer,[6] which seems to be an interesting unit with the donor-acceptor approach, assuming that regioregularity does

not pose a problem.

Obviously, the polymers with the best efficiencies have a LUMO that is very near PCBM's LUMO level, which could hinder the charge transfer processes. Also, the fact that the optimal band gap is 1.4 eV implies that their HOMO levels are near or over the maximum of -5.3 eV, which is presumed to be the maximum allowed for air stability.[31, 58] Encapsulation could be used to avoid air exposure, but this is far from ideal. Regarding the LUMO offset criterion, P8 and P9 both have a calculated LUMO level under -3.8 eV according to this model, yet they still have an experimental PCE of 4.0% and 4.7%, respectively. Moreover, regarding air stability, both P1 (P3HT) and P28 have a calculated HOMO level of, respectively, -4.98 and -5.04 eV, and they both possess an experimental PCE of over 5%. Therefore, provided efficient experimental procedures to isolate the compounds from air exposure, these candidates should not be disregarded as they show promising results in terms of PCE. Of course, the inefficient charge transfer and poor stability are two important problems for every high performance device and need to be further investigated. However, assuming an efficient charge transfer, a good stability, and a good morphology of the device, the PCE reported in Table 4.I should be reachable by those polymers.

4.2.4 Conclusions

In this work, we have discussed how theoretical calculations based on the Kohn-Sham energy levels of density functional theory used in conjunction with Scharber's model can provide a guide to find promising polymers for photovoltaic cells. Detailed calculations on 30 different polymers were used to assess the predicting power of the model. It was found that the PCE obtained with the model provides an indication of the maximum value that could be reached if we assume the device possesses good morphology. New polymers that could reach a high power conversion efficiency have been shown, but they might suffer from other recurrent problems like charge separation and stability. The latter could be corrected if we use a device with an electron donor that has lower energy levels. However, to ensure en effective charge separation process, this would require an acceptor with lower energy levels as well. The model could there-

Table 4.I: **Donor Polymers That Could Reach High Efficiencies When Used With PCBM**[†]

	PCE (exp)	PCE (max)	E_{opt} (eV)	HOMO (eV)	LUMO (eV)
P7	0.8%	8.9%	1.72	−5.52	−3.79
P8	4.0%	9.6%	1.41	−5.22	−3.80
P9	4.7%	10.4%	1.36	−5.23	−3.87
P10	5.5%	9.2%	1.53	−5.29	−3.76
P13	2.8%	9.2%	1.46	−5.26	−3.81
P16	4.4%	8.6%	1.49	−5.25	−3.75
P101	-	8.2%	1.54	−5.25	−3.71
P102	-	10.5%	1.31	−5.24	−3.93
P103	-	8.4%	1.51	−5.24	−3.73
P104	-	8.4%	1.60	−5.32	−3.72
P105	-	7.9%	1.61	−5.29	−3.68
P106	-	9.1%	1.42	−5.21	−3.80
P107	-	8.9%	1.73	−5.52	−3.79
P108	-	8.6%	1.17	−5.04	−3.87
P109	-	8.1%	1.23	−5.05	−3.82
P110[††]	-	10.2%	1.35	−5.36	−4.01
P111	-	8.9%	1.47	−5.25	−3.78
P112	-	8.4%	1.52	−5.25	−3.73

[†] Properties were calculated, respectively, with Equations (4.1), (5.6), (5.7) and (4.9).

[††] The LUMO of copolymer P110 is 0.08 eV too low to ensure charge separation with PCBM. However, this value is below the margin of error of 0.24 eV, established previously for the LUMO levels. This copolymer then still has a chance to be part of a functioning device with PCBM. The PCE calculation was corrected by shifting both HOMO and LUMO levels from the same amount in this particular case to ensure that the V_{OC} is always lower than $E_{opt} - 0.6$ eV and therefore avoiding extremely high PCE values over the 11.1% limit.

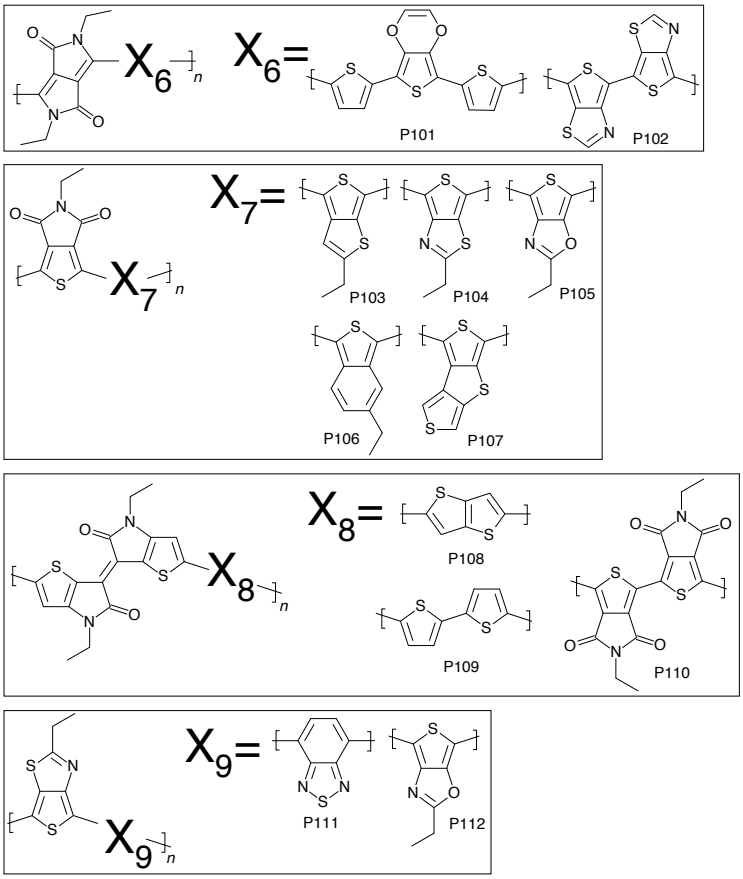

Figure 4.3: Structure of promising polymers of Table 4.I.

fore be extended to quickly calculate the efficiency of every possible pairing between polymers in an attempt to replace PCBM as an acceptor.

Acknowledgements. We thank the funding support of NSERC and the PV Innovation Network. NB acknowledges the Vanier Scholarship program. The calculations were done on the computational infrastructure provided by Calcul Québec and Compute Canada. We would also like to acknowledge the support of the Regroupement québécois sur les matériaux de pointe (RQMP) and the Centre québécois sur les matériaux fonctionnels (CQMF).

CHAPITRE 5

DESIGN DE POLYMÈRES SELON L'APPROCHE QUINOIDE-AROMATIQUE

5.1 Mise en contexte

L'espace moléculaire est particulièrement énorme à sonder. Dans la quête vers une efficacité toujours plus élevée, l'industrie de la photovoltaïque a besoin d'agencer les niveaux énergétiques des composants avec de plus en plus de précision. Le modèle de Scharber, étudié au Chapitre 4, a établi que le band gap optimal des polymères photovoltaïques devait se situer entre 1,1 et 1,4 eV, ce qui constitue encore aujourd'hui une plage de valeurs beaucoup plus basses que la norme et difficiles à atteindre. La synthèse de copolymères a été développée dans ce but. Sa prémisse est de pouvoir utiliser les propriétés avantageuses de chacun des monomères le composant. L'approche donneur-accepteur est sans conteste le paradigme le plus répandu du design de polymères. Basée sur une interprétation où les orbitales atomiques des monomères interagissent de façon liante et antiliante, cette approche stipule que les monomères dictent le potentiel d'ionisation et l'affinité électronique du copolymère les regroupant.

Cependant, après avoir analysé plus d'une centaine de copolymères différents avec l'étude du Chapitre 4, j'ai constaté que cette approche manquait de précision et donnait parfois des résultats complètement contraires à l'expérience. Les chimistes de synthèse semblaient plutôt en avoir recours a posteriori, ou pour limiter inutilement leurs choix de copolymérisation en séparant les monomères dans une dichotomie arbitraire de donneurs et d'accepteurs. En effet, deux monomères nommés accepteurs pourraient être combinés dans un copolymère aux propriétés très intéressantes.

Le record du monde en photovoltaïque organique, détenu à l'époque par Solarmer, était un copolymère dont l'efficacité était justifiée par sa forme quinoide. Cependant, la forme quinoide était utilisée sans explication adéquate et aucune recherche récente sur le sujet ne semblait vouloir expliquer cette description. Seuls quelques articles du début des années 1980, écrits par Jean-Luc Brédas, analysaient la question de la forme structurale

des polymères, mais son étude s'est limitée à quelques polymères aux caractéristiques très semblables.

Dans le but d'étendre cette relation à l'ensemble des polymères, les propriétés structurales de l'ensemble de la base de données récoltée dans le cadre de l'étude du Chapitre 4 ont été analysées. Plusieurs analyses ont été faites dans le but d'établir un lien entre la forme structurale, quinoide ou aromatique, et le band gap des copolymères. Ce lien sera présenté ce chapitre, et sera ensuite exploité dans le but d'offrir une nouvelle approche pour guider le design du band gap des polymères photovoltaïques.

Cette étude repose entièrement sur les calculs de ma base de données et de l'analyse que j'en ai faite. Josiane Gaudreau a été mentionnée comme coauteure, car elle a aidé à la récolte de données pour l'analyse structurale d'une dizaine de polymères pendant son stage d'été sous ma supervision.

Cet article établit un nouveau paradigme pour le design de polymères à petit band gaps, qui fonctionne de manière systématique avec tous les copolymères, peu importe leurs familles. L'utilisation de cette nouvelle approche nous permet de trouver des candidats qui nous échapperaient avec l'approche précédente de donneur-accepteur. De plus, les calculs DFT présagent pour une première fois l'existence d'une multitude de polymères avec des band gaps plus petit que 1 eV, ce qui facilite grandement l'accès à la plage intéressante de 1,1-1,4 eV pour la photovoltaïque organique.

Il est important de noter ici les limitations de cette étude. Par exemple, les polymères de type *ladder* où il n'y a pas de lien C-C intermonomère car les monomères sont fusionnés entre eux ne sont pas inclus dans cette étude, et sont d'excellents candidats pour atteindre la plage sous 0,5 eV déterminée par le gap minimal de Peierls. Il est bien connu, par exemple, qu'un nanoruban de graphène de largeur d'un cycle de benzène, le polyacène, présente théoriquement les caractéristiques d'un polymère métallique, même si la synthèse de ce dernier est pour le moment presque impossible.[119, 143] Les copolymères regroupant trois ou plus monomères différents sont également à étudier avec l'approche de ce chapitre. Certains dérivés du diketopyrrolopyrrole, donc la cellule primitive contient quatre unités différentes, ont été synthétisé avec un band gap optique près de 1 eV.[6] Il est donc évident que des copolymères intéressants se trouvent dans cette

catégorie.

Les candidats de cette étude n'ont toujours pas été synthétisés pour le moment, mais plusieurs sont en cours de synthèse dans le groupe de Mario Leclerc, y compris un polymère similaire au poly(TTD-TPD) de la Table 5.I. Il est cependant à noter que tous les polymères de cet article peuvent être synthétisés avec les procédés actuels, mais que la difficulté principale réside dans l'efficacité de ces procédés.

5.2 Low Band Gap Polymers Design Approach Based on a Mix of Aromatic and Quinoid Structures

Nicolas Bérubé, Josiane Gaudreau and Michel Côté

Département de physique, Université de Montréal, C. P. 6128 Succursale Centre-Ville, Montréal (Québec) H3C 3J7, Canada

This article establishes a link between the structural form of a polymer and its light absorption properties using density functional theory. According to a relationship established for 200 polymers from a wide range of different families, it is found that low band gap polymers can be designed with a mix of the quinoid and the aromatic structures. This characteristic can be obtained by synthesizing a copolymer containing quinoid monomers with aromatic ones. This promising approach of polymer design offers noticeably better predictions than the commonly used donor-acceptor approach and can be used as a fast method to obtain band gap properties of any copolymer using only information on homopolymers. Using this design approach, we present 31 new polymers with theoretical band gaps between 0.75 and 1.30 eV, 10 of which are under 1 eV.

5.2.1 Introduction

Organic electronics offer many advantages over their inorganic counterparts. The low-cost and flexible properties of polymers are useful in creating novel applications for various electronic devices. However, whereas low band gap inorganic semiconductor are readily available, it is still a challenge to find polymers with band gap lower than 1 eV. Such polymers would be suitable candidates for solar cells,[39, 66, 67, 127, 188, 208, 209, 235] light-emitting diodes,[132, 223] conductive inks,[24] and field-effect transistors.[49, 52, 65, 66, 79, 120, 122, 124, 200, 233]

The most common approach for low band gap polymer design is the donor-acceptor, also known as the push-pull approach.[28, 46, 80, 92] This method supposes that a copolymer's energy levels will be given by the lowest ionization potential and the highest electronic affinity of the monomers that compose it. Another way to look at the band gap is to consider the structure of the polymer. Polyacethylene is the textbook example that relates the atomic structure with the band gap through a Peierls deformation.[61, 169] In this case, the dimerization is so large that it results in a 2 eV electronic gap. We want to use this design principle to find other polymeric systems with lower band gap.

A polymer is naturally found in either its aromatic form, with single carbon bonds in between the monomers, or in its quinoid form, with double carbon bonds in between the monomers.[2, 43, 47, 48, 106, 117, 215, 216] Normally, their most stable form is the aromatic one, but one can force the quinoid form by fusing another aromatic cycle to the main cycle to force a double bond. This strategy is used to obtain the quinoid polymer isothianapthene[232] from the aromatic polythiophene.

The link between the quinoid form and the band gap has been theoretically investigated by Jean-Luc Brédas 25 years ago,[33, 38] but it has rarely been used as a design principle.[97, 98, 121, 130, 184, 185, 213, 218, 237] Brédas calculated the theoretical band gap of polythiophene by changing and forcing the bond length between carbon atoms, and he observed that the minimal band gap is obtained when the polymer is between its quinoid and aromatic form, where all bond lengths would be almost equal.

In the present article, we will generalize and expand the relation between the quinoid

structure and the band gap of polymers composed of stable molecules presently available using density functional theory. The latter is a very widely used method to obtain geometrical and electronic properties from ab initio methods.[9, 22, 31, 131, 166, 242] We will then build an approach to predict the band gap of copolymers using data on the monomers that compose it, and we will compare its efficiency to the donor-acceptor approach. We will find that the link between quinoid structure and band gap is more reliable than the donor-acceptor method as a guiding principle to find low band gap polymers. Finally, we will close with a discussion about improvements on charge mobilities and a list of 31 new polymers with low band gaps between 0.75 and 1.30 eV.

5.2.2 Methodology

This article's calculations use density functional theory (DFT)[41, 96, 148] and time-dependent density functional theory (TDDFT)[146, 187] as implemented in the Gaussian package,[72] using the B3LYP functional to treat the exchange-correlation energy[4, 20, 55, 147, 151, 193] and the $6-311g(d)$ basis set.[129] The polymers are all calculated in an isolated, one-dimensional periodic system, except for TDDFT calculations which are done on tetramers. Both the number of primitive cells considered in the exact-exchange and the k-point sampling are done automatically by the Gaussian software, since they depend on the length of the primitive cell. The exchange energy was calculated over a distance ranging from 5 to 17 primitive cells. Each copolymer calculation contains a number of k-points ranging from 9 to 46. The alkyl side chains are not considered in this study, since they do not influence the atomic structure of the backbone or the band gap results in any significant way. The band gaps are calculated with the Kohn-Sham energy levels of DFT, which can be related to the ionization potential according to Janak's theorem.[110] They are obtainable easily and rapidly for almost any polymer. Even though they strongly depend on the functional, this choice is made with a design purpose in mind since they can be used as guideline by spanning over a large number of possible candidates. Any bias is therefore presumed to be systematic through the study, and all trends and relations found would still be meaningful, especially if they apply to a very large number of polymers. We use a previous study[23] to relate the

obtained DFT/B3LYP band gap with the real observed optical gap in order to make realistic predictive results.

Our goal is to investigate the relationship between the optical gap of a copolymer and the degree of its aromatic or quinoid character. However, this notion is not well-defined. Ideally, we need a method to obtain a simple dimensionless dimerization parameter, which will be named Δ, which quantifies the quinoid or aromatic character of a polymer. This approach is unambiguous only in very precise cases where single and double bonds are precisely defined, like polyacethylene. The challenge lies in the cases where the single and double bonds are not clearly identifiable. For example, poly(*p*-phenylene) is problematic since the double and single bonds are actually delocalized in the aromatic cycle of the benzene monomer.

We find that a reliable way to quantify the quinoid character in relation to the band gap was to simply calculate the ratio of intermonomer carbon bond lengths over the average intramonomer carbon bond lengths, as shown in Figure 5.1. This is justified by the fact that in the aromatic form there are more double carbon bonds in the monomer whereas the intermonomer bonds will be single bonds. Therefore, the parameter Δ of aromatic polymers is greater than 1. In the quinoid cases, it is the opposite, meaning that Δ is lower than 1. Other attempts have been made to perform different averages and ratios to define Δ. The simpler attempts were to calculate the ratio of the extremes of the bond lengths instead of their average or to only consider the intermonomer bonds. The more elaborate approaches were to weight each bond according to how it is affected by the transition from the aromatic to the quinoid form or according to its position relating to the shortest path between the monomer extremities. Another one was to include the variance of the carbon bonds in the calculations. While the simpler approaches were inconclusive, the more complex ones did not improve the results in any significant way.

Since the aromatic and quinoid character is mostly expressed through the dimerization of unsaturated carbon chains, we choose to exclude every interatomic distance that is not between carbon atoms. The noncarbon atoms directly affect the precise energy levels of the polymer, namely the ionization potential and the electronic affinity.[45, 121] However, the modifications that comes from noncarbon atoms often applies equally on both

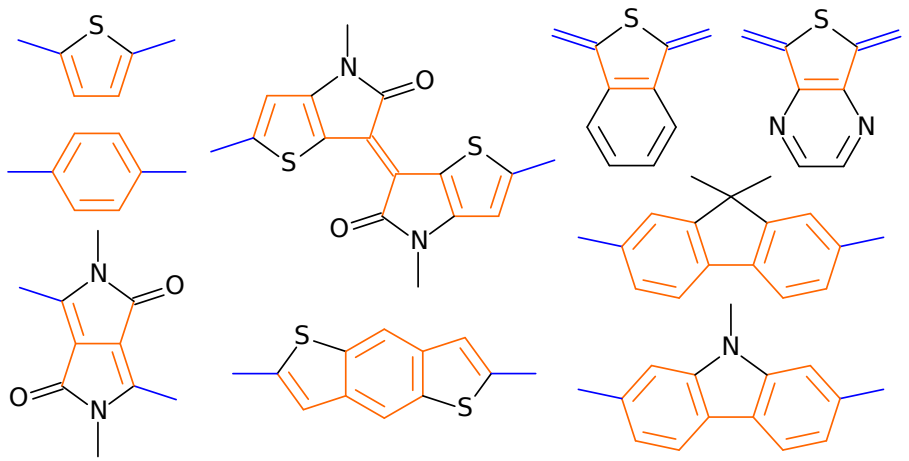

Figure 5.1: A few examples of the bonds considered in the calculation of the parameter Δ, namely sp^2-hybridized carbon bonds in the shortest path cycles. For a specific polymer, Δ is the ratio of the average of intermonomer (blue) bonds over the average of intramonomer (orange) bonds. This choice is made to improve the comparison between isothianaphthene and thioenopyrazine, or between fluorene and carbazole, illustrated on the right.

the ionization potential and the electronic affinity, leaving the band gap unchanged. One can obviously compare bonds with oxygen, nitrogen, or sulfur atoms, but these results need to be compared to the equilibrium distance of the respective bonds and be weighted accordingly in the bond lengths average. Instead, in the intramonomer bonds average, we choose to include all sp^2-hybridized carbon bonds that are in the main cycles, namely the aromatic cycles that include the shortest path between the monomers extremities. Figure 5.1 contains a few examples of the considered carbon bonds. This choice is made to include polymers from very different families, while still being able to adequately compare similar polymers. For example, thienopyrazine and isothianaphthene have very similar structures: an aromatic cycle fused to the main thiophene backbone. There is no reason why the carbon bonds in isothianaphthene should be considered while the nitrogen bonds in thienopyrazine should not. Therefore, we only consider the effect of the fused aromatic cycles on the main cycle, in this case the thiophene cycle. The choice to include sp^2-hybridized bonds is made to compare fluorene and carbazole units analogously. One can argue that this choice for the parameter Δ is ambiguous. However, Δ

only serves as an intermediate quantity in the prediction model of the following section, and its precise definition is not central to the approach.

5.2.3 Results and discussion

Results of the calculated band gap in function of the quinoid character, represented by Δ, for 87 homopolymers and 113 copolymers are shown in Figure 5.2. One observes the same relation as in Brédas article,[38] with low band gaps lying in between the quinoid and aromatic polymers. The main difference with Brédas' study is that instead of a single polymer with forced geometry, those are 200 different polymers from notably different families, all with relaxed geometrical configurations. Homopolymers and copolymers all seem to follow the same quantitative relationship. The linear fits of Figure 5.2 correspond to the following equations:

$$E_{opt} = (\Delta - 0.991) \times 53.3 \text{ eV} \quad \text{for aromatic} \tag{5.1}$$

$$E_{opt} = (\Delta - 0.993) \times (-39.0 \text{ eV}) \quad \text{for quinoid} \tag{5.2}$$

One can note that the slopes of both fits are not the same, but such a detail does not matter in the construction of the future prediction model, as we shall see later. It is also worth noting that the two fits do not intersect at $\Delta = 1$, but at $\Delta = 0.992$. Even in Brédas' article,[38] where the definition of the parameter was less ambiguous owing to the atomic structure of polythiophene, the fits intersect slightly in the quinoid zone of the graph. This is surprising but understandable, as it supposes that either a true metallic polymer would be slightly quinoid or that some new effect needs to be taken into account for very low band gaps. However, there is a zone present below 0.5 eV that seems to be unattainable. This excluded region is explained by the Peierls theorem, which states that one-dimensional periodic materials have nonzero band gap and that their true metallic state is an unstable one.[95, 169, 182] An example of this fact is polyacetylene, whose band gap is strongly correlated to the chain dimerization.[61, 181, 204, 205] It is also worth noting that this zone depends on the functional used in our DFT calculations, namely the percentage of exact exchange.[61] The B3LYP functional is preferred since

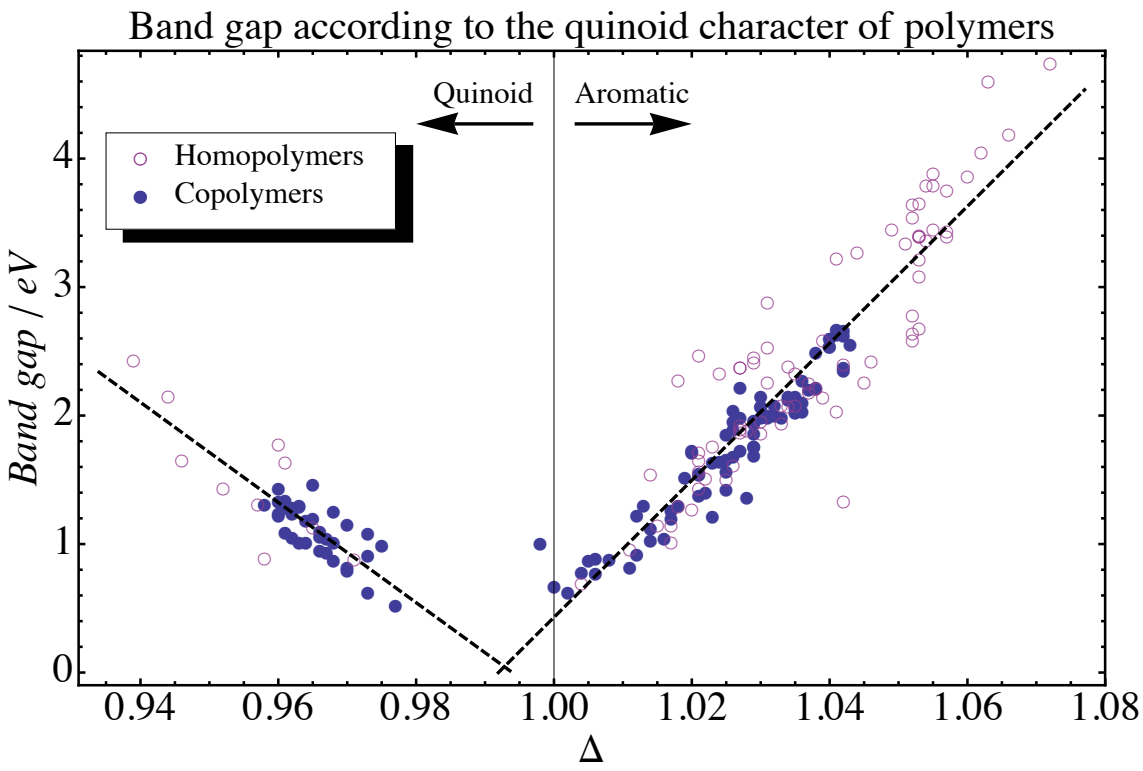

Figure 5.2: Calculated band gap of 87 homopolymers and 113 copolymers according to the quinoid or aromatic character represented by parameter Δ. Quinoid polymers are in the left section of the graph ($\Delta < 1$) while aromatic polymers are on the right ($\Delta > 1$).

its exact exchange percentage is empirically fit to best describe those properties.[20] For the rest of the article, we define Peierls' minimal gap as PMG = 0.5 eV and the quinoid-aromatic threshold at $\Delta = 0.992$.

The existence of such an exclusion zone is emphasized by the fact that there are very similar copolymers that are situated at both limits. For example, polythienopyrazine (pTPy) is a quinoid polymer with $\Delta = 0.957$, while polythienothiazole (pTTz) and polydithienothiophene (pDTT) are both similar aromatic polymers with $\Delta = 1.018$ and $\Delta = 1.023$, respectively. All three of them have the same basic structure, namely, a main thiophene chain with an aromatic cycle fused on it, as illustrated in Figure 5.3. The copolymer of thienopyrazine and thienothiazole (pTPy-TTz) is quinoid, with $\Delta = 0.968$. However, the copolymer of thienopyrazine and dithienothiophene (pTPy-DTT) is aro-

matic, with $\Delta = 1.008$. This supposes that they both got excluded from the Peierls zone, one on the quinoid side and one on the aromatic side. This is further emphasized by the fact that both copolymers have very similar theoretical band gaps: 0.87 and 0.88 eV, respectively.

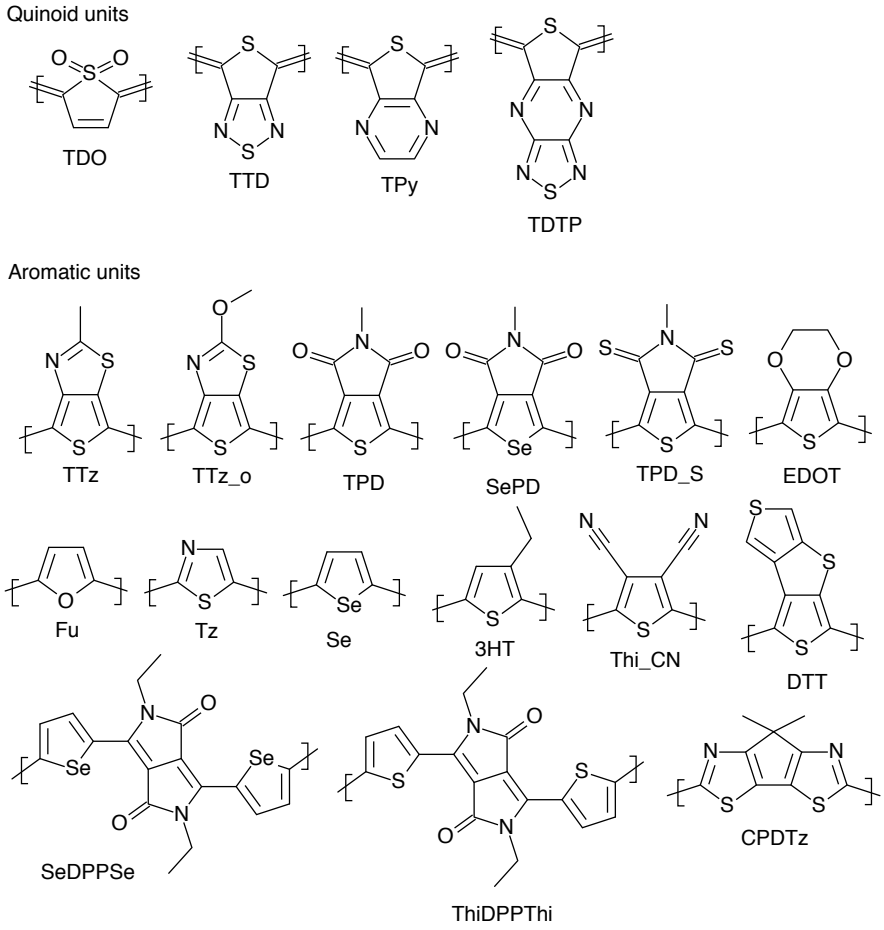

Figure 5.3: Units of copolymers from Table 5.I.

The space of possible polymers is seemingly endless. For example, from a bank of just 100 monomers, there is almost 5000 different copolymers that can combine two of them. The well-known polymer PCDTBT[207] is composed of four monomer units, which is one of almost 4 million possibilities. If we can predict the band gap of copolymers only with data from the monomers and homopolymers, we can guide our design

path without having to launch more expensive and complicated calculations on growingly convoluted polymers. We can also know instantly which are the most suitable candidates to pair with new monomers or find out which couples are the most interesting to consider with a novel synthesizing method.

The two approaches that are considered here are the donor-acceptor one and this study's novel quinoid-aromatic one. Both approaches try to predict the band gap of 113 copolymers from separate, independent DFT calculations on the monomers that compose them or, more precisely, on the homopolymers those monomers form. We prefer to use the energy levels of the homopolymers as they are much closer to the copolymer's than the monomer's energy levels. This is explained by the fact that the homopolymers' calculations include the interactions between the monomers which is crucial to pinpoint the exact energy levels. In addition, the end groups of any finite oligomers dictate whether it stands in its aromatic or quinoid form, which in turn dictates the band gap,[125, 191, 196] as opposed to periodic polymers that can freely alternate between the two forms during a geometrical optimization. For these reasons, the approaches only consider the energy levels of the periodic homopolymers formed by the monomers that are used as the building blocks of the more complex copolymers. The donor-acceptor approach takes the lowest ionization potential (IP) and the highest electronic affinity (EA) of the present homopolymers to calculate the new copolymer band gap $E_{g\,\mathrm{DA}}$ with their difference, according to the equation

$$E_{g\,\mathrm{DA}} = min[\mathrm{IP}] - max[\mathrm{EA}] \tag{5.3}$$

Of course, if Equation 5.3 returns a negative value, the band gap is fixed to zero.

This study's quinoid-aromatic approach assumes that each homopolymer brings either its aromatic or quinoid structure into the copolymer to various degrees and that the band gap is calculated according to the relation of Figure 5.2. However, in order to quantify the degree to which the units will bring their quinoid or aromatic character, it is more appropriate to consider the average of the band gaps instead of the average of the Δ parameters since Δ is ill-defined. Therefore, the band gap of a copolymer composed

of two aromatic or two quinoid monomers is simply the average of the two band gaps, weighted by the number of carbon bonds in each monomer. A copolymer mixing an aromatic and quinoid unit is slightly more complex. Let us assume that both units have the same number of carbon bonds, so that we do not have to worry about the weighted average. If we define the band gap of the homopolymer composed of the aromatic unit as $E_g(A)$ and the quinoid one as $E_g(Q)$, the band gap of the resulting copolymer is simply

$$E_{g\,\mathrm{qui}} = \frac{\left|E_g(A) - E_g(Q)\right|}{2} + PMC \tag{5.4}$$

where *PMC* is Peierls' minimal gap, fixed at 0.5 eV. The previous examples are specific cases of a general approach. Assuming N is the number of carbon bonds in a specific unit, E_g is the band gap of the homopolymer made from this unit, and q the value $+1$ for aromatic units and -1 for quinoid ones, the general formula to predict the band gap of a copolymer is

$$E_{g\,\mathrm{qui}} = \frac{\left|\sum qN(E_g - PMC)\right|}{\sum N} + PMC \tag{5.5}$$

where the sums are over all units that compose the copolymer. The standard deviation of Equation 5.5 compared to the DFT calculated band gap is 0.4 eV. A greater value of *PMC* lowers the standard deviation. For this reason, the excluded zone width was taken to be as big as possible, but still smaller than the lowest band gap we calculated of 0.52 eV, which was, in our case, with the poly(thienothiazole-thienopyrrole) copolymer.

Figure 5.4 compares the predictions of the two approaches. One can see that even though the donor-acceptor approach is sensible, it completely fails, even in a qualitative way, to predict the band gaps of copolymers. This approach also widely underestimates the band gaps, as shown by the fact that the majority of the points are below the dashed line, and even returns zero band gaps for a lot of polymers. The standard deviation of the donor-acceptor approach is 0.6 eV, which is greater than the previously mentioned 0.4 eV value for the quinoid-aromatic approach.

The quinoid-aromatic method, while lacking precise quantitative predictions, still holds very well in a qualitative way. After establishing Equation 5.5, we attempted to

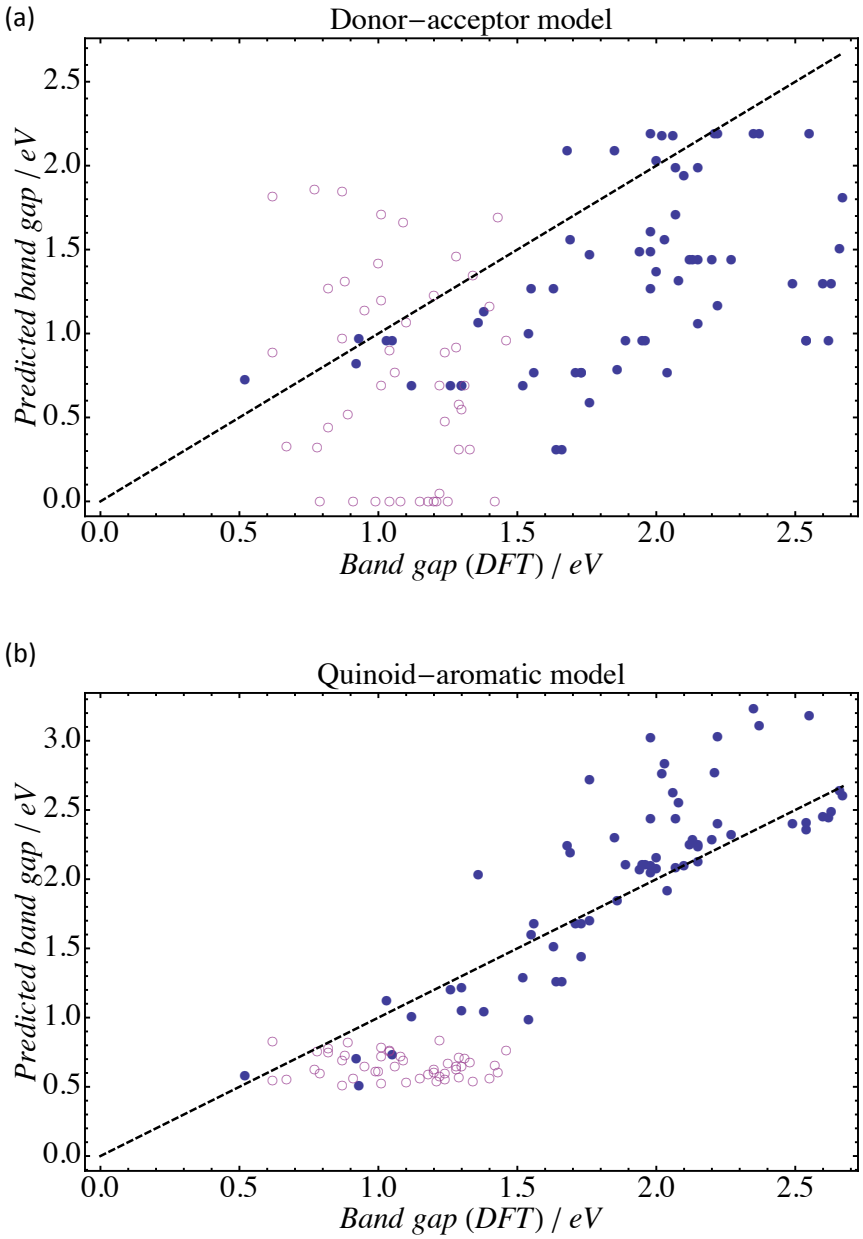

Figure 5.4: Comparison of the two approaches for designing low band gap polymers. The x-axis represents the model's prediction for the copolymer band gap based simply on the data of the homopolymers. The y-axis represents the more demanding DFT calculation of the band gap of the copolymers. The dashed line is the $y = x$ line. The empty circles were all calculated after the models were established. (a) Donor-acceptor approach, calculated with Equation 5.3. (b) Quinoid-aromatic approach, calculated with Equation 5.5.

test and refine our method by finding low band gap polymers. Therefore, from our results on 83 homopolymers, all the copolymers that the quinoid-aromatic approach predicted to have a band gap lower than 1 eV were calculated more thoroughly with DFT in order to verify their band gaps and to obtain the levels of their ionization potentials and electronic affinities. Those subsequent calculations are represented by the empty circles of Figure 5.4. According to density functional theory, half of those promising copolymers have indeed a band gap under 1 eV, while all of them are still under 1.5 eV. By comparison, some of the polymers that the donor-acceptor method predicts to have a band gap under 1 eV actually have, according to complete DFT calculations, band gaps of up to 2.5 eV. The quantitative predictive power of the donor-acceptor approach is found to be very unreliable. The quinoid-aromatic approach is a more efficient way to span the tens of thousands of combinations of monomers, before starting more expensive calculations or long synthesis processes.

As a side note, a polymer that balances between its aromatic and quinoid form has equal length carbon bonds through the polymer chain. However, one can ask if this form is stable, if the polymer is fragile, and how it deforms when optically excited. All those factors affect the charge mobility of the polymer, a crucial parameter in organic photonics.[214] Time-dependent density functional theory calculations were conducted on tetramers in order to find out whether low band gap polymers would have lower reorganization energy upon excitation, and therefore a better mobility, according to Marcus theory.[17, 21, 145] The reorganization energy is obtained by doing a geometrical optimization of an optically excited tetramer with TDDFT and by calculating the energy gained by the geometrical reorganization of the atoms. This energy is then compared to the band gap of the polymer, which is nonetheless very strongly correlated with the band gap of the tetramer.[35] The results are shown in Figure 5.5. It is clearly shown that oligomers with lower band gaps have also lower reorganization energy.

Table 5.I and Figure 5.3 report 31 stable copolymers with theoretical band gaps between 0.75 and 1.30 eV, 10 of which are under the 1 eV threshold. Each one of them is designed with the quinoid-aromatic approach in mind, which consists of mixing a quinoid and an aromatic monomer in order to find a balance between those two forms

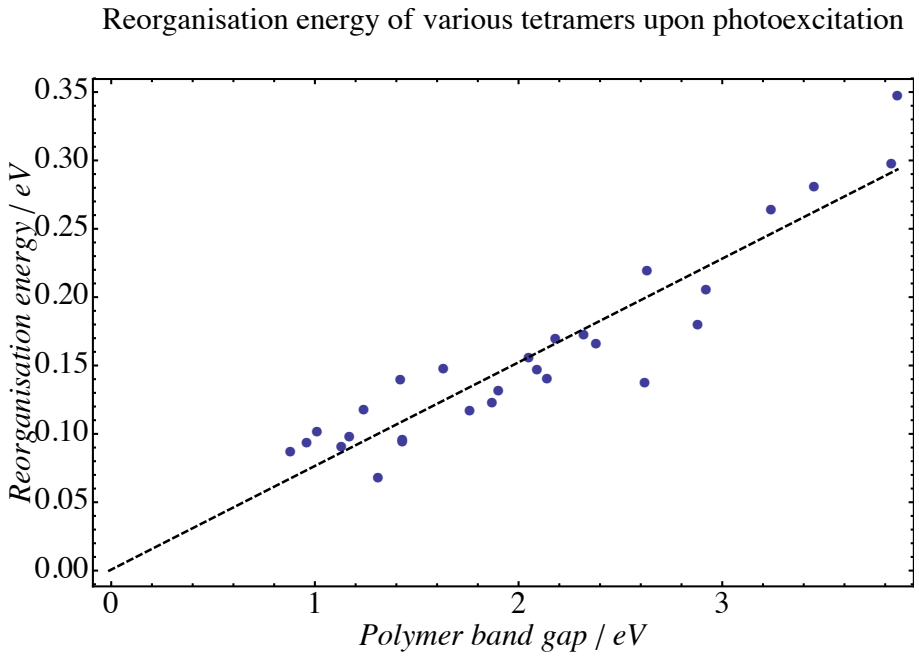

Figure 5.5: Reorganization energy of tetramers upon photoexcitation calculated with TDDFT, according to the homopolymer's band gap calculated with DFT. The dashed line is a linear fit of the data points.

and lower the band gap.

The band gaps and ionization potentials are calculated with linear fits in order to match empirical data of polymers more adequately, according to the following equations:[23]

$$E_{opt} = 0.68 * (\mathrm{LUMO}_{\mathrm{DFT/B3LYP}} - \mathrm{HOMO}_{\mathrm{DFT/B3LYP}}) + 0.33\ \mathrm{eV} \tag{5.6}$$

$$\mathrm{HOMO} = 0.68 * \mathrm{HOMO}_{\mathrm{DFT/B3LYP}} - 1.92\ \mathrm{eV} \tag{5.7}$$

In particular, Equation 6 provides the experimental optical gap of polymers within 0.1 eV.[23] Table 5.II compares the theoretical gap to the experimental one for a few known polymers: poly(3-hexylthiophene) (P3HT),[102] poly(carbazole-dithophene-benzothiadiazole) (PCDTBT),[167] poly(diketopyrrolopyrrole-quaterthiophene) (PDPPQT),[231] and poly(benzodithiophene-thienothiophene) (PBDTTT).[141] The

ionization potentials are all over 5 eV in order to limit ourselves to polymers that would be near or over the air stability threshold, which is believed to be around 5.3 eV.[31, 58] DFT calculations are an easy way to identify which units are quinoid and which units simply have a weaker aromatic character, and it was found that true stable quinoid units remain pretty scarce. The quinoid units listed in Table 5.I were the most promising ones. Those units are thiophene dioxide (TDO), thienothiadizaole (TTD), thienopyrazine (TPy), and thiadiazolothienopyrazine (TDTP), all of which have been already synthesized on their own.[184, 185]

Out of these results, we single out two interesting cases: poly(TTD-SePD) and poly(TTD-TPD). Both polymers are predicted to have a very low band gaps of 0.75 and 0.85 eV, respectively, and high ionization potentials that indicate a good air stability. They both contain symmetrical units, meaning that regioregularity should not be a problem for the synthesis. Solubility can easily be improved by adding alkyl side chains to the SePD or the TPD unit without affecting the electronic properties. Moreover, they demonstrate the advantages of the quinoid-aromatic approach since the donor-acceptor one returns high band gap values around 1.85 eV for both copolymers. The TTD, SePD, and TPD homopolymers all have band gaps around 2 eV, but the mix of the quinoid TTD and the aromatic SePD or TPD lowers the band gap to values under 1 eV.

5.2.4 Conclusions

In conclusion, low band gaps are obtained with polymers that carefully balance between their quinoid and aromatic structures. This approach is more reliable than the more commonly used donor-acceptor approach of polymer design. Low band gap polymers possess lower reorganization energy according to time-dependent density functional theory which is correlated to a higher charge mobility. New stable polymers with predicted band gaps around 1 eV are shown. The prediction efficiency of this promising approach could be improved if we include other information on the homopolymer like torsion angle[34, 36] or individual bond lengths instead of averages. Consideration of the non-carbon atoms could also help to predict the individual energy levels[45, 121] instead of only the band gaps.

Table 5.I: **Stable Low Band Gap Polymers Found with the Quinoid-Aromatic Approach**[†]

	E_g (eV)	IP (eV)		E_g (eV)	IP (eV)
TDO-DTT	0.95 (0.91)	5.43 (5.16)	TTD-SePD	0.75 (0.62)	5.22 (4.86)
TDO-EDOT	1.00 (0.99)	5.15 (4.75)	TTD-Thi_CN	0.78 (0.67)	5.71 (5.57)
TDO-SeDPPSe	1.04 (1.04)	5.40 (5.12)	TTD-TPD	0.85 (0.77)	5.27 (4.93)
TDO-3HT	1.07 (1.08)	5.51 (5.28)	TTD-ThiDPPThi	0.89 (0.82)	5.14 (4.73)
TDO-TTz_o	1.11 (1.15)	5.39 (5.10)	TTD-TPDf	0.92 (0.87)	5.29 (4.96)
TDO-CPDTz	1.15 (1.21)	5.60 (5.41)	TTD-SeDPPSe	0.98 (0.95)	5.18 (4.80)
TDO-TTz	1.18 (1.25)	5.44 (5.18)	TTD-TPD_S	1.01 (1.00)	5.53 (5.31)
TDO-Se	1.30 (1.42)	5.76 (5.65)	TTD-CPDTz	1.02 (1.01)	5.17 (4.78)
TDTP-SeDPPSe	1.04 (1.04)	5.36 (5.06)	TTD-DTT	1.07 (1.09)	5.10 (4.67)
TDTP-CPDTz	1.08 (1.10)	5.39 (5.10)	TTD-Fu	1.20 (1.28)	5.09 (4.66)
TDTP-EDOT	1.14 (1.20)	5.03 (4.57)	TTD-3HT	1.24 (1.34)	5.04 (4.59)
TDTP-DTT	1.17 (1.24)	5.29 (4.96)	TTD-Se	1.30 (1.43)	5.19 (4.81)
TDTP-Se	1.20 (1.28)	5.42 (5.14)	TPy-SeDPPSe	0.75 (0.62)	4.99 (4.51)
TDTP-3HT	1.20 (1.29)	5.26 (4.92)	TPy-DTT	0.93 (0.88)	4.95 (4.46)
TDTP-TTz_o	1.21 (1.29)	5.24 (4.88)	TPy-Tz	1.15 (1.20)	5.25 (4.89)
TDTP-TTz	1.23 (1.33)	5.28 (4.94)			

[†] Theoretical properties shown are the optical band gap and the ionization potential, and were corrected respectively with Equations 5.6 and 5.7. Values in parentheses correspond to the corresponding DFT/B3LYP data.

Table 5.II: **Comparison between the Theoretical Band Gap Calculated with Equation 5.6 and the Experimental Optical Gap for Known Polymers.**

Polymer	Theoretical gap[23]	Experimental gap[102, 141, 167, 231]
P3HT	1.75	1.8
PCDTBT	1.80	1.9
PDPPQT	1.41	1.4
PBDTTT	1.62	1.6

Acknowledgements. We thank the funding support of NSERC and the PV Innovation Network. N.B. acknowledges the Vanier Scholarship program. The calculations were done on the computational infrastructure provided by Calcul Québec and Compute Canada. We also acknowledge the support of the Regroupement québécois sur les matériaux de pointe (RQMP) and the Centre québécois sur les matériaux fonctionnels (CQMF).

CHAPITRE 6

CONCLUSION

Cette thèse s'attarde sur la caractérisation et l'exploration des méthodes de design de polymères pour l'électronique organique. La photovoltaïque organique est un domaine en plein essor, ce qui signifie qu'il y a encore place à beaucoup d'améliorations. Les défis actuels au niveau du design de polymères sont néanmoins nombreux, et il n'est pas rare d'avoir à sacrifier des propriétés intéressantes au profit d'autres. Il est important d'avoir des polymères solubles, peu coûteux, stables, possédant un faible band gap et des niveaux électroniques judicieusement alignés.

La solubilité est généralement assurée par l'augmentation de l'entropie du polymère créée par l'ajout de groupements fonctionnels et de longues chaines de carbone. Néanmoins, ces chaines ont des effets importants et particulièrement difficiles à prédire sur la morphologie et la miscibilité des composantes. La morphologie du dispositif organique influence grandement les rendements des cellules solaires, mais elle peut difficilement être contrôlée et joue, pour le moment, un rôle mineur sur le design de nouveaux polymères. La morphologie est souvent considérée lors de la synthèse du polymère, et sort donc du contexte de cette thèse qui est plutôt centrée sur l'aspect théorique sur une échelle atomique et électronique.

La stabilité des polymères est étudiée au Chapitre 2 dans le cadre du diketopyrrolopyrrole. En effet, les polymères aux propriétés électroniques intéressantes sont parfois malheureusement instables. La technique de sulfuration présentée dans ce chapitre a pour effet de diminuer le band gap au coût de la stabilité du polymère. Il est donc important d'identifier les causes de cette instabilité afin de pouvoir l'éviter lors du design de nouveaux polymères. Un lien est établi entre la stabilité des composantes et la profondeur du puits de potentiel autour des positions d'équilibre calculées des composés de diketopyrrolopyrrole et de thienopyrroledione. Ce lien permet d'augmenter la stabilité des polymères en substituant les thiophènes par des furanes, ce qui redonnant une forme plane au polymère et assurait un profond puits de potentiel.

Il serait judicieux d'explorer la présence de ce lien pour d'autres composés organiques instables. Considérant que le polythiophène n'est pas plan et possède donc un faible puits de potentiel, le lien établi dans ce chapitre ne peut être généralisé. Il faut considérer les niveaux électroniques, qui influencent les procédés d'oxydation, et la disposition de la charge dans les liens interatomiques, qui témoignent de leur stabilité et ont un effet sur la dégradation. Puisqu'aucun composé contenant du soufre n'était stable à la lumière dans cette étude, le problème reste encore incomplet et les causes dépassent la simple planarité.

La technique de sulfuration est cependant très utile puisque son effet de diminution du band gap s'est avéré systématique sur tous les composants. Il serait donc très intéressant de l'appliquer sur d'autres molécules organiques contenant des groupements carbonyles. Les calculs théoriques sont très efficaces pour prédire le band gap des composés, et il serait donc possible de facilement explorer l'espace moléculaire.

Une autre limitation importante de la photovoltaïque organique est la perte énergétique située entre l'absorption de la lumière et la collecte des porteurs de charges aux électrodes. L'origine de cette perte énergétique est encore mal comprise, et il est donc nécessaire d'étudier la dynamique électronique des porteurs de charge des dispositifs photovoltaïques organiques. Le technique de *femtosecond stimulated Raman spectroscopy*, décrite au Chapitre 3 permet de voir l'évolution des vibrations moléculaires sur une échelle de temps de la femtoseconde. La difficulté de la caractérisation de cette dynamique consiste à établir le lien entre les spectres de vibrations et les états électroniques d'excitons, de polarons et de séparation de charges. Cette caractérisation est grandement simplifiée par les calculs théoriques de vibration de l'état fondamental et des états excités qui peuvent être comparés aux spectres expérimentaux. De plus, le fait que la séparation de charge se produise avant 300 fs est un nouveau résultat controversé. Il est donc important d'avoir des calculs théoriques qui corroborent les résultats de l'étude. Il serait judicieux de pouvoir accomplir cette technique de sonde sur d'autres polymères, spécialement sur des polymères des dispositifs à faible efficacité afin de pouvoir tester si le délai de séparation de charge est plus long dans ceux-ci. Cela signifierait que le court délai de 300 fs est responsable de la haute efficacité et qu'il serait ainsi nécessaire de

comprendre ses causes afin de les reproduire.

Bien que les calculs théoriques permettent une amélioration de la caractérisation des polymères existants, il faut également définir leur place dans le design des polymères avant l'étape de synthèse. L'utilité des calculs théoriques est autant dans la rapidité par rapport au temps nécessaire afin d'effectuer l'expérience que dans la possibilité de sonder des propriétés électroniques inaccessibles aux équipements de laboratoire actuels. La possibilité de prédire l'efficacité des cellules solaires à partir de calculs théoriques utilisés avec le modèle de Scharber est ainsi étudiée dans le Chapitre 4. Cette étude a permis d'établir que la précision des calculs sur les valeurs des band gaps ainsi que du voltage du dispositif sont de l'ordre du dixième d'électronvolt. Cette précision n'est cependant pas partagée pour le potentiel d'ionisation et l'affinité électronique. Ces deux propriétés ont une influence directe sur la stabilité à l'air et au transfert de charge à l'hétérojonction. Il est donc crucial d'augmenter la précision sur ces valeurs pour s'assurer de la viabilité du dispositif. La caractérisation de la fonctionnelle B3LYP dans ce chapitre devrait donc être répétée pour différentes fonctionnelles, ou pour des méthodes de calculs réputées pour avoir une meilleure précision sur les niveaux électroniques, comme la GW.

Il est également important de faire le suivi des polymères proposés aux Chapitres 4 et 5. Les rares polymères qui ont été synthétisés suite à cette étude semblent respecter les prédictions théoriques. La synthèse de ces candidats est très importante pour confirmer le pouvoir prédictif de ces méthodes, mais également pour s'assurer de l'applicabilité des outils théoriques développés au cours de cette thèse.

Les calculs DFT sont également utiles pour établir des liens entre les propriétés et ainsi les utiliser à notre avantage dans le design de polymères efficaces en électronique organique. Un défi principal de ce domaine est la quête vers des polymères à petits band gaps, pouvant ainsi fonctionner dans l'infrarouge, à plus basse énergie ou pouvant être de bons candidats pour des transistors. Les polymères à petits band gaps sont également utiles dans l'ajustement des valeurs des band gaps dans le design de polymères photovoltaïques nécessitant un band gap précis situé entre 1,1 et 1,4 eV. L'étude du Chapitre 5 établit un lien entre le band gap d'un polymère et la forme structurale, aromatique ou quinoide, adoptée par les atomes de carbone composant sa chaîne principale. La forme

structurale est presque impossible à sonder expérimentalement et les calculs théoriques sont nécessaires pour comprendre les liens qui l'unissent aux propriétés électroniques. Ce lien est exploité pour établir un modèle de prédiction des band gaps de copolymères surpassant l'approche standard de donneur-accepteur utilisée dans la littérature. Cependant, l'approche aromatique-quinoide a été développée dans un esprit de simplicité et d'accessibilité, et il reste encore à développer son efficacité. Par exemple, il faudrait l'appliquer aux copolymères regroupant trois ou plus monomères dans sa cellule primitive pour voir si l'approche s'applique toujours dans cette situation. De plus, le fait de considérer les atomes qui ne sont pas du carbone pourrait grandement l'améliorer. Il serait également possible de s'intéresser à la prédiction des niveaux électroniques plutôt que le band gap dans le but d'avoir une description plus complète du polymère. De plus, même si l'approche aromatique-quinoide s'applique de façon systématique à tous les polymères étudiés, peu importe leurs composantes de base, elle est incomplète puisqu'elle ne s'applique aux polymères de type *ladder* où les liens intermonomères n'existent pas.

Finalement, les travaux de cette thèse montrent l'utilité des calculs théoriques de DFT dans le cadre de la photovoltaïque organique. Les méthodes plus avancées telles la GW ou les fonctionnelles plus complexes que la B3LYP ne font pas l'objet de ce travail puisqu'il est principalement centré sur les collaborations concrètes avec les groupes de recherches expérimentaux, spécialement avec les chimistes de synthèse. La complexité de ces dispositifs nécessite la pluridisciplinarité entre physiciens et chimistes, entre théoriciens et expérimentateurs. Il est donc important d'utiliser et de caractériser les méthodes de calculs établies, simples, connues et rapides, consistant le compromis adéquat. Le design des polymères se base d'abord sur l'exploration de l'espace moléculaire, et cette exploration doit se faire rapidement sur un grand nombre de molécules, tout en utilisant les liens établis pour guider notre recherche. Le développement des méthodes de calculs pourra également s'avérer crucial pour comprendre les propriétés électroniques des interfaces des dispositifs organiques, qui échappent encore à la compréhension des scientifiques. Les exemples cités précédemment constituent un excellent point d'exploration pour de nombreuses futures collaborations.

BIBLIOGRAPHIE

[1] U.S. Energy Information Administration. Levelized cost of new generation resources in the annual energy outlook 2013, consulté le 11 février 2014. http://www.eia.gov/forecasts/aeo/electricity_generation.cfm.

[2] Ayyappanpillai Ajayaghosh. Donor-acceptor type low band gap polymers: Polysquaraines and related systems. *Chem. Soc. Rev.*, 32:181–191, 2003. URL http://dx.doi.org/10.1039/B204251G.

[3] Maher Al-Ibrahim, H.-Klaus Roth, Uladzimir Zhokhavets, Gerhard Gobsch et Steffi Sensfuss. Flexible large area polymer solar cells based on poly(3-hexylthiophene)/fullerene. *Sol. Energy Mater. Sol. Cells*, 85(1):13–20, 2005. ISSN 0927-0248. URL http://www.sciencedirect.com/science/article/pii/S0927024804001187.

[4] Kaj van Alem, Ernst J. R. Sudhölter et Han Zuilhof. Quantum chemical calculations on α-substituted ethyl cations: A comparison between b3lyp and post-hf methods. *J. Phys. Chem. A*, 102(52):10860–10868, 1998. URL http://pubs.acs.org/doi/abs/10.1021/jp983114u.

[5] Nicolas Allard, Réda Badrou Aïch, David Gendron, Pierre-Luc T. Boudreault, Christian Tessier, Salima Alem, Shing-Chi Tse, Ye Tao et Mario Leclerc. Germafluorenes: New heterocycles for plastic electronics. *Macromolecules*, 43(5):2328–2333, 2010. URL http://pubs.acs.org/doi/abs/10.1021/ma9025866.

[6] Nicolas Allard, Ahmed Najari, Jean-Remi Pouliot, Agnieszka Pron, Francois Grenier et Mario Leclerc. Easy and versatile synthesis of new poly(thieno[3,4-d]thiazole)s. *Polym. Chem.*, 3:2875–2879, 2012. URL http://dx.doi.org/10.1039/C2PY20422C.

[7] K. Aryanpour, D. Psiachos et S. Mazumdar. Theory of interfacial charge-transfer

complex photophysics in π-conjugated polymer-fullerene blends. *Phys. Rev. B*, 81:085407, Feb 2010. URL http://link.aps.org/doi/10.1103/PhysRevB.81.085407.

[8] Raja Shahid Ashraf, Auke Jisk Kronemeijer, David Ian James, Henning Sirringhaus et Iain McCulloch. A new thiophene substituted isoindigo based copolymer for high performance ambipolar transistors. *Chem. Commun.*, 48:3939–3941, 2012. URL http://dx.doi.org/10.1039/C2CC30169E.

[9] A. Azazi, A. Mabrouk et K. Alimi. Theoretical investigation on the photophysical properties of low-band-gap copolymers for photovoltaic devices. *Comput. Theor. Chem.*, 978(1-3):7–15, 2011. ISSN 2210-271X. URL http://www.sciencedirect.com/science/article/pii/S2210271X11004440.

[10] Brian Azzopardi, Christopher J. M. Emmott, Antonio Urbina, Frederik C. Krebs, Joseph Mutale et Jenny Nelson. Economic assessment of solar electricity production from organic-based photovoltaic modules in a domestic environment. *Energy Environ. Sci.*, 4:3741–3753, 2011. URL http://dx.doi.org/10.1039/C1EE01766G.

[11] Réda Badrou Aïch, Nicolas Blouin, Angélique Bouchard et Mario Leclerc. Electrical and Thermoelectric Properties of Poly(2,7-Carbazole) Derivatives. *Chem. Mater.*, 21(4):751–757, février 2009. URL http://pubs.acs.org/doi/abs/10.1021/cm8031175.

[12] A A Bakulin, A Rao, V G Pavelyev, P H M van Loosdrecht, M S Pshenichnikov, D Niedzialek, Jerome Cornil, David Beljonne et Richard H Friend. The Role of Driving Energy and Delocalized States for Charge Separation in Organic Semiconductors. *Science*, 335(6074):1340–1344, 2012. URL http://www.sciencemag.org/content/335/6074/1340.abstract.

[13] Artem A Bakulin, Dmitry Martyanov, Dmitry Yu Paraschuk, Paul H M van Loos-

drecht et Maxim S Pshenichnikov. Charge-transfer complexes of conjugated polymers as intermediates in charge photogeneration for organic photovoltaics. *Chem. Phys. Lett.*, 482(1-3):99–104, 2009. URL http://www.sciencedirect.com/science/article/pii/S0009261409011580.

[14] Natalie Banerji. Sub-picosecond delocalization in the excited state of conjugated homopolymers and donor–acceptor copolymers. *J. Mater. Chem. C*, 1(18):3052, 2013. URL http://pubs.rsc.org/en/content/articlelanding/2013/tc/c3tc00005b.

[15] Natalie Banerji, Sarah R Cowan, Mario Leclerc, Eric Vauthey et Alan J Heeger. Exciton Formation, Relaxation, and Decay in PCDTBT. *J. Am. Chem. Soc.*, 132 (49):17459–17470, 2010. URL http://pubs.acs.org/doi/abs/10.1021/ja105290e.

[16] Natalie Banerji, Eric Gagnon, Pierre-Yves Morgantini, Sebastian Valouch, Ali Reza Mohebbi, Jung Hwa Seo, Mario Leclerc et Alan J Heeger. Breaking Down the Problem: Optical Transitions, Electronic Structure, and Photoconductivity in Conjugated Polymer PCDTBT and in Its Separate Building Blocks. *J. Phys. Chem. C*, 116(21):11456–11469, mai 2012. URL http://pubs.acs.org/doi/abs/10.1021/jp301639e.

[17] Paul F. Barbara, Thomas J. Meyer et Mark A. Ratner. Contemporary issues in electron transfer research. *J. Phys. Chem.*, 100(31):13148–13168, 1996. URL http://pubs.acs.org/doi/abs/10.1021/jp9605663.

[18] S. Barth et H. Bässler. Intrinsic photoconduction in ppv-type conjugated polymers. *Phys. Rev. Lett.*, 79:4445–4448, Dec 1997. URL http://link.aps.org/doi/10.1103/PhysRevLett.79.4445.

[19] Serge Beaupré, Michel Belletête, Gilles Durocher et Mario Leclerc. Rational design of poly(2,7-carbazole) derivatives for photovoltaic applications. *Ma-*

cromol. Theory Simul., 20(1):13–18, 2011. ISSN 1521-3919. URL http://dx.doi.org/10.1002/mats.201000061.

[20] Axel D. Becke. Density-functional thermochemistry. iii. the role of exact exchange. *J. Chem. Phys.*, 98(7):5648–5652, 1993. URL http://link.aip.org/link/?JCP/98/5648/1.

[21] David Beljonne, Jérôme Cornil, Luca Muccioli, Claudio Zannoni, Jean-Luc Brédas et Frédéric Castet. Electronic processes at organic-organic interfaces: Insight from modeling and implications for opto-electronic devices. *Chem. Mater.*, 23 (3):591–609, 2011. URL http://pubs.acs.org/doi/abs/10.1021/cm1023426.

[22] Nicolas Berton, Chiara Ottone, Vanessa Labet, Rémi de Bettignies, Séverine Bailly, André Grand, Christophe Morell, Saïd Sadki et Frédéric Chandezon. New alternating copolymers of 3,6-carbazoles and dithienylbenzothiadiazoles: Synthesis, characterization, and application in photovoltaics. *Macromol. Chem. Phys.*, 212(19):2127–2141, 2011. ISSN 1521-3935. URL http://dx.doi.org/10.1002/macp.201100209.

[23] Nicolas Bérubé, Vincent Gosselin, Josiane Gaudreau et Michel Côté. Designing polymers for photovoltaic applications using ab initio calculations. *J. Phys. Chem. C*, 117(16):7964–7972, 2013. URL http://pubs.acs.org/doi/abs/10.1021/jp309800f.

[24] Sambhu Bhadra, Dipak Khastgir, Nikhil K. Singha et Joong Hee Lee. Progress in preparation, processing and applications of polyaniline. *Prog. Polym. Sci.*, 34 (8):783–810, 2009. ISSN 0079-6700. URL http://www.sciencedirect.com/science/article/pii/S0079670009000355.

[25] Johan C. Bijleveld, Veronique S. Gevaerts, Daniele Di Nuzzo, Mathieu Turbiez, Simon G. J. Mathijssen, Dago M. de Leeuw, Martijn M. Wienk et René A. J. Janssen. Efficient solar cells based on an easily accessible diketopyrrolopyrrole

polymer. *Adv. Mater.*, 22(35):E242–E246, 2010. ISSN 1521-4095. URL http://dx.doi.org/10.1002/adma.201001449.

[26] Johan C. Bijleveld, Bram P. Karsten, Simon G. J. Mathijssen, Martijn M. Wienk, Dago M. de Leeuw et Rene A. J. Janssen. Small band gap copolymers based on furan and diketopyrrolopyrrole for field-effect transistors and photovoltaic cells. *J. Mater. Chem.*, 21:1600–1606, 2011. URL http://dx.doi.org/10.1039/C0JM03137B.

[27] Johan C. Bijleveld, Arjan P. Zoombelt, Simon G. J. Mathijssen, Martijn M. Wienk, Mathieu Turbiez, Dago M. de Leeuw et René A. J. Janssen. Poly(diketopyrrolopyrrole-terthiophene) for ambipolar logic and photovoltaics. *J. Am. Chem. Soc.*, 131(46):16616–16617, 2009. URL http://pubs.acs.org/doi/abs/10.1021/ja907506r.

[28] Laure Biniek, Bob C. Schroeder, Christian B. Nielsen et Iain McCulloch. Recent advances in high mobility donor-acceptor semiconducting polymers. *J. Mater. Chem.*, 22:14803–14813, 2012. URL http://dx.doi.org/10.1039/C2JM31943H.

[29] Eric R. Bittner et Carlos Silva. Noise-induced quantum coherence drives photo-carrier generation dynamics at polymeric semiconductor heterojunctions. *Nat. Commun.*, 5:3119, 2014. URL http://www.nature.com/ncomms/2014/140129/ncomms4119/full/ncomms4119.html.

[30] Nicolas Blouin, A Michaud et M Leclerc. A Low-Bandgap Poly(2,7-Carbazole) Derivative for Use in High-Performance Solar Cells. *Adv. Mater.*, 19(17):2295–2300, septembre 2007. URL http://onlinelibrary.wiley.com/doi/10.1002/adma.200602496/abstract.

[31] Nicolas Blouin, Alexandre Michaud, David Gendron, Salem Wakim, Emily Blair, Rodica Neagu-Plesu, Michel Belletête, Gilles Durocher, Ye Tao et Mario Leclerc. Toward a rational design of poly(2,7-carbazole) derivatives for solar cells. *J. Am.*

Chem. Soc., 130(2):732–742, 2008. URL http://pubs.acs.org/doi/abs/10.1021/ja0771989.

[32] BP. Statistical review of world energy 2013, consulté le 11 février 2014. http://www.bp.com/content/dam/bp/pdf/statistical-review/statistical_review_of_world_energy_2013.pdf.

[33] J. L. Brédas. Relationship between band gap and bond length alternation in organic conjugated polymers. *J. Chem. Phys.*, 82(8):3808–3811, 1985. URL http://link.aip.org/link/?JCP/82/3808/1.

[34] J. L. Brédas et A. J. Heeger. Theoretical investigation of gas-phase torsion potentials along conjugated polymer backbones: Polyacetylene, polydiacetylene, and polythiophene. *Macromolecules*, 23(4):1150–1156, 1990. URL http://pubs.acs.org/doi/abs/10.1021/ma00206a038.

[35] J. L. Brédas, R. Silbey, D. S. Boudreaux et R. R. Chance. Chain-length dependence of electronic and electrochemical properties of conjugated systems: Polyacetylene, polyphenylene, polythiophene, and polypyrrole. *J. Am. Chem. Soc.*, 105(22):6555–6559, 1983. URL http://pubs.acs.org/doi/abs/10.1021/ja00360a004.

[36] J. L. Brédas, G. B. Street, B. Thémans et J. M. André. Organic polymers based on aromatic rings (polyparaphenylene, polypyrrole, polythiophene): Evolution of the electronic properties as a function of the torsion angle between adjacent rings. *J. Chem. Phys.*, 83(3):1323–1329, 1985. URL http://link.aip.org/link/?JCP/83/1323/1.

[37] Jean-Luc Brédas, David Beljonne, Veaceslav Coropceanu et Jérôme Cornil. Charge-transfer and energy-transfer processes in π-conjugated oligomers and polymers: A molecular picture. *Chem. Rev.*, 104(11):4971–5004, 2004. URL http://pubs.acs.org/doi/abs/10.1021/cr040084k.

[38] J.L. Brédas. Theoretical design of polymeric conductors. *Synth. Met.*, 17(1-3): 115–121, 1987. ISSN 0379-6779. URL http://www.sciencedirect.com/science/article/pii/0379677987907259.

[39] Eva Bundgaard et Frederik C. Krebs. Low band gap polymers for organic photovoltaics. *Sol. Energy Mater. Sol. Cells*, 91(11):954–985, 2007. ISSN 0927-0248. URL http://www.sciencedirect.com/science/article/pii/S0927024807000451.

[40] Karl Burkart. Sneak peak of konarka's roll-up solar charger, consulté le 28 février 2014. http://www.mnn.com/green-tech/gadgets-electronics/blogs/sneak-peak-of-konarkas-roll-up-solar-charger.

[41] Klaus Capelle. A bird's-eye view of density-functional theory. *Braz. J. Phys.*, 36:1318–1343, 12 2006. ISSN 0103-9733. URL http://www.scielo.br/scielo.php?script=sci_arttext&pid=S0103-97332006000700035&nrm=iso.

[42] Claudia M. Cardona, Wei Li, Angel E. Kaifer, David Stockdale et Guillermo C. Bazan. Electrochemical considerations for determining absolute frontier orbital energy levels of conjugated polymers for solar cell applications. *Adv. Mater.*, 23 (20):2367–2371, 2011. ISSN 1521-4095. URL http://dx.doi.org/10.1002/adma.201004554.

[43] Chiu-Hsiang Chen, Chao-Hsiang Hsieh, Martin Dubosc, Yen-Ju Cheng et Chain-Shu Hsu. Synthesis and characterization of bridged bithiophene-based conjugated polymers for photovoltaic applications: Acceptor strength and ternary blends. *Macromolecules*, 43(2):697–708, 2010. URL http://pubs.acs.org/doi/abs/10.1021/ma902206u.

[44] Guan-Yu Chen, Chien-Ming Chiang, Dhananjay Kekuda, Shang-Che Lan, Chih-Wei Chu et Kung-Hwa Wei. Synthesis and characterization of a narrow-bandgap

polymer containing alternating cyclopentadithiophene and diketo-pyrrolo-pyrrole units for solar cell applications. *J. Polym. Sci., Part A: Polym. Chem.*, 48(7): 1669–1675, 2010. ISSN 1099-0518. URL http://dx.doi.org/10.1002/pola.23931.

[45] Hsiang-Yu Chen, Jianhui Hou, Shaoqing Zhang, Yongye Liang, Guanwen Yang, Yang Yang, Luping Yu, Yue Wu et Gang Li. Polymer solar cells with enhanced open-circuit voltage and efficiency. *Nat. Photonics*, 3(11):649–653, 2009. URL http://dx.doi.org/10.1038/nphoton.2009.192.

[46] Junwu Chen et Yong Cao. Development of novel conjugated donor polymers for high-efficiency bulk-heterojunction photovoltaic devices. *Acc. Chem. Res.*, 42(11):1709–1718, 2009. URL http://pubs.acs.org/doi/abs/10.1021/ar900061z.

[47] Wen-Chang Chen et Samson A. Jenekhe. Model compound studies of small bandgap conjugated poly(heteroarylene methines). *Macromol. Chem. Phys.*, 199(4):655–666, 1998. ISSN 1521-3935. URL http://dx.doi.org/10.1002/(SICI)1521-3935(19980401)199:4<655::AID-MACP655>3.0.CO;2-U.

[48] Wen-Chang Chen, Cheng-Liang Liu, Cheng-Tyng Yen, Fu-Chuan Tsai, Christopher J. Tonzola, Nicholas Olson et Samson A. Jenekhe. Theoretical and experimental characterization of small band gap poly(3,4-ethylenedioxythiophene methine)s. *Macromolecules*, 37(16):5959–5964, 2004. URL http://pubs.acs.org/doi/abs/10.1021/ma049557f.

[49] Zhuoying Chen, Mi Jung Lee, Raja Shahid Ashraf, Yun Gu, Sebastian Albert-Seifried, Martin Meedom Nielsen, Bob Schroeder, Thomas D. Anthopoulos, Martin Heeney, Iain McCulloch et Henning Sirringhaus. High-performance ambipolar diketopyrrolopyrrole-thieno[3,2-b]thiophene copolymer field-effect transistors with balanced hole and electron mobilities. *Adv. Mater.*, 24(5):647–652,

2012. ISSN 1521-4095. URL http://dx.doi.org/10.1002/adma.201102786.

[50] Mike Chino. Solar powered bus shelter unveiled in san francisco, consulté le 28 février 2014. http://inhabitat.com/solar-powered-bus-shelter-unveiled-in-san-francisco/.

[51] Ta-Ya Chu, Jianping Lu, Serge Beaupré, Yanguang Zhang, Jean-Rémi Pouliot, Salem Wakim, Jiayun Zhou, Mario Leclerc, Zhao Li, Jianfu Ding et Ye Tao. Bulk heterojunction solar cells using thieno[3,4-c]pyrrole-4,6-dione and dithieno[3,2-b:2',3'-d]silole copolymer with a power conversion efficiency of 7.3%. *J. Am. Chem. Soc.*, 133(12):4250–4253, 2011. URL http://pubs.acs.org/doi/abs/10.1021/ja200314m.

[52] Lay-Lay Chua, Jana Zaumseil, Jui-Fen Chang, Eric C.-W. Ou, Peter K.-H. Ho, Henning Sirringhaus et Richard H. Friend. General observation of n-type field-effect behaviour in organic semiconductors. *Nature*, 434(7030):194–199, 2005. ISSN 0028-0836. URL http://dx.doi.org/10.1038/nature03376.

[53] Tracey M Clarke et James R Durrant. Charge Photogeneration in Organic Solar Cells. *Chem. Rev.*, 110(11):6736–6767, 2010. URL http://pubs.acs.org/doi/abs/10.1021/cr900271s.

[54] David C Coffey, Bryon W Larson, Alexander W Hains, James B Whitaker, Nikos Kopidakis, Olga V Boltalina, Steven H Strauss et Garry Rumbles. An Optimal Driving Force for Converting Excitons into Free Carriers in Excitonic Solar Cells. *J. Phys. Chem. C*, 116(16):8916–8923, avril 2012. URL http://pubs.acs.org/doi/abs/10.1021/jp302275z.

[55] Aron J. Cohen, Paula Mori-Sánchez et Weitao Yang. Fractional charge perspective on the band gap in density-functional theory. *Phys. Rev. B*, 77:115123, Mar 2008. URL http://link.aps.org/doi/10.1103/PhysRevB.77.115123.

[56] Brian A. Collins, Eliot Gann, Lewis Guignard, Xiaoxi He, Christopher R. McNeill et Harald Ade. Molecular miscibility of polymer−fullerene blends. *J. Phys. Chem. Lett.*, 1(21):3160–3166, 2010. URL http://pubs.acs.org/doi/abs/10.1021/jz101276h.

[57] Swati De, Tero Kesti, Manisankar Maiti, Fengling Zhang, Olle Inganäs, Arkady Yartsev, Torbjörn Pascher et Villy Sundstrom. Exciton dynamics in alternating polyfluorene/fullerene blends. *Chem. Phys.*, 350(1-3):14–22, juin 2008. URL http://www.sciencedirect.com/science/article/pii/S0301010407005435.

[58] D.M. de Leeuw, M.M.J. Simenon, A.R. Brown et R.E.F. Einerhand. Stability of n-type doped conducting polymers and consequences for polymeric microelectronic devices. *Synth. Met.*, 87(1):53–59, 1997. ISSN 0379-6779. URL http://www.sciencedirect.com/science/article/pii/S0379677997800975.

[59] Gilles Dennler, Markus C. Scharber et Christoph J. Brabec. Polymer-fullerene bulk-heterojunction solar cells. *Adv. Mater.*, 21(13):1323–1338, 2009. ISSN 1521-4095. URL http://dx.doi.org/10.1002/adma.200801283.

[60] Letian Dou, Jun You, Jingbi Yang, Chun-Chao Chen, Youjun He, Seiichiro Murase, Tom Moriarty, Keith Emery, Gang Li et Yang Yang. Tandem polymer solar cells featuring a spectrally matched low-bandgap polymer. *Nat. Photonics*, 6(3):180–185, 2012. ISSN 1749-4885. URL http://dx.doi.org/10.1038/nphoton.2011.356.

[61] Guillaume Dumont, Paul Boulanger, Michel Côté et Matthias Ernzerhof. Peierls instability in carbon nanotubes: A first-principles study. *Phys. Rev. B*, 82:035419, Jul 2010. URL http://link.aps.org/doi/10.1103/PhysRevB.82.035419.

[62] Daniel A. Eisenberg, Mengjing Yu, Carl W. Lam, Oladele A. Ogunsei-

tan et Julie M. Schoenung. Comparative alternative materials assessment to screen toxicity hazards in the life cycle of {CIGS} thin film photovoltaics. *J. Hazard. Mater.*, 260(0):534 – 542, 2013. ISSN 0304-3894. URL http://www.sciencedirect.com/science/article/pii/S030438941300407X.

[63] Nieves Espinosa et Frederik C. Krebs. Life cycle analysis of organic tandem solar cells: When are they warranted ? *Sol. Energy Mater. Sol. Cells*, 120, Part B(0): 692 – 700, 2014. ISSN 0927-0248. URL http://www.sciencedirect.com/science/article/pii/S0927024813004716.

[64] Fabian Etzold, Ian A Howard, Ralf Mauer, Michael Meister, Tae-Dong Kim, Kwang-Sup Lee, Nam Seob Baek et Frédéric Laquai. Ultrafast Exciton Dissociation Followed by Nongeminate Charge Recombination in PCDTBT:PCBM Photovoltaic Blends. *J. Am. Chem. Soc.*, 133(24):9469–9479, 2011. URL http://pubs.acs.org/doi/abs/10.1021/ja201837e.

[65] Antonio Facchetti. Semiconductors for organic transistors. *Mater. Today*, 10(3):28 – 37, 2007. ISSN 1369-7021. URL http://www.sciencedirect.com/science/article/pii/S1369702107700172.

[66] Antonio Facchetti. π-conjugated polymers for organic electronics and photovoltaic cell applications. *Chem. Mater.*, 23(3):733–758, 2011. URL http://pubs.acs.org/doi/abs/10.1021/cm102419z.

[67] Antonio Facchetti. Polymer donor-polymer acceptor (all-polymer) solar cells. *Mater. Today*, 16(4):123 – 132, 2013. ISSN 1369-7021. URL http://www.sciencedirect.com/science/article/pii/S1369702113001053.

[68] Antonio Facchetti, Myung-Han Yoon, Charlotte L. Stern, Geoffrey R. Hutchison, Mark A. Ratner et Tobin J. Marks. Building blocks for n-type molecular and polymeric electronics. perfluoroalkyl- versus alkyl-functionalized oligo-

thiophenes (n = 2-6). systematic synthesis, spectroscopy, electrochemistry, and solid-state organization. *J. Am. Chem. Soc.*, 126(41):13480–13501, 2004. URL http://pubs.acs.org/doi/abs/10.1021/ja048988a.

[69] Donald G. Farnum, Goverdhan Mehta, George G.I. Moore et Frederick P. Siegal. Attempted reformatskii reaction of benzonitrile, 1,4-diketo-3,6-diphenylpyrrolo[3,4-c]pyrrole. a lactam analogue of pentalene. *Tetrahedron Lett.*, 15(29):2549 – 2552, 1974. ISSN 0040-4039. URL http://www.sciencedirect.com/science/article/pii/S0040403901932022.

[70] Forbes. Solar grid parity comes to spain, consulté le 11 février 2014. http://www.forbes.com/sites/peterdetwiler/2012/12/26/solar-grid-parity-comes-to-spain/.

[71] M. J. Frisch, G. W. Trucks, H. B. Schlegel, G. E. Scuseria, M. A. Robb, J. R. Cheeseman, J. A. Montgomery, Jr., T. Vreven, K. N. Kudin, J. C. Burant, J. M. Millam, S. S. Iyengar, J. Tomasi, V. Barone, B. Mennucci, M. Cossi, G. Scalmani, N. Rega, G. A. Petersson, H. Nakatsuji, M. Hada, M. Ehara, K. Toyota, R. Fukuda, J. Hasegawa, M. Ishida, T. Nakajima, Y. Honda, O. Kitao, H. Nakai, M. Klene, X. Li, J. E. Knox, H. P. Hratchian, J. B. Cross, V. Bakken, C. Adamo, J. Jaramillo, R. Gomperts, R. E. Stratmann, O. Yazyev, A. J. Austin, R. Cammi, C. Pomelli, J. W. Ochterski, P. Y. Ayala, K. Morokuma, G. A. Voth, P. Salvador, J. J. Dannenberg, V. G. Zakrzewski, S. Dapprich, A. D. Daniels, M. C. Strain, O. Farkas, D. K. Malick, A. D. Rabuck, K. Raghavachari, J. B. Foresman, J. V. Ortiz, Q. Cui, A. G. Baboul, S. Clifford, J. Cioslowski, B. B. Stefanov, G. Liu, A. Liashenko, P. Piskorz, I. Komaromi, R. L. Martin, D. J. Fox, T. Keith, M. A. Al-Laham, C. Y. Peng, A. Nanayakkara, M. Challacombe, P. M. W. Gill, B. Johnson, W. Chen, M. W. Wong, C. Gonzalez et J. A. Pople. Gaussian 03, Revision C.02, 2003. Gaussian, Inc., Wallingford, CT, 2004.

[72] M. J. Frisch, G. W. Trucks, H. B. Schlegel, G. E. Scuseria, M. A. Robb, J. R.

Cheeseman, G. Scalmani, V. Barone, B. Mennucci, G. A. Petersson, H. Nakatsuji, M. Caricato, X. Li, H. P. Hratchian, A. F. Izmaylov, J. Bloino, G. Zheng, J. L. Sonnenberg, M. Hada, M. Ehara, K. Toyota, R. Fukuda, J. Hasegawa, M. Ishida, T. Nakajima, Y. Honda, O. Kitao, H. Nakai, T. Vreven, J. A. Montgomery, Jr., J. E. Peralta, F. Ogliaro, M. Bearpark, J. J. Heyd, E. Brothers, K. N. Kudin, V. N. Staroverov, R. Kobayashi, J. Normand, K. Raghavachari, A. Rendell, J. C. Burant, S. S. Iyengar, J. Tomasi, M. Cossi, N. Rega, J. M. Millam, M. Klene, J. E. Knox, J. B. Cross, V. Bakken, C. Adamo, J. Jaramillo, R. Gomperts, R. E. Stratmann, O. Yazyev, A. J. Austin, R. Cammi, C. Pomelli, J. W. Ochterski, R. L. Martin, K. Morokuma, V. G. Zakrzewski, G. A. Voth, P. Salvador, J. J. Dannenberg, S. Dapprich, A. D. Daniels, Ö. Farkas, J. B. Foresman, J. V. Ortiz, J. Cioslowski et D. J. Fox. *Gaussian 09*. Gaussian, Inc., Wallingford, CT, 2009.

[73] Renee R Frontiera, Jyotishman Dasgupta et Richard A Mathies. Probing Interfacial Electron Transfer in Coumarin 343 Sensitized TiO 2Nanoparticles with Femtosecond Stimulated Raman. *J. Am. Chem. Soc.*, 131(43):15630–15632, novembre 2009. URL `http://pubs.acs.org/doi/abs/10.1021/ja907188b`.

[74] Renee R. Frontiera, Chong Fang, Jyotishman Dasgupta et Richard A. Mathies. Probing structural evolution along multidimensional reaction coordinates with femtosecond stimulated raman spectroscopy. *Phys. Chem. Chem. Phys.*, 14:405–414, 2012. URL `http://dx.doi.org/10.1039/C1CP22767J`.

[75] Tomotsumi Fujisawa, Mark Creelman et Richard A. Mathies. Structural dynamics of a noncovalent charge transfer complex from femtosecond stimulated Raman spectroscopy. *J. Phys. Chem. B*, 116(35):10453–10460, 2012. URL `http://pubs.acs.org/doi/abs/10.1021/jp3001306`.

[76] Jian Gao et John K Grey. Resonance Raman overtones reveal vibrational displacements and dynamics of crystalline and amorphous poly(3-hexylthiophene) chains in fullerene blends. *J. Chem. Phys.*, 139(4):044903,

2013. URL http://scitation.aip.org/content/aip/journal/jcp/139/4/10.1063/1.4815819.

[77] Simon Gélinas, Olivier Pare-Labrosse, Colin-Nadeau Brosseau, Sebastian Albert-Seifried, Christopher R Mcneill, Kiril R Kirov, Ian A Howard, Richard Leonelli, Richard H Friend et Carlos Silva. The Binding Energy of Charge-Transfer Excitons Localized at Polymeric Semiconductor Heterojunctions. *J. Phys. Chem. C*, 115(14):7114–7119, 2011. URL http://pubs.acs.org/doi/abs/10.1021/jp200466y.

[78] Simon Gélinas, Akshay Rao, Abhishek Kumar, Samuel L. Smith, Alex W. Chin, Jenny Clark, Tom S. van der Poll, Guillermo C. Bazan et Richard H. Friend. Ultrafast long-range charge separation in organic semiconductor photovoltaic diodes. *Science*, 2014. URL http://www.sciencemag.org/content/early/2013/12/11/science.1246249.

[79] Gerwin H. Gelinck, H. Edzer A. Huitema, Erik van Veenendaal, Eugenio Cantatore, Laurens Schrijnemakers, Jan B. P. H. van der Putten, Tom C. T. Geuns, Monique Beenhakkers, Jacobus B. Giesbers, Bart-Hendrik Huisman, Eduard J. Meijer, Estrella Mena Benito, Fred J. Touwslager, Albert W. Marsman, Bas J. E. van Rens et Dago M. de Leeuw. Flexible active-matrix displays and shift registers based on solution-processed organic transistors. *Nat. Mater.*, 3(2):106–110, 2004. URL http://dx.doi.org/10.1038/nmat1061.

[80] David Gendron et Mario Leclerc. New conjugated polymers for plastic solar cells. *Energy Environ. Sci.*, 4:1225–1237, 2011. URL http://dx.doi.org/10.1039/C1EE01072G.

[81] Peter M. W. Gill, Benny G. Johnson, John A. Pople et Michael J. Frisch. An investigation of the performance of a hybrid of hartree-fock and density functional theory. *Int. J. Quantum Chem.*, 44(S26):319–331, 1992. ISSN 1097-461X. URL http://dx.doi.org/10.1002/qua.560440828.

[82] G Grancini, M Maiuri, D Fazzi, A Petrozza, H-J Egelhaaf, D Brida, G Cerullo et G Lanzani. Hot exciton dissociation in polymer solar cells. *Nat. Mater.*, 12:29–33, 2012. URL http://www.nature.com/nmat/journal/v12/n1/full/nmat3502.html.

[83] Martin A. Green, Keith Emery, Yoshihiro Hishikawa, Wilhelm Warta et Ewan D. Dunlop. Solar cell efficiency tables (version 39). *Prog. Photovolt. Res. Appl.*, 20 (1):12–20, 2012. ISSN 1099-159X. URL http://dx.doi.org/10.1002/pip.2163.

[84] G M Greetham, Pierre Burgos, Qian Cao, Ian P Clark, Peter S Codd, Richard C Farrow, Michael W George, Moschos Kogimtzis, Pavel Matousek, A W Parker, Mark R Pollard, David A Robinson, Zhi-Jun Xin et Michael Towrie. ULTRA: A Unique Instrument for Time-Resolved Spectroscopy. *Appl. Spectroscopy*, 64(12): 1311–1319, novembre 2010. URL http://www.opticsinfobase.org/as/abstract.cfm?uri=as-64-12-1311.

[85] Xugang Guo, Hao Xin, Felix Sunjoo Kim, Arawwawala D. T. Liyanage, Samson A. Jenekhe et Mark D. Watson. Thieno[3,4-c]pyrrole-4,6-dione-based donor-acceptor conjugated polymers for solar cells. *Macromolecules*, 44(2):269–277, 2011. URL http://pubs.acs.org/doi/abs/10.1021/ma101878w.

[86] Johannes Hachmann, Roberto Olivares-Amaya, Sule Atahan-Evrenk, Carlos Amador-Bedolla, Roel S. Sànchez-Carrera, Aryeh Gold-Parker, Leslie Vogt, Anna M. Brockway et Alàn Aspuru-Guzik. The harvard clean energy project: Large-scale computational screening and design of organic photovoltaics on the world community grid. *J. Phys. Chem. Lett.*, 2(17):2241–2251, 2011. URL http://pubs.acs.org/doi/abs/10.1021/jz200866s.

[87] Christopher M. Hadad, Paul R. Rablen et Kenneth B. Wiberg. C−o and c−s bonds: stability, bond dissociation energies, and resonance stabilization. *J. Org. Chem.*, 63(24):8668–8681, 1998. URL http://pubs.acs.org/doi/abs/10.1021/jo972180%2B.

[88] Markus Hallermann, Stephan Haneder et Enrico Da Como. Charge-transfer states in conjugated polymer/fullerene blends: Below-gap weakly bound excitons for polymer photovoltaics. *Appl. Phys. Lett.*, 93(5):053307, 2008. URL http://scitation.aip.org/content/aip/journal/apl/93/5/10.1063/1.2969295.

[89] Markus Hallermann, Ilka Kriegel, Enrico Da Como, Josef M Berger, Elizabeth Von Hauff et Jochen Feldmann. Charge Transfer Excitons in Polymer/Fullerene Blends: The Role of Morphology and Polymer Chain Conformation. *Adv. Funct. Mater.*, 19(22):3662–3668, 2009. URL http://onlinelibrary.wiley.com/doi/10.1002/adfm.200901398/abstract.

[90] J. J. M. Halls, J. Cornil, D. A. dos Santos, R. Silbey, D.-H. Hwang, A. B. Holmes, J. L. Brédas et R. H. Friend. Charge- and energy-transfer processes at polymer/polymer interfaces: A joint experimental and theoretical study. *Phys. Rev. B*, 60:5721–5727, Aug 1999. URL http://link.aps.org/doi/10.1103/PhysRevB.60.5721.

[91] Zhimin Hao et Abul Iqbal. Some aspects of organic pigments. *Chem. Soc. Rev.*, 26:203–213, 1997. URL http://dx.doi.org/10.1039/CS9972600203.

[92] E.E. Havinga, W. ten Hoeve et H. Wynberg. Alternate donor-acceptor small-band-gap semiconducting polymers ; polysquaraines and polycroconaines. *Synth. Met.*, 55(1):299–306, 1993. ISSN 0379-6779. URL http://www.sciencedirect.com/science/article/pii/037967799390949W.

[93] Lars Hedin. New method for calculating the one-particle green's function with application to the electron-gas problem. *Phys. Rev.*, 139:A796–A823, Aug 1965. URL http://link.aps.org/doi/10.1103/PhysRev.139.A796.

[94] Lars Hedin et Stig Lundqvist. Effects of electron-electron and electron-photon

interaction on the one-electron states of solids. *Solid State Physics*, 23:1, 1969. URL http://www.sciencedirect.com/science/article/pii/S0081194708606153.

[95] A. J. Heeger, S. Kivelson, J. R. Schrieffer et W. P. Su. Solitons in conducting polymers. *Rev. Mod. Phys.*, 60:781–850, Jul 1988. URL http://link.aps.org/doi/10.1103/RevModPhys.60.781.

[96] P. Hohenberg et W. Kohn. Inhomogeneous electron gas. *Phys. Rev.*, 136: B864–B871, Nov 1964. URL http://link.aps.org/doi/10.1103/PhysRev.136.B864.

[97] Sung Y. Hong, Si J. Kwon et Shi C. Kim. Electronic structures of new pi-conjugated cyclic polymers with quinoid structures. *J. Chem. Phys.*, 103(5):1871–1877, 1995. URL http://link.aip.org/link/?JCP/103/1871/1.

[98] I. Hoogmartens, P. Adriaensens, D. Vanderzande, J. Gelan, C. Quattrocchi, R. Lazzaroni et J. L. Brédas. Low-bandgap conjugated polymers. a joint experimental and theoretical study of the structure of polyisothianaphthene. *Macromolecules*, 25(26):7347–7356, 1992. URL http://pubs.acs.org/doi/abs/10.1021/ma00052a043.

[99] Jianhui Hou, Hsiang-Yu Chen, Shaoqing Zhang, Ruby I. Chen, Yang Yang, Yue Wu et Gang Li. Synthesis of a low band gap polymer and its application in highly efficient polymer solar cells. *J. Am. Chem. Soc.*, 131(43):15586–15587, 2009. URL http://pubs.acs.org/doi/abs/10.1021/ja9064975.

[100] Jianhui Hou, Hsiang-Yu Chen, Shaoqing Zhang, Gang Li et Yang Yang. Synthesis, characterization, and photovoltaic properties of a low band gap polymer based on silole-containing polythiophenes and 2,1,3-benzothiadiazole. *J. Am. Chem. Soc.*, 130(48):16144–16145, 2008. URL http://pubs.acs.org/doi/abs/10.1021/ja806687u.

[101] Jianhui Hou, Mi-Hyae Park, Shaoqing Zhang, Yan Yao, Li-Min Chen, Juo-Hao Li et Yang Yang. Bandgap and molecular energy level control of conjugated polymer photovoltaic materials based on benzo[1,2-b:4,5-b']dithiophene. *Macromolecules*, 41(16):6012–6018, 2008. URL http://pubs.acs.org/doi/abs/10.1021/ma800820r.

[102] Jianhui Hou, Zhan'ao Tan, Yong Yan, Youjun He, Chunhe Yang et Yongfang Li. Synthesis and photovoltaic properties of two-dimensional conjugated polythiophenes with bi(thienylenevinylene) side chains. *J. Am. Chem. Soc.*, 128(14): 4911–4916, 2006. URL http://pubs.acs.org/doi/abs/10.1021/ja060141m.

[103] Lijun Huo, Jianhui Hou, Hsiang-Yu Chen, Shaoqing Zhang, Yang Jiang, Teresa L. Chen et Yang Yang. Bandgap and molecular level control of the low-bandgap polymers based on 3,6-dithiophen-2-yl-2,5-dihydropyrrolo[3,4-c]pyrrole-1,4-dione toward highly efficient polymer solar cells. *Macromolecules*, 42(17):6564–6571, 2009. URL http://pubs.acs.org/doi/abs/10.1021/ma9012972.

[104] Geoffrey R. Hutchison, Mark A. Ratner et Tobin J. Marks. Accurate prediction of band gaps in neutral heterocyclic conjugated polymers. *J. Phys. Chem. A*, 106(44): 10596–10605, 2002. URL http://pubs.acs.org/doi/abs/10.1021/jp025999m.

[105] Geoffrey R. Hutchison, Mark A. Ratner et Tobin J. Marks. Electronic structure and band gaps in cationic heterocyclic oligomers. multidimensional analysis of the interplay of heteroatoms, substituents, molecular length, and charge on redox and transparency characteristics. *J. Phys. Chem. B*, 109(8):3126–3138, 2005. URL http://pubs.acs.org/doi/abs/10.1021/jp046579v.

[106] Y. Ikenoue, F. Wudl et A.J. Heeger. A novel substituted poly(isothianaphthene). *Synth. Met.*, 40(1):1–12, 1991. ISSN 0379-6779. URL http://www.sciencedirect.com/science/article/pii/037967799191483Q.

[107] A. Iqbal, M. Jost, R. Kirchmayr, J. Pfenninger, A. Rochat et O. Wallquist. The synthesis and properties of 1,4-diketo-pyrrolo[3,4-c]pyrroles. *Bull. Soc. Chim. Belges*, 97(8-9):615–644, 1988. ISSN 0037-9646. URL http://dx.doi.org/10.1002/bscb.19880970804.

[108] Nicholas E. Jackson, Brett M. Savoie, Kevin L. Kohlstedt, Monica Olvera de la Cruz, George C. Schatz, Lin X. Chen et Mark A. Ratner. Controlling conformations of conjugated polymers and small molecules: The role of nonbonding interactions. *J. Am. Chem. Soc.*, 135(28):10475–10483, 2013. URL http://pubs.acs.org/doi/abs/10.1021/ja403667s.

[109] Askat E Jailaubekov, Adam P Willard, John R Tritsch, Wai-Lun Chan, Na Sai, Raluca Gearba, Loren G Kaake, Kenrick J Williams, Kevin Leung, Peter J Rossky et X Y Zhu. Hot charge-transfer excitons set the time limit for charge separation at donor/acceptor interfaces in organic photovoltaics. *Nat. Mater.*, 11(12): 1–8, 2012. URL http://www.nature.com/nmat/journal/v12/n1/full/nmat3500.html.

[110] J. F. Janak. Proof that $\partial e/\partial n_i = \varepsilon$ in density-functional theory. *Phys. Rev. B*, 18:7165–7168, Dec 1978. URL http://link.aps.org/doi/10.1103/PhysRevB.18.7165.

[111] Benjamin G. Janesko. Comparing modern density functionals for conjugated polymer band structures: Screened hybrid, minnesota, and rung 3.5 approximations. *J. Chem. Phys.*, 134(18):–, 2011. URL http://scitation.aip.org/content/aip/journal/jcp/134/18/10.1063/1.3589145.

[112] Jang Jo, David Gendron, Ahmed Najari, Ji Sun Moon, Shinuk Cho, Mario Leclerc et Alan J. Heeger. Bulk heterojunction solar cells based on a low-bandgap carbazole-diketopyrrolopyrrole copolymer. *Appl. Phys. Lett.*, 97(20):203303, 2010. URL http://link.aip.org/link/?APL/97/203303/1.

[113] Jang Jo, Seok-In Na, Seok-Soon Kim, Tae-Woo Lee, Youngsu Chung, Seok-

Ju Kang, Doojin Vak et Dong-Yu Kim. Three-dimensional bulk heterojunction morphology for achieving high internal quantum efficiency in polymer solar cells. *Adv. Funct. Mater.*, 19(15):2398–2406, 2009. ISSN 1616-3028. URL http://dx.doi.org/10.1002/adfm.200900183.

[114] Jae Woong Jung, Feng Liu, Thomas P. Russell et Won Ho Jo. A high mobility conjugated polymer based on dithienothiophene and diketopyrrolopyrrole for organic photovoltaics. *Energy Environ. Sci.*, 5:6857–6861, 2012. URL http://dx.doi.org/10.1039/C2EE21149A.

[115] Joseph Kalowekamo et Erin Baker. Estimating the manufacturing cost of purely organic solar cells. *Sol. Energy*, 83(8):1224 – 1231, 2009. ISSN 0038-092X. URL http://www.sciencedirect.com/science/article/pii/S0038092X09000322.

[116] Catherine Kanimozhi, P. Balraju, G. D. Sharma et Satish Patil. Synthesis of diketopyrrolopyrrole containing copolymers: A study of their optical and photovoltaic properties. *J. Phys. Chem. B*, 114(9):3095–3103, 2010. URL http://pubs.acs.org/doi/abs/10.1021/jp909183x.

[117] Michinori Karikomi, Chitoshi Kitamura, Shoji Tanaka et Yoshiro Yamashita. New narrow-bandgap polymer composed of benzobis(1,2,5-thiadiazole) and thiophenes. *J. Am. Chem. Soc.*, 117(25):6791–6792, 1995. URL http://pubs.acs.org/doi/abs/10.1021/ja00130a024.

[118] J. Y. Kim, S. H. Kim, H.-H. Lee, K. Lee, W. Ma, X. Gong et A. J. Heeger. New architecture for high-efficiency polymer photovoltaic cells using solution-based titanium oxide as an optical spacer. *Adv. Mater.*, 18(5):572–576, 2006. ISSN 1521-4095. URL http://dx.doi.org/10.1002/adma.200501825.

[119] S. Kivelson et O. L. Chapman. Polyacene and a new class of quasi-one-dimensional conductors. *Phys. Rev. B*, 28:7236–7243, Dec 1983. URL http://link.aps.org/doi/10.1103/PhysRevB.28.7236.

[120] Hagen Klauk. Organic thin-film transistors. *Chem. Soc. Rev.*, 39:2643–2666, 2010. URL http://dx.doi.org/10.1039/B909902F.

[121] Nabil Kleinhenz, Liqiang Yang, Huaxing Zhou, Samuel C. Price et Wei You. Low-band-gap polymers that utilize quinoid resonance structure stabilization by thienothiophene: Fine-tuning of homo level. *Macromolecules*, 44(4):872–877, 2011. URL http://pubs.acs.org/doi/abs/10.1021/ma1024126.

[122] A. Knobloch, A. Manuelli, A. Bernds et W. Clemens. Fully printed integrated circuits from solution processable polymers. *J. Appl. Phys.*, 96(4):2286–2291, 2004. URL http://link.aip.org/link/?JAP/96/2286/1.

[123] Takashi Kobayashi, J Hamazaki, M Arakawa, H Kunugita, K Ema, K Ochiai, M Rikukawa et K Sanui. Self-trapped exciton dynamics in highly ordered and disordered films of polythiophene derivative. *Phys. Rev. B*, 62(13):8580, 2000. URL http://journals.aps.org/prb/abstract/10.1103/PhysRevB.62.8580.

[124] H. Koezuka, A. Tsumura et T. Ando. Field-effect transistor with polythiophene thin film. *Synth. Met.*, 18(1-3):699–704, 1987. ISSN 0379-6779. URL http://www.sciencedirect.com/science/article/pii/0379677987909647.

[125] Makoto Komatsu, Jotaro Nakazaki, Satoshi Uchida, Takaya Kubo et Hiroshi Segawa. A donor-acceptor type organic dye connected with a quinoidal thiophene for dye-sensitized solar cells. *Phys. Chem. Chem. Phys.*, 15:3227–3232, 2013. URL http://dx.doi.org/10.1039/C2CP43598E.

[126] Floris B. Kooistra, Joop Knol, Fredrik Kastenberg, Lacramioara M. Popescu, Wiljan J. H. Verhees, Jan M. Kroon et Jan C. Hummelen. Increasing the open circuit voltage of bulk-heterojunction solar cells by raising the lumo level of the acceptor. *Org. Lett.*, 9(4):551–554, 2007. URL http://pubs.acs.org/doi/abs/10.1021/ol062666p.

[127] Frederik C. Krebs, Mikkel Jørgensen, Kion Norrman, Ole Hagemann, Jan Alstrup, Torben D. Nielsen, Jan Fyenbo, Kaj Larsen et Jette Kristensen. A complete process for production of flexible large area polymer solar cells entirely using screen printing - first public demonstration. *Sol. Energy Mater. Sol. Cells*, 93(4):422–441, 2009. ISSN 0927-0248. URL http://www.sciencedirect.com/science/article/pii/S0927024808004595.

[128] R. Krishnan, J. S. Binkley, R. Seeger et J. A. Pople. Self-consistent molecular orbital methods. xx. a basis set for correlated wave functions. *J. Chem. Phys.*, 72 (1):650–654, 1980. URL http://link.aip.org/link/?JCP/72/650/1.

[129] R. Krishnan, J. S. Binkley, R. Seeger et J. A. Pople. Self-consistent molecular orbital methods. xx. a basis set for correlated wave functions. *J. Chem. Phys.*, 72 (1):650–654, 1980. URL http://link.aip.org/link/?JCP/72/650/1.

[130] Renee Kroon, Martijn Lenes, Jan C. Hummelen, Paul W. M. Blom et Bert de Boer. Small bandgap polymers for organic solar cells (polymer material development in the last 5 years). *Polym. Rev.*, 48(3):531–582, 2008. URL http://dx.doi.org/10.1080/15583720802231833.

[131] Jamin Ku, Yves Lansac et Yun Hee Jang. Time-dependent density functional theory study on benzothiadiazole-based low-band-gap fused-ring copolymers for organic solar cell applications. *J. Phys. Chem. C*, 115(43):21508–21516, 2011. URL http://pubs.acs.org/doi/abs/10.1021/jp2062207.

[132] Abhishek P. Kulkarni, Christopher J. Tonzola, Amit Babel et Samson A. Jenekhe. Electron transport materials for organic light-emitting diodes. *Chem. Mater.*, 16(23):4556–4573, 2004. URL http://pubs.acs.org/doi/abs/10.1021/cm0494731.

[133] Kock Yee. Law. Organic photoconductive materials: recent trends and develop-

ments. *Chem. Rev.*, 93(1):449–486, 1993. URL http://pubs.acs.org/doi/abs/10.1021/cr00017a020.

[134] M. Leclerc, A. Najari et Y. Zou. Novel photoactive polymers. WO Patent 2011/063534 A, 2011.

[135] J Lee, K Vandewal, SR Yost, ME Bahlke, L Goris, MA Baldo, JV Manca et T Van Voorhis. Charge Transfer State Versus Hot Exciton Dissociation in Polymer− Fullerene Blended Solar Cells. *J. Am. Chem. Soc.*, 132(34): 11878–11880, 2010. URL http://pubs.acs.org/doi/abs/10.1021/ja1045742.

[136] Michael R. Lee, Robert D. Eckert, Karen Forberich, Gilles Dennler, Christoph J. Brabec et Russell A. Gaudiana. Solar power wires based on organic photovoltaic materials. *Science*, 324(5924):232–235, 2009. URL http://www.sciencemag.org/content/324/5924/232.abstract.

[137] Martijn Lenes, Gert-Jan A. H. Wetzelaer, Floris B. Kooistra, Sjoerd C. Veenstra, Jan C. Hummelen et Paul W. M. Blom. Fullerene bisadducts for enhanced open-circuit voltages and efficiencies in polymer solar cells. *Adv. Mater.*, 20(11): 2116–2119, 2008. ISSN 1521-4095. URL http://dx.doi.org/10.1002/adma.200702438.

[138] Simon Lévesque, David Gendron, Nicolas Bérubé, François Grenier, Mario Leclerc et Michel Côté. Supporting information for thiocarbonyl substitution in 1,4-dithioketopyrrolopyrrole and thienopyrroledithione derivatives: an experimental and theoretical study, consulté le 28 février 2014. http://pubs.acs.org/doi/suppl/10.1021/jp411300h/suppl_file/jp411300h_si_001.pdf.

[139] Yongye Liang, Danqin Feng, Yue Wu, Szu-Ting Tsai, Gang Li, Claire Ray et Luping Yu. Highly efficient solar cell polymers developed via fine-tuning of structu-

ral and electronic properties. *J. Am. Chem. Soc.*, 131(22):7792–7799, 2009. URL http://pubs.acs.org/doi/abs/10.1021/ja901545q.

[140] Yongye Liang, Yue Wu, Danqin Feng, Szu-Ting Tsai, Hae-Jung Son, Gang Li et Luping Yu. Development of new semiconducting polymers for high performance solar cells. *J. Am. Chem. Soc.*, 131(1):56–57, 2009. URL http://pubs.acs.org/doi/abs/10.1021/ja808373p.

[141] Yongye Liang, Zheng Xu, Jiangbin Xia, Szu-Ting Tsai, Yue Wu, Gang Li, Claire Ray et Luping Yu. For the bright future−bulk heterojunction polymer solar cells with power conversion efficiency of 7.4%. *Adv. Mater.*, 22(20):E135–E138, 2010. ISSN 1521-4095. URL http://dx.doi.org/10.1002/adma.200903528.

[142] Yongye Liang et Luping Yu. A new class of semiconducting polymers for bulk heterojunction solar cells with exceptionally high performance. *Acc. Chem. Res.*, 43(9):1227–1236, 2010. URL http://pubs.acs.org/doi/abs/10.1021/ar1000296.

[143] Alejandro López-Bezanilla, François Triozon et Stephan Roche. Chemical functionalization effects on armchair graphene nanoribbon transport. *Nano Lett.*, 9(7):2537–2541, 2009. URL http://pubs.acs.org/doi/abs/10.1021/nl900561x. PMID: 19505128.

[144] Andrzej. Maciejewski et Ronald P. Steer. The photophysics, physical photochemistry, and related spectroscopy of thiocarbonyls. *Chem. Rev.*, 93(1):67–98, 1993. URL http://pubs.acs.org/doi/abs/10.1021/cr00017a005.

[145] Rudolph A. Marcus. Electron transfer reactions in chemistry. theory and experiment. *Rev. Mod. Phys.*, 65:599–610, Jul 1993. URL http://link.aps.org/doi/10.1103/RevModPhys.65.599.

[146] Miguel A. L. Marques. *Time-Dependent Density Functional Theory*, volume 706 de *Lecture Notes in Physics*. Springer, 2006.

[147] M Marsman, J Paier, A Stroppa et G Kresse. Hybrid functionals applied to extended systems. *J. Phys.: Condens. Matter*, 20(6):064201, 2008. URL http://stacks.iop.org/0953-8984/20/i=6/a=064201.

[148] Richard M. Martin. *Electronic Structure: Basic Theory and Practical Methods*. Cambridge University Press, 2004.

[149] David W. McCamant. Re-Evaluation of Rhodopsin's Relaxation Kinetics Determined from Femtosecond Stimulated Raman Lineshapes. *J. Phys. Chem. B*, 115(29):9299–9305, 2011. URL http://dx.doi.org/10.1021/jp2028164.

[150] David W McCamant, Philipp Kukura, Sangwoon Yoon et Richard A Mathies. Femtosecond broadband stimulated Raman spectroscopy: Apparatus and methods. *Rev. Sci. Instrum.*, 75(11):4971, 2004. URL http://scitation.aip.org/content/aip/journal/rsi/75/11/10.1063/1.1807566.

[151] Theresa M. McCormick, Colin R. Bridges, Elisa I. Carrera, Paul M. DiCarmine, Gregory L. Gibson, Jon Hollinger, Lisa M. Kozycz et Dwight S. Seferos. Conjugated polymers: Evaluating dft methods for more accurate orbital energy modeling. *Macromolecules*, 46(10):3879–3886, 2013. URL http://pubs.acs.org/doi/abs/10.1021/ma4005023.

[152] V. D. Mihailetchi, P. W. M. Blom, J. C. Hummelen et M. T. Rispens. Cathode dependence of the open-circuit voltage of polymer:fullerene bulk heterojunction solar cells. *J. Appl. Phys.*, 94(10):6849–6854, 2003. URL http://link.aip.org/link/?JAP/94/6849/1.

[153] Amanda H. Miller. Konarka markets building-integrated solar, consulté le 28 février 2014. http://www.cleanenergyauthority.com/solar-energy-news/konarka-markets-building-integated-solar-051612.

[154] J. Mizuguchi. Electronic characterization of 1-keto-4-thioketo-3,6-diphenylpyrrolo[3,4-c]pyrrole in solution and in the solid state. *J. Phys. Chem. A*, 105(7):1125–1130, 2001. URL http://pubs.acs.org/doi/abs/10.1021/jp0027905.

[155] Jin Mizuguchi. Temperature dependence of the dark conductivity and photoconductivity in evaporated thin films of 1,4-dithioketo-3,6-diphenyl-pyrrolo-[3,4-c]-pyrrole under a high vacuum or in the atmosphere of oxygen or hydrogen. *J. Appl. Phys.*, 66(7):3111–3113, 1989. URL http://scitation.aip.org/content/aip/journal/jap/66/7/10.1063/1.344143.

[156] Jin Mizuguchi et Seiji Homma. Intermolecular charge transfer in 1,4-dithioketo-3,6-diphenyl-pyrrolo-[3,4-c]-pyrrole. *J. Appl. Phys.*, 66(7):3104–3110, 1989. URL http://scitation.aip.org/content/aip/journal/jap/66/7/10.1063/1.344142.

[157] Arne C Morteani, Paiboon Sreearunothai, Laura M Herz, Richard H Friend et Carlos Silva. Exciton Regeneration at Polymeric Semiconductor Heterojunctions. *Phys. Rev. Lett.*, 92(24):247402, juin 2004. URL http://journals.aps.org/prl/abstract/10.1103/PhysRevLett.92.247402.

[158] P. Morvillo et E. Bobeico. Tuning the lumo level of the acceptor to increase the open-circuit voltage of polymer-fullerene solar cells: A quantum chemical study. *Sol. Energy Mater. Sol. Cells*, 92(10):1192 – 1198, 2008. ISSN 0927-0248. URL http://www.sciencedirect.com/science/article/pii/S0927024808001438.

[159] Shaul Mukamel. Multidimensional femtosecond correlation spectroscopies of electronic and vibrational excitations. *Annu. Rev. Phys. Chem.*, 51(1):691–729, 2000. URL http://www.annualreviews.org/doi/abs/10.1146/annurev.physchem.51.1.691.

[160] Shaul Mukamel et Jason D. Biggs. Communication: Comment on the effec-

tive temporal and spectral resolution of impulsive stimulated raman signals. *J. Chem. Phys.*, 134(16):161101, 2011. URL http://scitation.aip.org/content/aip/journal/jcp/134/16/10.1063/1.3581889.

[161] Ahmed Najari, Serge Beaupré, Philippe Berrouard, Yingping Zou, Jean-Rémi Pouliot, Charlotte Lepage-Pérusse et Mario Leclerc. Synthesis and characterization of new thieno[3,4-c]pyrrole-4,6-dione derivatives for photovoltaic applications. *Adv. Funct. Mater.*, 21(4):718–728, 2011. ISSN 1616-3028. URL http://dx.doi.org/10.1002/adfm.201001771.

[162] Noel M. O'Boyle, Casey M. Campbell et Geoffrey R. Hutchison. Computational design and selection of optimal organic photovoltaic materials. *J. Phys. Chem. C*, 115(32):16200–16210, 2011. URL http://pubs.acs.org/doi/abs/10.1021/jp202765c.

[163] Roberto Olivares-Amaya, Carlos Amador-Bedolla, Johannes Hachmann, Sule Atahan-Evrenk, Roel S. Sànchez-Carrera, Leslie Vogt et Alàn Aspuru-Guzik. Accelerated computational discovery of high-performance materials for organic photovoltaics by means of cheminformatics. *Energy Environ. Sci.*, 4:4849–4861, 2011. URL http://dx.doi.org/10.1039/C1EE02056K.

[164] Giovanni Onida, Lucia Reining et Angel Rubio. Electronic excitations: Density-functional versus many-body green's-function approaches. *Rev. Mod. Phys.*, 74:601–659, Jun 2002. URL http://link.aps.org/doi/10.1103/RevModPhys.74.601.

[165] R Österbacka, XM Jiang, CP An, B Horovitz et ZV Vardeny. Photoinduced quantum interference antiresonances in π-conjugated polymers. *Phys. Rev. Lett.*, 88 (22):226401, 2002. URL http://journals.aps.org/prl/abstract/10.1103/PhysRevLett.88.226401.

[166] Laxman Pandey, Chad Risko, Joseph E. Norton et Jean-Luc Brédas. Donor-acceptor copolymers of relevance for organic photovoltaics: A theoretical in-

vestigation of the impact of chemical structure modifications on the electronic and optical properties. *Macromolecules*, 45(16):6405–6414, 2012. URL http://pubs.acs.org/doi/abs/10.1021/ma301164e.

[167] Sung Heum Park, Anshuman Roy, Serge Beaupré, Shinuk Cho, Nelson Coates, Ji Sun Moon, Daniel Moses, Mario Leclerc, Kwanghee Lee et Alan J. Heeger. Bulk heterojunction solar cells with internal quantum efficiency approaching 100%. *Nat. Photonics*, 3(5):297–302, 2009. ISSN 1749-4885. URL http://dx.doi.org/10.1038/nphoton.2009.69.

[168] J. Peet, J. Y. Kim, N. E. Coates, W. L. Ma, D. Moses, A. J. Heeger et G. C. Bazan. Efficiency enhancement in low-bandgap polymer solar cells by processing with alkane dithiols. *Nat. Mater.*, 6(7):497–500, 2007. ISSN 1476-1122. URL http://dx.doi.org/10.1038/nmat1928.

[169] Rudolf Peierls. *Quantum Theory of Solids*. Oxford University Press, 1955.

[170] Ryan D Pensack et John B Asbury. Barrierless Free Carrier Formation in an Organic Photovoltaic Material Measured with Ultrafast Vibrational Spectroscopy. *J. Am. Chem. Soc.*, 131(44):15986–15987, 2009. URL http://pubs.acs.org/doi/abs/10.1021/ja906293q.

[171] Claudia Piliego, Thomas W. Holcombe, Jessica D. Douglas, Claire H. Woo, Pierre M. Beaujuge et Jean M. J. Fréchet. Synthetic control of structural order in n-alkylthieno[3,4-c]pyrrole-4,6-dione-based polymers for efficient solar cells. *J. Am. Chem. Soc.*, 132(22):7595–7597, 2010. URL http://pubs.acs.org/doi/abs/10.1021/ja103275u.

[172] Martin Pomerantz, Ananda S. Amarasekara et H. V. Rasika Dias. Synthesis and solid-state structures of dimethyl 2,2‘-bithiophenedicarboxylates. *J. Org. Chem.*, 67(20):6931–6937, 2002. URL http://pubs.acs.org/doi/abs/10.1021/jo020307b. PMID: 12353985.

[173] Samuel C. Price, Andrew C. Stuart, Liqiang Yang, Huaxing Zhou et Wei You. Fluorine substituted conjugated polymer of medium band gap yields 7% efficiency in polymer-fullerene solar cells. *J. Am. Chem. Soc.*, 133(12):4625–4631, 2011. URL http://pubs.acs.org/doi/abs/10.1021/ja1112595.

[174] Françoise Provencher, David Beljonne, Jean-Luc Brédas et Carlos Silva. Charge photogeneration dynamics in polymer solar cells. *Nat. Mater.*, submitted, 2013.

[175] Françoise Provencher, Maciej Sakowicz, Colin-Nadeau Brosseau, Gianluca Latini, Serge Beaupre, Mario Leclerc, Luke X. Reynolds, Saif A. Haque, Richard Leonelli et Carlos Silva. Slow geminate-charge-pair recombination dynamics at polymer: Fullerene heterojunctions in efficient organic solar cells. *J. Polym. Sci., Part B: Polym. Phys.*, 50(20):1395–1404, août 2012. URL http://onlinelibrary.wiley.com/doi/10.1002/polb.23139/abstract.

[176] Gang Qian, Ji Qi, James A. Davey, James S. Wright et Zhi Yuan Wang. Family of diazapentalene chromophores and narrow-band-gap polymers: Synthesis, halochromism, halofluorism, and visible–near infrared photodetectivity. *Chem. Mater.*, 24(12):2364–2372, 2012. URL http://pubs.acs.org/doi/abs/10.1021/cm300938s.

[177] Ruiping Qin, Weiwei Li, Cuihong Li, Chun Du, Clemens Veit, Hans-Frieder Schleiermacher, Mattias Andersson, Zhishan Bo, Zhengping Liu, Olle Inganäs, Uli Wuerfel et Fengling Zhang. A planar copolymer for high efficiency polymer solar cells. *J. Am. Chem. Soc.*, 131(41):14612–14613, 2009. URL http://pubs.acs.org/doi/abs/10.1021/ja9057986.

[178] Hydro Québec. Tarifs résidentiels d'électricité, consulté le 11 février 2014. http://www.hydroquebec.com/residentiel/comprendre-la-facture/tarification/tarifs-residentiels-d-electricite/tarif-d/.

[179] V. Pushkara Rao. The photoreactivity of thiocarbonyl compounds. *Sulfur reports*, 12(2):359–399, 1992. URL http://www.tandfonline.com/doi/abs/10.1080/01961779208048948.

[180] Matthew E Reish, Sanghun Nam, Wonho Lee, Han Young Woo et Keith C Gordon. A Spectroscopic and DFT Study of the Electronic Properties of Carbazole-Based D–A Type Copolymers. *J. Phys. Chem. C*, 116(40):21255–21266, octobre 2012. URL http://pubs.acs.org/doi/abs/10.1021/jp307552z.

[181] Michael J. Rice. Charged π-phase kinks in lightly doped polyacetylene. *Phys. Lett. A*, 71(1):152–154, 1979. ISSN 0375-9601. URL http://www.sciencedirect.com/science/article/pii/0375960179909058.

[182] M.J. Rice et S. Strässler. Theory of a quasi-one-dimensional band-conductor. *Solid State Commun.*, 13(1):125–128, 1973. ISSN 0038-1098. URL http://www.sciencedirect.com/science/article/pii/0038109873900835.

[183] Minze T. Rispens, Auke Meetsma, Roman Rittberger, Christoph J. Brabec, N. Serdar Sariciftci et Jan C. Hummelen. Influence of the solvent on the crystal structure of pcbm and the efficiency of mdmo-ppv:pcbm 'plastic' solar cells. *Chem. Commun.*, pages 2116–2118, 2003. URL http://dx.doi.org/10.1039/B305988J.

[184] J. Roncali. Molecular engineering of the band gap of π-conjugated systems: Facing technological applications. *Macromol. Rapid Commun.*, 28(17):1761–1775, 2007. ISSN 1521-3927. URL http://dx.doi.org/10.1002/marc.200700345.

[185] Jean Roncali. Synthetic principles for bandgap control in linear π-conjugated systems. *Chem. Rev.*, 97(1):173–206, 1997. URL http://pubs.acs.org/doi/abs/10.1021/cr950257t.

[186] Andrea Rozzi, Carlo, Sarah Maria Falke, Nicola Spallanzani, Angel Rubio, Elisa Molinari, Daniele Brida, Margherita Maiuri, Giulio Cerullo, Heiko Schramm, Jens Christoffers et Christoph Lienau. Quantum coherence controls the charge separation in a prototypical artificial light-harvesting system. *Nat. Commun.*, 4: 1602, mars 2013. URL http://www.nature.com/ncomms/journal/v4/n3/full/ncomms2603.html.

[187] Erich Runge et E. K. U. Gross. Density-functional theory for time-dependent systems. *Phys. Rev. Lett.*, 52:997–1000, Mar 1984. URL http://link.aps.org/doi/10.1103/PhysRevLett.52.997.

[188] N. S. Sariciftci, L. Smilowitz, A. J. Heeger et F. Wudl. Photoinduced electron transfer from a conducting polymer to buckminsterfullerene. *Science*, 258(5087): 1474–1476, 1992. URL http://www.sciencemag.org/content/258/5087/1474.abstract.

[189] M. C. Scharber, D. Mühlbacher, M. Koppe, P. Denk, C. Waldauf, A. J. Heeger et C. J. Brabec. Design rules for donors in bulk-heterojunction solar cells−towards 10 % energy-conversion efficiency. *Adv. Mater.*, 18(6):789–794, 2006. ISSN 1521-4095. URL http://dx.doi.org/10.1002/adma.200501717.

[190] Cody W Schlenker, Kung-Shih Chen, Hin-Lap Yip, Chang-Zhi Li, Liam R Bradshaw, Stefan T Ochsenbein, Feizhi Ding, Xiaosong S Li, Daniel R Gamelin, Alex K-Y Jen et David S Ginger. Polymer Triplet Energy Levels Need Not Limit Photocurrent Collection in Organic Solar Cells. *J. Am. Chem. Soc.*, 134(48): 19661–19668, novembre 2012. URL http://pubs.acs.org/doi/abs/10.1021/ja306110b.

[191] U. Schlick, F. Teichert et M. Hanack. Electrochemical and spectroelectrochemical investigations of small-bandgap π-conjugated polymers and their precursors. *Synth. Met.*, 92(1):75–85, 1998. ISSN 0379-6779. URL http://www.sciencedirect.com/science/article/pii/S037967799880026X.

[192] Gregory D Scholes. Quantum-Coherent Electronic Energy Transfer: Did Nature Think of It First ? *J. Phys. Chem. Lett.*, 1(1):2–8, 2010. URL http://pubs.acs.org/doi/abs/10.1021/jz900062f.

[193] A. Seidl, A. Görling, P. Vogl, J. A. Majewski et M. Levy. Generalized kohn-sham schemes and the band-gap problem. *Phys. Rev. B*, 53:3764–3774, Feb 1996. URL http://link.aps.org/doi/10.1103/PhysRevB.53.3764.

[194] Robert F. Service. Outlook brightens for plastic solar cells. *Science*, 332(6027): 293, 2011. URL http://www.sciencemag.org/content/332/6027/293.short.

[195] C-X Sheng, T Basel, B Pandit et Zeev Valy Vardeny. Photoexcitation dynamics in polythiophene/fullerene blends for photovoltaic applications. *Org. Electron.*, 13(6):1031–1037, juin 2012. URL http://www.sciencedirect.com/science/article/pii/S1566119912000948.

[196] H.-Y. Shin, J. H. Woo, M. J. Gwon, M. Barthelemy, M. Vomir, T. Muto, K. Takaishi, M. Uchiyama, D. Hashizume, T. Aoyama, D.-W. Kim, S. Yoon, J.-Y. Bigot, J. W. Wu et J. C. Ribierre. Exciton diffusion in near-infrared absorbing solution-processed organic thin films. *Phys. Chem. Chem. Phys.*, 15:2867–2872, 2013. URL http://dx.doi.org/10.1039/C2CP43705H.

[197] William Shockley et Hans J. Queisser. Detailed balance limit of efficiency of p-n junction solar cells. *J. Appl. Phys.*, 32(3):510–519, 1961. URL http://scitation.aip.org/content/aip/journal/jap/32/3/10.1063/1.1736034.

[198] Cephas E. Small, Song Chen, Jegadesan Subbiah, Chad M. Amb, Sai-Wing Tsang, Tzung-Han Lai, John R. Reynolds et Franky So. High-efficiency inverted dithienogermole-thienopyrrolodione-based polymer solar cells. *Nat. Photonics*, 6(2):115–120, 2012. ISSN 1749-4885. URL http://dx.doi.org/10.1038/nphoton.2011.317.

[199] Anatoliy N. Sokolov, Sule Atahan-Evrenk, Rajib Mondal, Hylke B. Akkerman, Roel S. Sànchez-Carrera, Sergio Granados-Focil, Joshua Schrier, Stefan C.B. Mannsfeld, Arjan P. Zoombelt, Zhenan Bao et Alàn Aspuru-Guzik. From computational discovery to experimental characterization of a high hole mobility organic crystal. *Nat. Commun.*, 2:437, 2002. URL http://dx.doi.org/10.1038/ncomms1451.

[200] Prashant Sonar, Tae-Jun Ha et Ananth Dodabalapur. A fluorenone based low band gap solution processable copolymer for air stable and high mobility organic field effect transistors. *Chem. Commun.*, 49:1588–1590, 2013. URL http://dx.doi.org/10.1039/C2CC37131F.

[201] Roar R. Søndergaard, Markus Hösel et Frederik C. Krebs. Roll-to-roll fabrication of large area functional organic materials. *J. Polym. Sci., Part B: Polym. Phys.*, 51 (1):16–34, 2013. ISSN 1099-0488. URL http://dx.doi.org/10.1002/polb.23192.

[202] R. P. Steer et V. Ramamurthy. Photophysics and intramolecular photochemistry of thiones in solution. *Acc. Chem. Res.*, 21(10):380–386, 1988. URL http://pubs.acs.org/doi/abs/10.1021/ar00154a005.

[203] Ben G. Streeman et Sanjay Kumar Banerjee. *Solid State Electronic Devices*. Pearson Prentice Hall, 2006.

[204] W. P. Su, J. R. Schrieffer et A. J. Heeger. Soliton excitations in polyacetylene. *Phys. Rev. B*, 22:2099–2111, Aug 1980. URL http://link.aps.org/doi/10.1103/PhysRevB.22.2099.

[205] W. P. Su, J. R. Schrieffer et A. J. Heeger. Erratum: Soliton excitations in polyacetylene. *Phys. Rev. B*, 28:1138–1138, Jul 1983. URL http://link.aps.org/doi/10.1103/PhysRevB.28.1138.

[206] Lei Sun, Fu-Quan Bai, Zeng-Xia Zhao et Hong-Xing Zhang. Design of new benzothiadiazole-based linear and star molecules with dif-

ferent functional groups as solar cells materials: A theoretical approach. *Sol. Energy Mater. Sol. Cells*, 95(7):1800 – 1810, 2011. ISSN 0927-0248. URL http://www.sciencedirect.com/science/article/pii/S0927024811000663.

[207] Yanming Sun, Christopher J. Takacs, Sarah R. Cowan, Jung Hwa Seo, Xiong Gong, Anshuman Roy et Alan J. Heeger. Efficient, air-stable bulk heterojunction polymer solar cells using moox as the anode interfacial layer. *Adv. Mater.*, 23 (19):2226–2230, 2011. ISSN 1521-4095. URL http://dx.doi.org/10.1002/adma.201100038.

[208] C. W. Tang. Two-layer organic photovoltaic cell. *Appl. Phys. Lett.*, 48(2):183–185, 1986. URL http://link.aip.org/link/?APL/48/183/1.

[209] Yaqi Tang et Christopher R. McNeill. All-polymer solar cells utilizing low band gap polymers as donor and acceptor. *J. Polym. Sci., Part B: Polym. Phys.*, 51(6): 403–409, 2013. ISSN 1099-0488. URL http://dx.doi.org/10.1002/polb.23233.

[210] Raphael Tautz, Enrico Da Como, Thomas Limmer, Jochen Feldmann, Hans-Joachim Egelhaaf, Elizabeth Von Hauff, Vincent Lemaur, David Beljonne, Seyfullah Yilmaz, Ines Dumsch, Sybille Allard et Ullrich Scherf. Structural correlations in the generation of polaron pairs in low-bandgap polymers for photovoltaics. *Nat. Commun.*, 3:970–8, 2012. URL http://www.nature.com/ncomms/journal/v3/n7/full/ncomms1967.html.

[211] Barry C. Thompson, Young-Gi Kim et John R. Reynolds. Spectral broadening in meh-ppv:pcbm-based photovoltaic devices via blending with a narrow band gap cyanovinylene−dioxythiophene polymer. *Macromolecules*, 38(13):5359–5362, 2005. URL http://pubs.acs.org/doi/abs/10.1021/ma0505934.

[212] M Tong, N Coates, Daniel Moses, Alan J Heeger, Serge Beaupré et M Leclerc. Charge carrier photogeneration and decay dynamics in the poly(2,7-carbazole)

copolymer PCDTBT and in bulk heterojunction composites with $PC_{70}BM$. *Phys. Rev. B*, 81(12):125210, 2010. URL http://journals.aps.org/prb/abstract/10.1103/PhysRevB.81.125210.

[213] J. M. Toussaint et J. L. Brédas. Theoretical analysis of the geometric and electronic structure of small-band-gap polythiophenes: Poly(5,5'-bithiophene methine) and its derivatives. *Macromolecules*, 26(19):5240–5248, 1993. URL http://pubs.acs.org/doi/abs/10.1021/ma00071a040.

[214] Despina Triantou, Spyridon Soulis, Sofia Koureli, Antonietta De Sio et Elizabeth von Hauff. Thiophene-based copolymers synthesized by electropolymerization for application as hole transport layer in organic solar cells. *J. Appl. Polym. Sci.*, 127(1):585–592, 2013. ISSN 1097-4628. URL http://dx.doi.org/10.1002/app.37831.

[215] Tomokazu Umeyama, Kohei Hirose, Kei Noda, Kazumi Matsushige, Tetsuya Shishido, Hironobu Hayashi, Yoshihiro Matano, Noboru Ono et Hiroshi Imahori. Thermal conversion of precursor polymer to low bandgap conjugated polymer containing isothianaphthene dimer subunits. *J. Phys. Chem. C*, 116(1):1256–1264, 2012. URL http://pubs.acs.org/doi/abs/10.1021/jp208775x.

[216] Tomokazu Umeyama, Yusuke Watanabe, Masaaki Oodoi, Douvogianni Evgenia, Tetsuya Shishido et Hiroshi Imahori. Synthesis of low bandgap polymers based on thienoquinodimethane units and their applications in bulk heterojunction solar cells. *J. Mater. Chem.*, 22:24394–24402, 2012. URL http://dx.doi.org/10.1039/C2JM33637E.

[217] J.K.J. van Duren, A. Dhanabalan, P.A. van Hal et R.A.J. Janssen. Low-bandgap polymer photovoltaic cells. *Synth. Met.*, 121(1-3):1587–1588, 2001. ISSN 0379-6779. URL http://www.sciencedirect.com/science/article/pii/S0379677900013072.

[218] H.A.M. van Mullekom, J.A.J.M. Vekemans, E.E. Havinga et E.W. Meijer. Developments in the chemistry and band gap engineering of donor-acceptor substituted conjugated polymers. *Mater. Sci. Eng. R Rep.*, 32(1):1–40, 2001. ISSN 0927-796X. URL http://www.sciencedirect.com/science/article/pii/S0927796X00000292.

[219] Koen Vandewal, Steve Albrecht, Eric T. Hoke, Kenneth R. Graham, Johannes Widmer, Jessica D. Douglas, Marcel Schubert, William R. Mateker, Jason T. Bloking, George F. Burkhard, Alan Sellinger, Jean M.J̃. Fréchet, Aram Amassian, Moritz K. Riede, Michael D. McGehee, Dieter Neher et Alberto Salleo. Efficient charge generation by relaxed charge-transfer states at organic interfaces. *Nat. Mater.*, 13:63–68, 2014. URL http://www.nature.com/nmat/journal/v13/n1/full/nmat3807.html.

[220] Eric Vauthey, Anthony W. Parker, Bohdana Nohova et David Phillips. Time-resolved resonance Raman study of the rate of separation of a geminate ion pair into free ions in a medium polarity solvent. *J. Am. Chem. Soc.*, 116(20):9182–9186, 1994. URL http://pubs.acs.org/doi/abs/10.1021/ja00099a037.

[221] Dirk Veldman, Stefan C. J. Meskers et René A. J. Janssen. The energy of charge-transfer states in electron donor–acceptor blends: Insight into the energy losses in organic solar cells. *Adv. Funct. Mater.*, 19(12):1939–1948, 2009. ISSN 1616-3028. URL http://dx.doi.org/10.1002/adfm.200900090.

[222] Eric Verploegen, Rajib Mondal, Christopher J. Bettinger, Seihout Sok, Michael F. Toney et Zhenan Bao. Effects of thermal annealing upon the morphology of polymer–fullerene blends. *Adv. Funct. Mater.*, 20(20):3519–3529, 2010. ISSN 1616-3028. URL http://dx.doi.org/10.1002/adfm.201000975.

[223] P.S. Vincett, W.A. Barlow, R.A. Hann et G.G. Roberts. Electrical conduction and low voltage blue electroluminescence in vacuum-deposited organic films. *Thin Solid Films*, 94(2):171–183, 1982. ISSN 0040-

6090. URL http://www.sciencedirect.com/science/article/pii/0040609082905090.

[224] Olof Wallquist et R. Lenz. 20 years of dpp pigments – future perspectives. *Macromol. Symp.*, 187(1):617–630, 2002. ISSN 1521-3900. URL http://dx.doi.org/10.1002/1521-3900(200209)187:1<617::AID-MASY617>3.0.CO;2-5.

[225] Ergang Wang, Li Wang, Linfeng Lan, Chan Luo, Wenliu Zhuang, Junbiao Peng et Yong Cao. High-performance polymer heterojunction solar cells of a polysilafluorene derivative. *Appl. Phys. Lett.*, 92(3):033307, 2008. URL http://link.aip.org/link/?APL/92/033307/1.

[226] Yanmin Wang, Wei Wei, Xin Liu et Yijie Gu. Research progress on polymer heterojunction solar cells. *Sol. Energy Mater. Sol. Cells*, 98(0):129–145, 2012. ISSN 0927-0248. URL http://www.sciencedirect.com/science/article/pii/S092702481100568X.

[227] Benjamin Watts, Warwick J. Belcher, Lars Thomsen, Harald Ade et Paul C. Dastoor. A quantitative study of pcbm diffusion during annealing of p3ht:pcbm blend films. *Macromolecules*, 42(21):8392–8397, 2009. URL http://pubs.acs.org/doi/abs/10.1021/ma901444u.

[228] D. Weißbach, G. Ruprecht, A. Huke, K. Czerski, S. Gottlieb et A. Hussein. Energy intensities, {EROIs} (energy returned on invested), and energy payback times of electricity generating power plants. *Energy*, 52(0):210 – 221, 2013. ISSN 0360-5442. URL http://www.sciencedirect.com/science/article/pii/S0360544213000492.

[229] Paul Westacott, John R. Tumbleston, Safa Shoaee, Sarah Fearn, James H. Bannock, James B. Gilchrist, Sandrine Heutz, John deMello, Martin Heeney, Harald Ade, James Durrant, David S. McPhail et Natalie Stingelin. On the role of inter-

mixed phases in organic photovoltaic blends. *Energy Environ. Sci.*, 6:2756–2764, 2013. URL http://dx.doi.org/10.1039/C3EE41821A.

[230] Christian Wiebeler, Raphael Tautz, Jochen Feldmann, Elizabeth Von Hauff, Enrico Da Como et Stefan Schumacher. Spectral Signatures of Polarons in Conjugated Co-polymers. *J. Phys. Chem. B*, 117(16):4454–4460, avril 2013. URL http://pubs.acs.org/doi/abs/10.1021/jp3084869.

[231] Martijn M. Wienk, Mathieu Turbiez, Jan Gilot et René A. J. Janssen. Narrow-bandgap diketo-pyrrolo-pyrrole polymer solar cells: The effect of processing on the performance. *Adv. Mater.*, 20(13):2556–2560, 2008. ISSN 1521-4095. URL http://dx.doi.org/10.1002/adma.200800456.

[232] Fred Wudl, M. Kobayashi et A. J. Heeger. Poly(isothianaphthene). *J. Org. Chem.*, 49(18):3382–3384, 1984. URL http://pubs.acs.org/doi/abs/10.1021/jo00192a027.

[233] He Yan, Zhihua Chen, Yan Zheng, Christopher Newman, Jordan R. Quinn, Florian Dotz, Marcel Kastler et Antonio Facchetti. A high-mobility electron-transporting polymer for printed transistors. *Nature*, 457(7239):679–686, 2009. ISSN 0028-0836. URL http://dx.doi.org/10.1038/nature07727.

[234] Takeshi Yanai, David P Tew et Nicholas C Handy. A new hybrid exchange-correlation functional using the Coulomb-attenuating method (CAM-B3LYP). *Chem. Phys. Lett.*, 393:51 – 57, 2004. URL http://www.sciencedirect.com/science/article/pii/S0009261404008620.

[235] G. Yu, J. Gao, J. C. Hummelen, F. Wudl et A. J. Heeger. Polymer photovoltaic cells: Enhanced efficiencies via a network of internal donor-acceptor heterojunctions. *Science*, 270(5243):1789–1791, 1995. URL http://www.sciencemag.org/content/270/5243/1789.abstract.

[236] Mao-Chuan Yuan, Mao-Yuan Chiu, Shih-Pin Liu, Chia-Min Chen et Kung-Hwa Wei. A thieno[3,4-c]pyrrole-4,6-dione-based donor-acceptor polymer exhibi-

ting high crystallinity for photovoltaic applications. *Macromolecules*, 43(17): 6936–6938, 2010. URL http://pubs.acs.org/doi/abs/10.1021/ma101523a.

[237] Cheng Zhang, Jianyuan Sun, Rui Li, Suely Black et Sam-Shajing Sun. Synthesis and energy gap studies of a series of sulfone-substituted polyphenylenevinylenes (sf-ppvs). *Synth. Met.*, 160(1-2):16–21, 2010. ISSN 0379-6779. URL http://www.sciencedirect.com/science/article/pii/S0379677909004925.

[238] Qing T. Zhang et James M. Tour. Low optical bandgap polythiophenes by an alternating donor/acceptor repeat unit strategy. *J. Am. Chem. Soc.*, 119(21): 5065–5066, 1997. URL http://pubs.acs.org/doi/abs/10.1021/ja9640399.

[239] Qing T. Zhang et James M. Tour. Alternating donor/acceptor repeat units in polythiophenes. intramolecular charge transfer for reducing band gaps in fully substituted conjugated polymers. *J. Am. Chem. Soc.*, 120(22):5355–5362, 1998. URL http://pubs.acs.org/doi/abs/10.1021/ja972373e.

[240] Wei-Min Zhang, Torsten Meier, Vladimir Chernyak et Shaul Mukamel. Exciton-migration and three-pulse femtosecond optical spectroscopies of photosynthetic antenna complexes. *J. Chem. Phys.*, 108(18):108–120, 1998. URL http://scitation.aip.org/content/aip/journal/jcp/108/18/10.1063/1.476212.

[241] Erjun Zhou, Motoshi Nakamura, Takeshi Nishizawa, Yue Zhang, Qingshuo Wei, Keisuke Tajima, Chunhe Yang et Kazuhito Hashimoto. Synthesis and photovoltaic properties of a novel low band gap polymer based on n-substituted dithieno[3,2-b:2',3'-d]pyrrole. *Macromolecules*, 41(22):8302–8305, 2008. URL http://pubs.acs.org/doi/abs/10.1021/ma802052w.

[242] Huaxing Zhou, Liqiang Yang et Wei You. Rational design of high performance

conjugated polymers for organic solar cells. *Macromolecules*, 45(2):607–632, 2012. URL http://pubs.acs.org/doi/abs/10.1021/ma201648t.

[243] Yingping Zou, David Gendron, Réda Badrou-Aïch, Ahmed Najari, Ye Tao et Mario Leclerc. A high-mobility low-bandgap poly(2,7-carbazole) derivative for photovoltaic applications. *Macromolecules*, 42(8):2891–2894, 2009. URL http://pubs.acs.org/doi/abs/10.1021/ma900364c.

[244] Yingping Zou, Ahmed Najari, Philippe Berrouard, Serge Beaupré, Badrou Réda Aïch, Ye Tao et Mario Leclerc. A thieno[3,4-c]pyrrole-4,6-dione-based copolymer for efficient solar cells. *J. Am. Chem. Soc.*, 132(15):5330–5331, 2010. URL http://pubs.acs.org/doi/abs/10.1021/ja101888b.

ANNEXE I

SUPPLEMENTARY INFORMATION FOR *DIRECT OBSERVATION OF ULTRAFAST LONG-RANGE CHARGE SEPARATION AT POLYMER:FULLERENE HETEROJUNCTIONS*

I.1 Ultrafast polaron signature

We see in the blend FSRS spectra at room temperature that the 1350 cm^{-1} band, characteristic of positive polaron, appears as early as 100 fs.

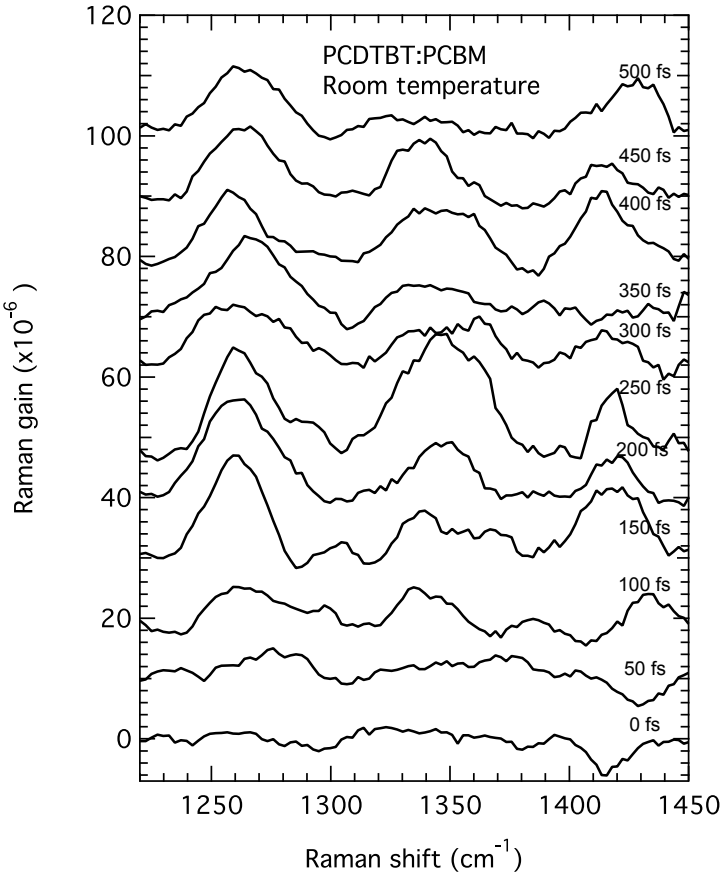

Figure I.1 – Transient stimulated resonance Raman spectra of PCDTBT: PCBM film at early times.

I.2 Calculated spectra

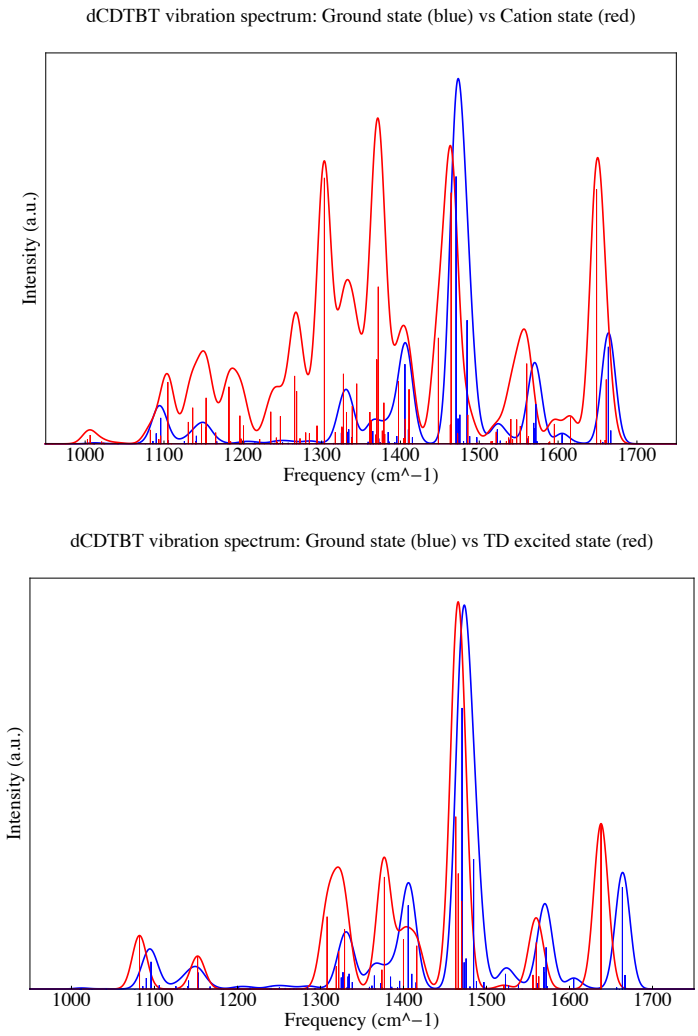

Figure I.2 – Calculated spectra for neat PCDTBT dimers in the ground state (blue) and either the cation (red, top) or the exciton (red, bottom).

I.3 Spontaneous Raman spectra

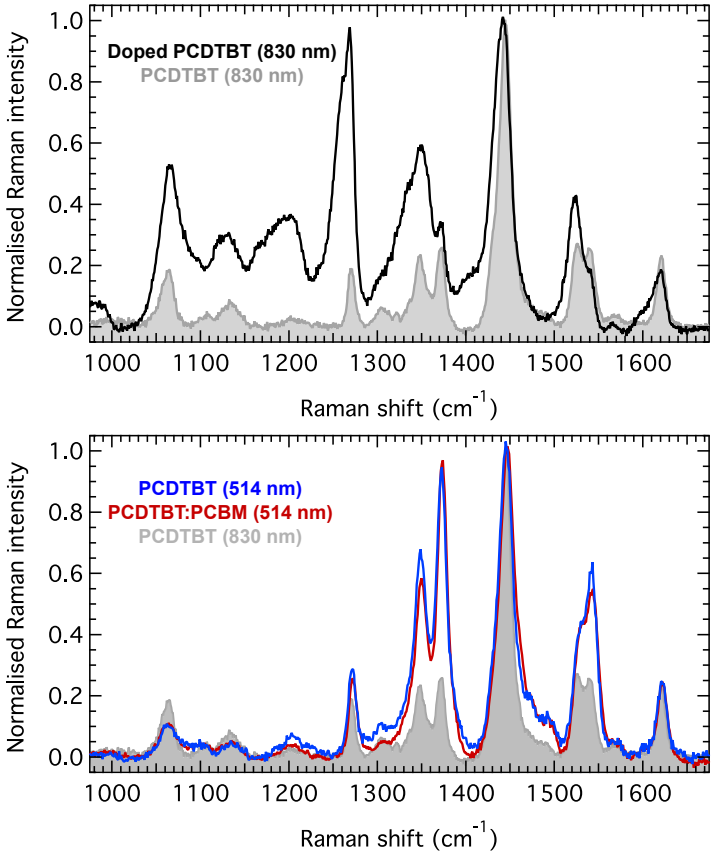

Figure I.3 – Steady-state spontaneous Raman spectra of doped PCDTBT (top) and neat PCDTBT and PCDTBT:PCBM (bottom) films under resonant conditions, compared to non-resonant Raman spectrum (gray area).

I.4 Normalised FSRS spectra

After 50 ps, we observe a decay of the 1261 and 1364 cm^{-1} bands which further emulate the relative intensities in the cationic spectrum.

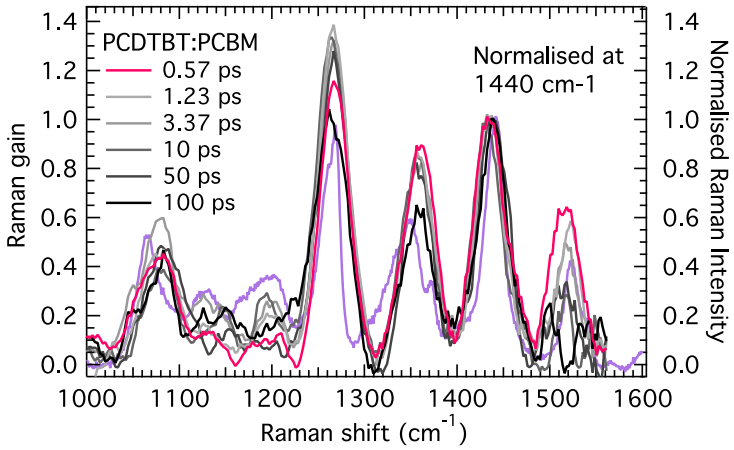

Figure I.4 – FSRS spectra of PCDTBT:PCBM film, normalised at 1440 cm^{-1} to show relative peak intensities evolution compared to steady-state spontaneous resonance Raman of doped PCDTBT (violet line). The spectral region between 1100 and 1230 cm^{-1} suffers from difficult background subtraction, which makes the evolution of the 1200 cm^{-1} band dynamics difficult to follow.

I.5 Characterisation of polymer thin films microstructure

In order to characterise the microstructure and molecular arrangement in this material system, X-ray diffraction experiments were performed. The corresponding powder diffractograms of drop-cast neat PCDTBT, neat PCBM and its blend film (1 part polymer : 4 parts fullerene by weight) are illustrated in Figure I.5. In agreement with the results of previous reports, the neat PCDTBT sample shows broad diffractions at angles with maximum intensities around 4° and 22°, suggesting crystallographic low conformational order.[31, 167] After blending the PCDTBT with the fullerene derivative, the broad diffraction at 4°, related to the neat polymer, can not be distinguished in the blend system with 80 wt% PCBM anymore. The presence of the fullerene derivative in excess obviously leads to further crystallographic disorder of the polymer chains. Crystalline domains of PCBM remain however within the blend when drop cast from DCB at 100 °C. Main diffractions of these PCBM domains were recorded at angles around 10, 17, 19° and reveal the molecular packing in complex crystallographic unit cells[183, 222] comparable to the diffractions of our neat PCBM sample.

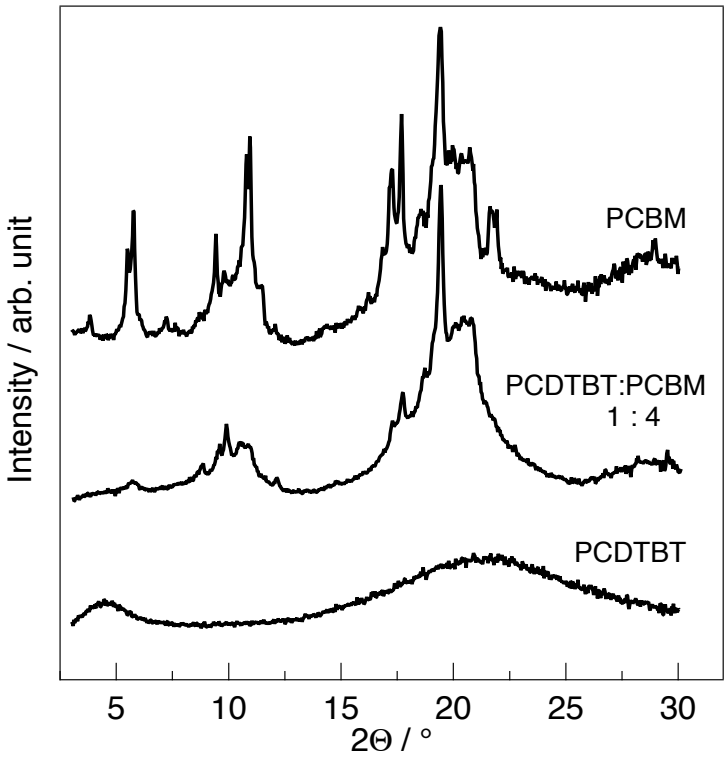

Figure I.5 – X-ray diffractograms of drop casted neat PCDTBT, neat PCBM and its blend (1 part polymer : 4 parts fullerene)

In order to gain further structural information of the neat polymer, the neat fullerene derivative and the blend system, we concentrate our efforts on combining optical and thermal characterisation techniques. Optical microscopic images of the films were taken at selected temperatures and compared to thermal transitions recorded from differential scanning calorimetry (DSC) experiments (see Figure I.6).

Following our film formation protocol smooth films are formed of the neat materials and the blend. During heating from 25 up to 300 °C the featureless films of the neat PCDTBT and the PCBM remain essentially unchanged. However, the transition of colour between 25 and 300 °C from dark purple to pink in the neat PCDTBT system indicate less conformational order and aggregation in the isotropic melt compared to the solid state of the polymer. For the blend, homogeneous and featureless films are formed which appear unchanged using our optical microscopic technique until a temperature

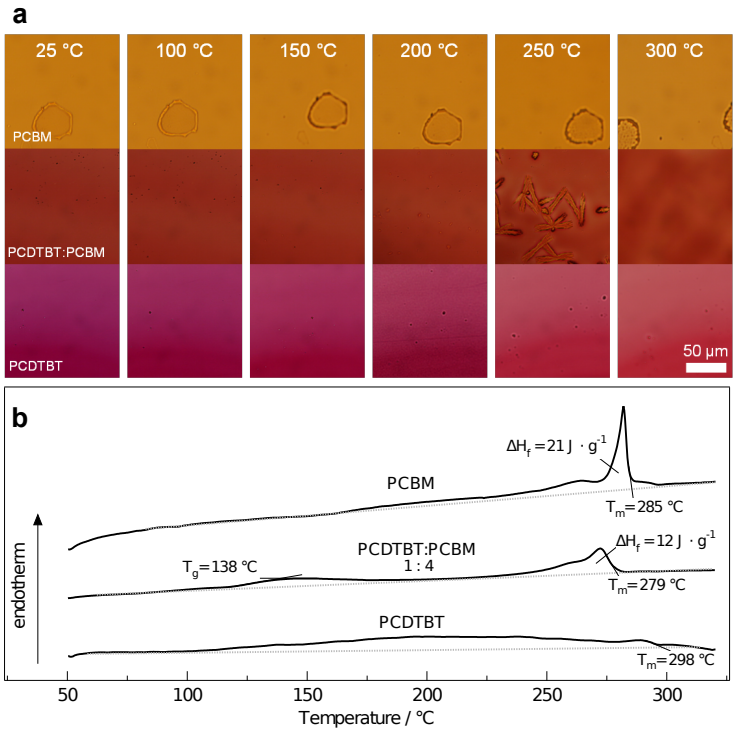

Figure I.6 – (a) Optical micrographs of PCDTBT, PCBM and its blend films at selected temperatures and (b) corresponding differential scanning calorimetric thermograms.

of approximately 200 °C is reached. At this temperature the formation of needle like PCBM crystallites could be observed which has been also reported for diverse polymer:fullerene systems during thermal treatment.[56, 227, 229] During further heating these PCBM features become clearly distinguishable in our experiment at a temperature of 250 °C. If the temperature is further increased to 300 °C both materials reach their liquid state. Investigations revealing kinetic information about the nucleation and growth rate of PCBM crystallites would give further insight into the mixing/demixing characteristics of this system but this is beyond the scope of this work.

The thermograms of the neat PCDTBT and neat PCBM films, drop-cast from solutions in DCB at 100 °C shown here, are in accordance with reported thermal induced conformational changes found for these systems.[31] Films of neat PCDTBT indicate an onset of thermal induced chain movements in disordered fraction above approxi-

mately 100 °C, which is supported by the reported glass transition temperature (T_g) of 130 °C.[31] Around 298 °C a weakly pronounced endotherm indicates the melting of more ordered regions of the polymer chains. The thermogram of neat PCBM films shows a pronounced melting peak of crystalline domains with an end of melting at approximately 285 °C. Please note that the main melting endotherm shows additional melting features at the on and off set of the main peak which we relate to different conformational arrangements of the fullerene derivative formed under our solidification/crystallisation conditions.

The elucidation of the complex morphology in polymer:fullerene systems has been subject of intense investigations. Pure polymer (amorphous and crystalline domains), pure fullerene (amorphous and crystalline domains) and intermixed phases (amorphous domains) have been reported, e. g. in systems containing poly 3-hexylthiophene (P3HT) and multiple C60 fullerene derivatives.[56, 227, 229] Our efforts in this study concentrate on the formation of possible pure amorphous, pure crystalline and intermixed domains of the fullerene component in the disordered polymer regions. In addition to the results of the X-ray diffraction experiments, a defined melting transition of PCDTBT can not be distinguished from the thermogram of the blend system, which also indicates a less ordered polymer arrangement if blended with PCBM. Please note, that in this experiment no exothermic transition due to crystallisation of the fullerene could be recorded.

Furthermore, our DSC data reveal that the fullerene derivative can mix with the selected polymer system. This idea is supported by the observed melting point depression of approximately 6 °C from 285 down to 279 °C for the residual crystalline fullerene component in the blend system. Additionally, the difference of the enthalpy of fusion (ΔH_f) of the fullerene derivative is reduced from approximately 21 down to around 12 J/g which one would expect in a partly miscible system. Please note that a weak endothermic transition at around 138 °C was recorded which could be related to the glass transition temperature of this blend system. Further investigations are ongoing to clarify this point but this out of the scope of this manuscript.

I.6 Baseline subtraction example

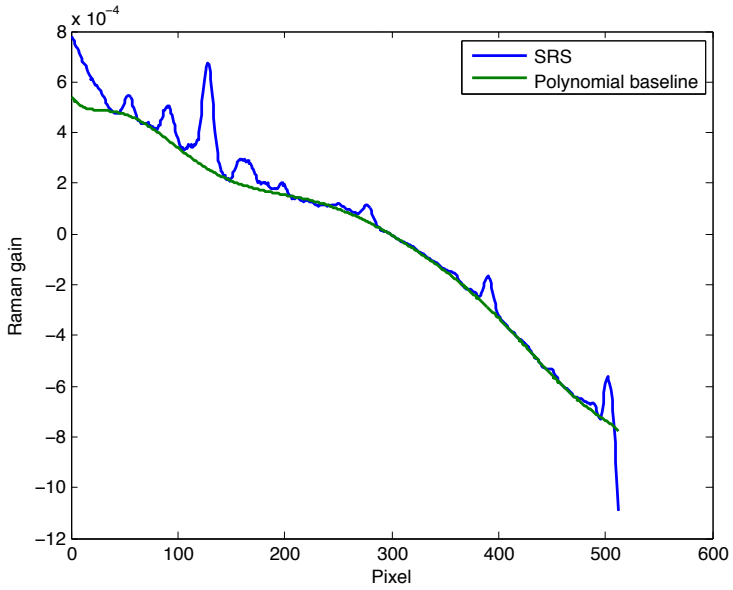

Figure I.7 – Example of polynomial baseline subtraction on smoothed FSRS spectrum.

I.7 FSRS spectra of PCDTBT and PCDTBT:PCBM at all recorded times

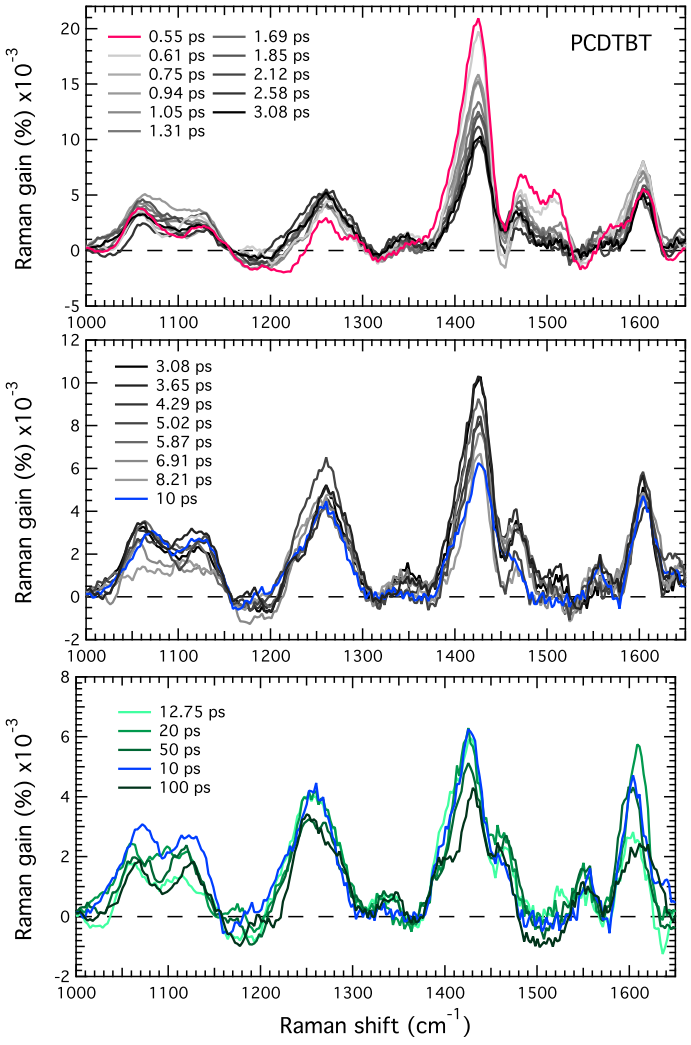

Figure I.8 – Transient Raman spectra of PCDTBT film from 0.55 ps to 100 ps, divided in three panels to better illustrate the spectral evolution.

xxx

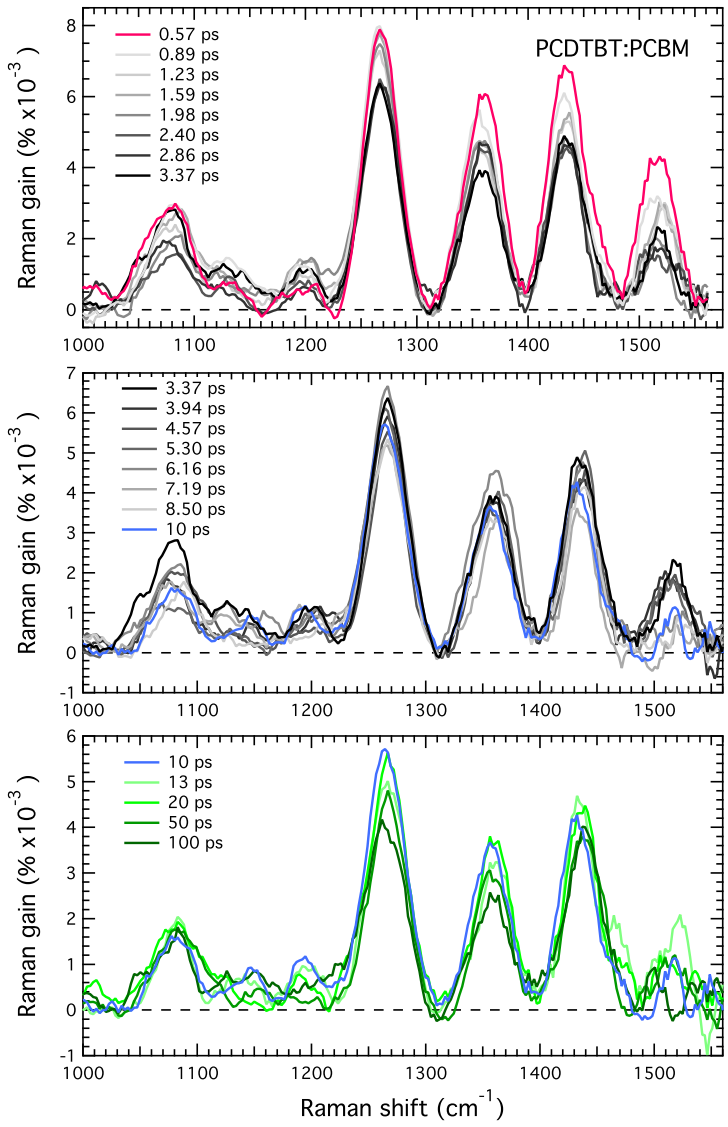

Figure I.9 – Transient Raman spectra of PCDTBT:PCBM film from 0.57 ps to 100 ps, divided in three panels to better illustrate the spectral evolution.

I.8 Molecular orbitals of the PCDTBT cation

The molecular orbitals of the cation differ from the neutral PCDTBT. In first approximation, since an electron is missing in the HOMO of the (formally neutral) polymer, the latter becomes the LUMO of the cationic PCDTBT. Similarly, the HOMO-1 of neat PCDTBT becomes the HOMO of cationic PCDTBT.

However, the cation breaks the spin symmetry of neutral PCDTBT because of the missing electron, which affects the HOMO of the cation. It is a mix of the HOMO and HOMO-1 of the neutral PCDTBT, and the HOMO of the cation sits 130 meV above the HOMO of neat PCDTBT.

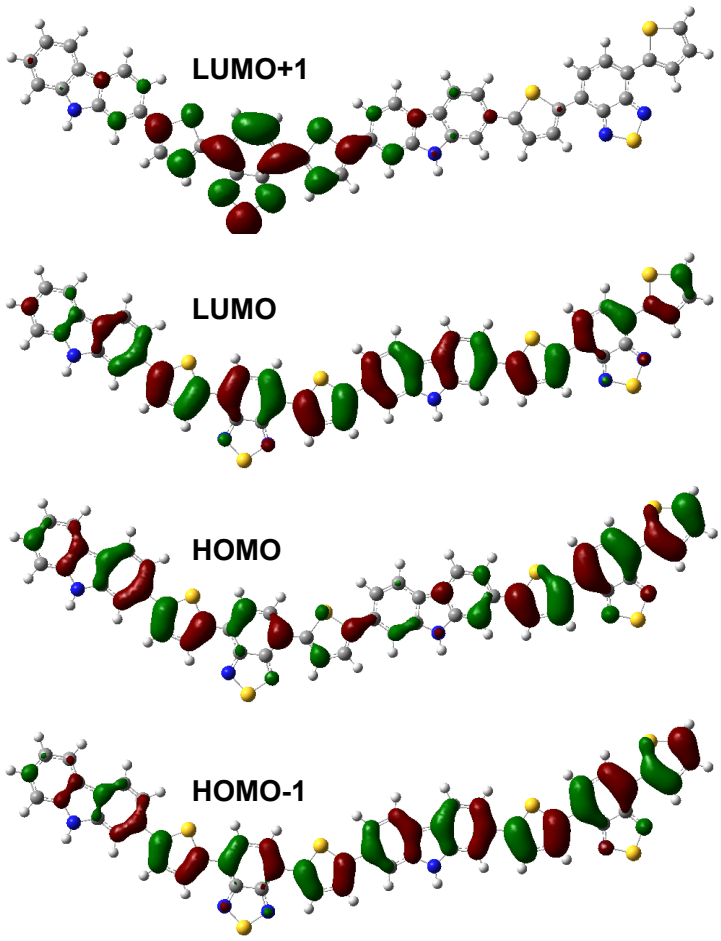

Figure I.10 – Molecular orbitals of the PCDTBT cation, from top to bottom.

I.9 Important Raman modes

In the blend film, the fast disappearing peak around 1513 cm^{-1} is a carbazole mode coupled to thiophenes. This mode is present in the resonance Raman of doped PCDTBT and have a calculated frequency of 1540 cm^{-1}:

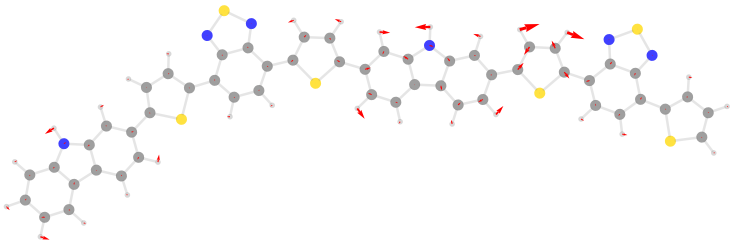

Figure I.11 – Cationic PCDTBT calculated vibrational mode at 1540 cm^{-1}.

The same carbazole mode exists in the neat PCDTBT, but since the electronic density is different, it couples to the thiophenes to a lesser extent, resulting in almost no Raman activity/intensity. This mode has a calculated frequency of 1543 cm^{-1}:

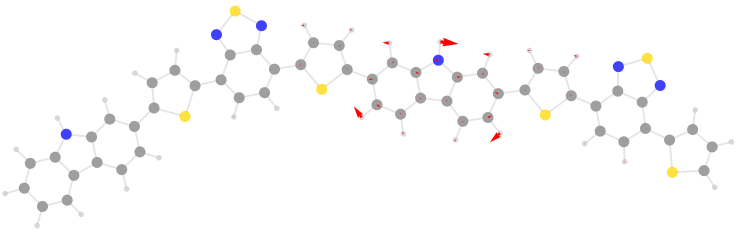

Figure I.12 – Neutral PCDTBT calculated vibrational mode at 1543 cm^{-1}

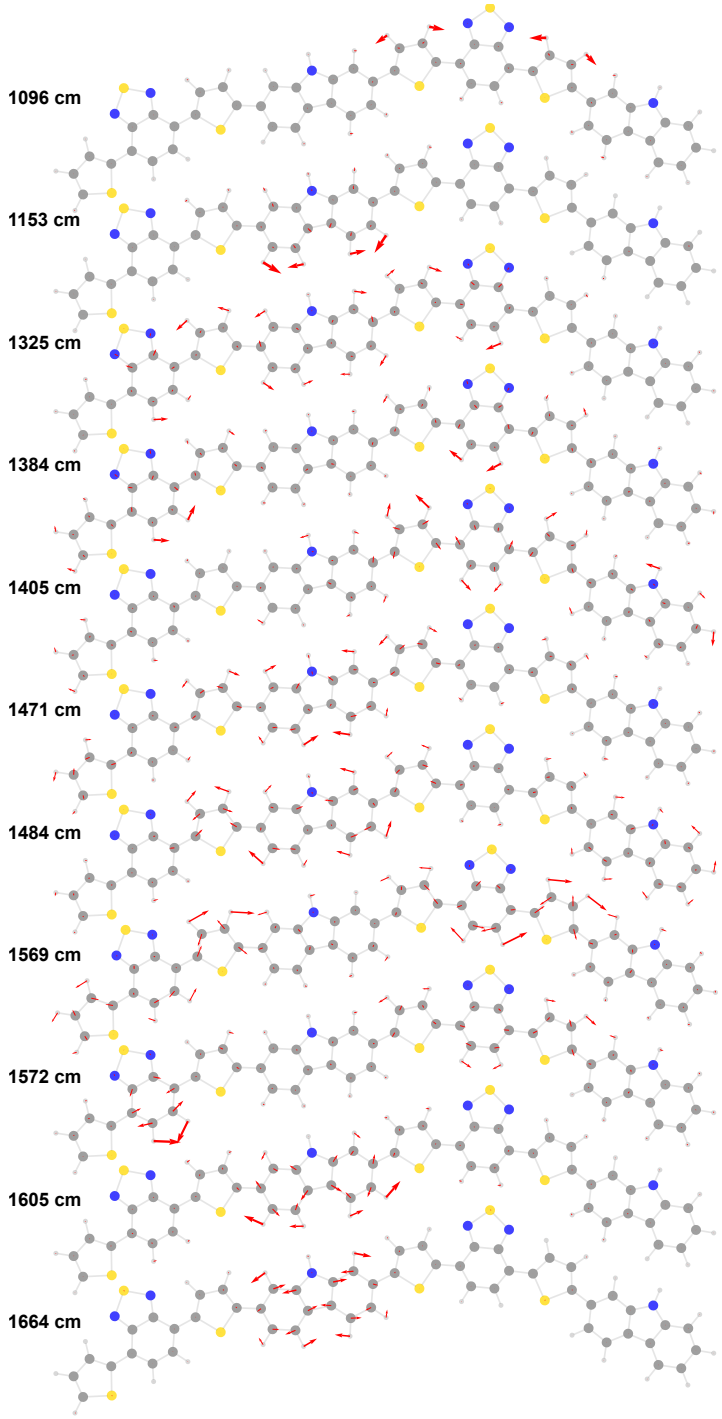

Figure I.13 – Neutral PCDTBT calculated vibrational modes.

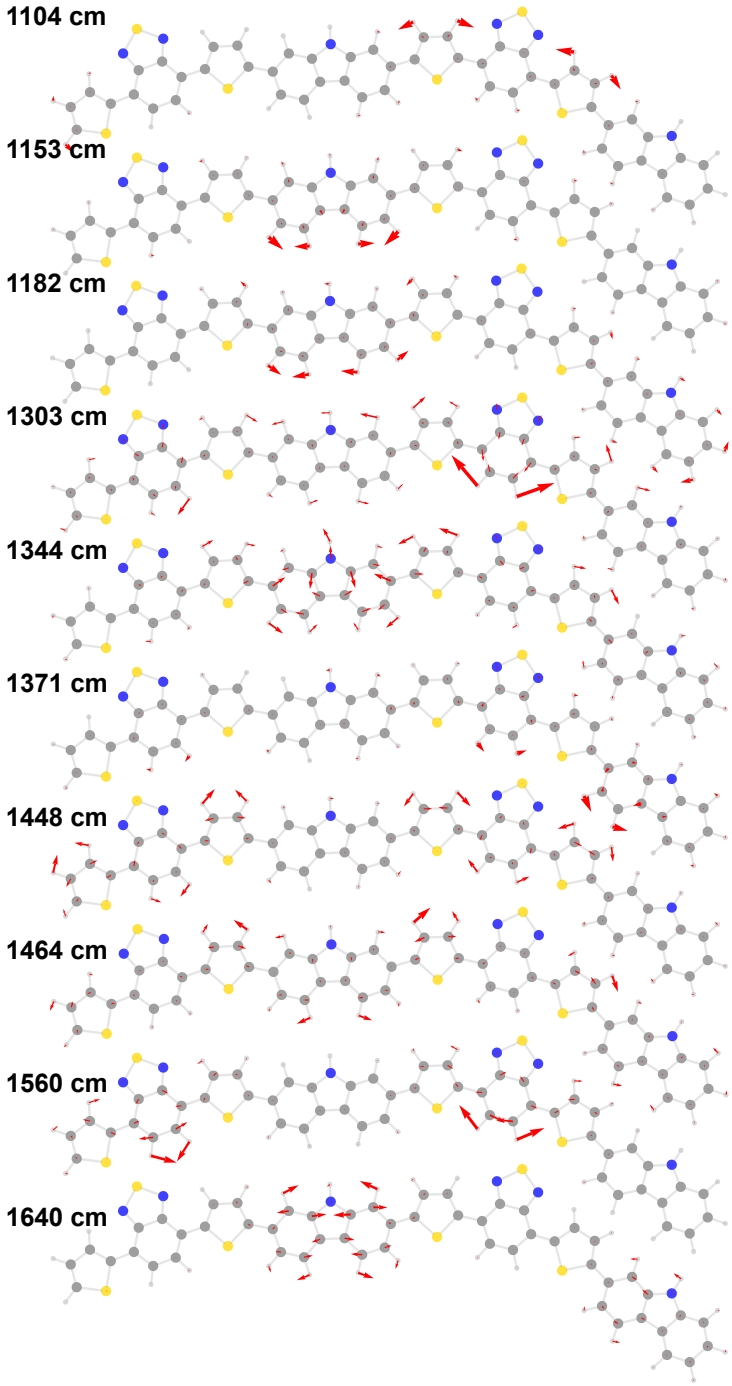

Figure I.14 – Cationic PCDTBT calculated vibrational modes.

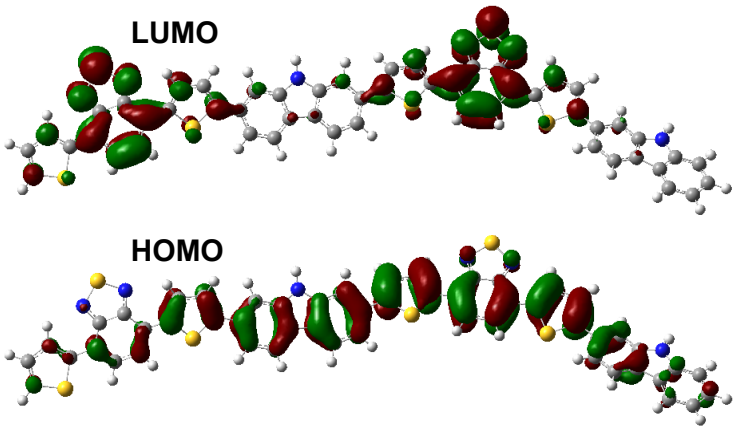

Figure I.15 – Neutral PCDTBT frontier orbitals. Note the shift of the electron density from the carbazole to the benzothiodiazole moiety, lengthening thus the carbazole C-C bonds.

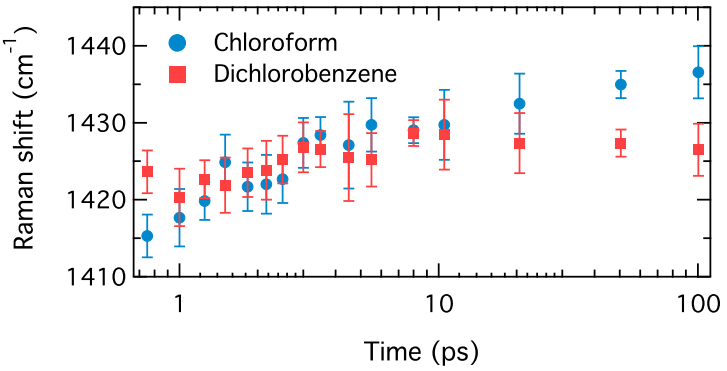

Figure I.16 – Change in frequency of the main FSRS band of PCDTBT (centered at 1425 cm^{-1}) in dilute solutions in chloroform and in dichlorobenzene as a function of time.